Development and Characterization of a Mechanical Surrogate Neck Prototype for Use in Helmet Certification Applications

by

Megan K. Ogle

A thesis submitted in partial fulfillment of the requirements of the degree of

Master of Science

Department of Mechanical Engineering

University of Alberta

ABSTRACT

Sport activities account for over half of all injuries in youths and young adults, with head injuries consistently ranked in the top five most common injury types. Despite mandated helmet use, contact sports, such as hockey and football, expose the players to a greater risk of suffering head and brain injuries compared to the general public due to high speed collisions between athletes. Nearly all current helmets are certified against linear acceleration, which has been found to be a contributor to focal traumatic brain injury (TBI) such as cerebral contusions and intracerebral hemorrhages. Biomechanical research on TBI, specifically mild traumatic brain injury, suggests a predictor variable for brain tissue damage is angular motion of the head. This has opened a debate in standard organizations about the validity of current helmet certification methods. Central to this debate is the development of a standardized surrogate neck model that offers lifelike biomechanical data in direct head impact testing.

The objective of this study is to develop and characterize a Phase 1 mechanical surrogate neck prototype for intended use in helmet certification experimental methods. The neck model is to exhibit realistic response, relative to the human cadaver, in both quasi-static bending and direct head impact to fill the gaps between currently available surrogate neck models and available cadaver data.

The Phase 1 neck model approximately matched the overall dimensions of a 50^{th} percentile human male. The neck prototype was characterized in flexion and extension sagittal bending as well as direct head impact, and was compared to previous cadaveric literature to ascertain whether the Phase 1 neck can offer head kinematics and upper neck kinetics comparable to cadaveric models. Bending moments ranging up to 2 Nm and head impacts up to 5 m/s were simulated. When subjected to sagittal bending, the summation of all vertebral rotations was 80% less than the

rotations presented in previous cadaver literature. In head impact, the Phase 1 neck yielded head kinematics within 35% and upper neck kinetics within 45% of those reported in the selected cadaveric literature. Although the peak results of the Phase 1 neck exceeded the 20% target to peak cadaver data, this Phase 1 attempt to characterize a novel mechanical surrogate neck prototype offered valuable insight to optimize the design in future iterations. Additionally, further testing of cadaveric necks to yield a broader dataset to which can be compared to the Phase 1 neck, and further testing of the prototype neck to understand whether it yields head kinematics comparable to what has been measured for athletes, is suggested.

The impact response of the Hybrid III neck and the Phase 1 neck were also compared. At 1.5 m/s impacts to the Hybrid III headform, it was found that differences in the Hybrid III headform COG kinematics exceeded 40% and the differences in upper neck kinetics exceeded 80% between the two neck models. These are important findings because it can be concluded that neck compliancy does in fact make a difference on the obtained biomechanical data, which contradicts the current assumption in helmet certification protocol.

The maximum inter-test variance of the Phase 1 neck was 44% in flexion rotations and 71% in extension rotations, respectively. In impact, the maximum inter-test variance of peak biomechanical measures was 38%. Although these values exceed the 20% inter-test variance target to achieve repeatability, these results show the variance of the Phase 1 neck is comparable to cadaver literature, which can be up to 40% in quasi-static bending and up to 140% in dynamic experiments.

Simple linear regression models of impact data showed biomechanical measures scale approximately linearly with impact speed, as evidenced by R^2 values of 0.90 or greater. Additionally, the Phase 1 neck sustained approximately 80 experiments without failure.

This thesis documents that the Phase 1 neck model is a durable component with inter-test variance comparable to cadaver literature. These results could be interpreted to convey that the Phase 1 neck is a first step towards a reusable neck model to be used in a controlled laboratory setting that could mimic cadaveric response. A neck model that exhibits realistic impact response, relative to the human, could increase the biofidelity of helmet certification and assessment experimental protocol.

PREFACE

This research project was completed in collaboration with Biokinetics, a Canadian consulting company whose primary focus is injury prevention. This collaboration was led by Dr. C. R. Dennison with Dr. J. P. Carey at the University of Alberta, and C. Withnall at Biokinetics. In addition, this project was partnered with the Faculty of Rehabilitation, specifically, Dr. G. Kawcuk and Ph. D. candidate P. Jun.

The robotic platform described in Chapter 4 was available in the Faculty of Rehabilitation laboratory. The guided free fall drop tower described in Chapter 5 and Chapter 6 was available in the Biomedical Instrumentation laboratory. This thesis is an original work completed by Megan Ogle. No part of this thesis has been previously published.

The contents of this thesis have been presented at the 2016 Alberta BME conference held in Banff, Alberta and the 2018 Injury Biomechanics Symposium held at Ohio State University.

ACKNOWLEDGEMENTS

I would first like to thank and acknowledge my supervisors, Dr. C. R. Dennison, and Dr. J. P. Carey. Their commitment and professional advice through research meetings, extensive revisions of written documents, and all other related discussions were invaluable to me. I am highly appreciative of their efforts.

I would also like to extend my thanks to all members of the Biomedical Instrumentation Laboratory for their assistance in experiments and collaboration. My experiments would not have run smoothly as they did without all your support.

TABLE OF CONTENTS

LIST OF FIGURES

LIST OF TABLES

1 INTRODUCTION

The problem with current mechanical surrogate neck models, the importance of developing a more biofidelic neck for helmet certification methods, and how the study objective of this thesis was defined is described in this chapter.

1.1 Motivation

In 2010, an estimated $26.8 billion in total economic costs were required to treat injuries in Canada [2]. According to Stats Canada, over half of all injuries in youths and young adults are sport related and, among these, head injuries are consistently ranked in the top five [3]. Traumatic brain injury (TBI) and mild traumatic brain injury (mTBI) pose a major health risk to individuals worldwide. These injuries are the result of high-energy traumas including, but not limited to, motor-vehicle accidents, sport activities, or military operations. These injuries to the brain are coupled with dire physical, behavioral, cognitive, and/or emotional affects, whose symptoms can interfere with normal brain function, which in turn disrupts an individual's quality of life [1].

Biomechanical research on mTBI suggests a mechanical predictor variable for brain tissue damage is angular motion of the head [4]. This has opened a debate in standard organizations about the validity of current helmet certification and assessment methods, in addition to how helmet testing could change to incorporate realistic approximations of the human upon impact. Central to this debate is the demand of a fully developed neck model that offers realistic rotations of the surrogate headform.

Multiple organizations have developed helmet certification standards and assessment metrics to evaluate the helmets ability to attenuate impact energy. Some organizations utilize helmeted anthropomorphic test device (ATD) head-neck models, which allow for angular rotation of the headform. However, ATD neck models are thought by many to be too mechanically stiff in bending to be considered a biofidelic model for direct head impact evaluation methods currently defined in helmet certification methods and assessment metrics.

A fully developed and characterized mechanical surrogate neck prototype is a vital component for realistic testing of head protection technology and helmet certification standards. A novel neck segment that behaves in a more biofidelic manner in direct head impact could offer much more realistic post-impact head-neck mechanics when compared to human head impact response. This realistic response is crucial if helmet assessment criteria were to include head rotation. The new neck segment could also reduce the reliance of flexible surrogate neck models that are considered too stiff.

1.2 Thesis Objective

The objective of this research is to design and characterize a Phase 1 mechanical surrogate neck prototype (hereafter referred to as Phase 1 neck) that offers realistic response in helmet certification and assessment experimental protocol. Specifically, this study will define a baseline characterization protocol to achieve realistic bending and impact responses of the Phase 1 neck design when compared to postmortem human subject (PMHS) data. The justification of comparing the Phase 1 neck response to PMHS and definition of these realistic responses are later defined in Chapter 2.

From the defined test protocol, this study will compare the quasi-static bending response of the Phase 1 neck in the sagittal plane to published PMHS cervical flexibility data. Additionally, a surrogate headform fixed to the Phase 1 neck will be impacted at several speeds and locations. The post-impact responses will be compared to the response of an available ATD neck model as well as to similar PMHS impact scenarios. Additionally, the focus of this study will establish whether the Phase 1 neck model is repeatable and can survive multiple tests without failure.

Successful development of a Phase 1 mechanical surrogate neck will pave a path to a more realistic neck model to be used in direct head impact research and helmet certification methods. Future considerations discussed throughout this thesis will allow for further development of the

mechanical surrogate neck model and will assist with design optimization to better match human cadaver impact response.

1.3 Thesis Organization

Chapter 2 begins with an overview of human cervical spine anatomy. Subsequently, the limitations when using in vivo and in vitro human neck models in helmet assessment methods are examined. The role that current ATD surrogate neck models play in human protective equipment certification is then discussed to identify the gaps between these neck models and currently available PMHS data. An overview of helmet development as well as current helmet certification and assessment metrics are then investigated. The design specifications of the Phase 1 neck are then outlined in a design specification matrix.

Chapter 3 includes a description of the development of the Phase 1 neck. Included in this description are the chosen geometrical measurements of the Phase 1 neck components as well as the chosen materials and their properties. The Phase 1 neck design is then justified using a decision matrix.

In Chapter 4, the Phase 1 neck quasi-static sagittal plane flexural stiffness experimental protocol and results are described. The quasi-static bending results are compared to similar published literature focused on PMHS cervical spine elastic range of motion (ROM) in the sagittal plane. Additionally, a coefficient of variation (CV) analysis is performed on the peak flexion and extension angular displacement values of the Phase 1 neck results.

Chapter 5 and Chapter 6 outline the Phase 1 neck impact experimental protocol methods, and the headform center of gravity (COG) kinematic and upper neck kinetic results are compared to the Hybrid III neck model and similar PMHS data focused on direct head impact tests, respectively. In addition, a CV analysis is performed on the peak biomechanical measures of the Phase 1 neck results.

The presented results and insight into the importance of the novel mechanical surrogate neck design is further detailed in Chapter 7. The Phase 1 neck design is compared to currently available ATD neck models, and limitations of the experimental protocol are discussed. Additionally, design change suggestions moving forward into phase 2 are proposed. The contributions of the work presented and suggested future work conclude this thesis in Chapter 8.

2 BACKGROUND

The purpose of this chapter is to orient the reader to cervical spine anatomy, cervical spine biomechanics, and currently available mechanical neck models so a comprehensive understanding of the limitations in current mechanical neck models can be reached. An interpretation of these limitations can help the reader grasp the design goals for the Phase 1 mechanical surrogate neck prototype. Additionally, sport helmet and current helmet certification and assessment metrics are outlined.

2.1 Human Cervical Spine Anatomy

To gain an understanding of movement within the human cervical spine, the anatomy and mechanics of movement within the human spinal column is discussed in this section. The human neck consists of the uppermost seven vertebral bodies of the spinal column, between the head and the thorax. The purpose of the human neck is to support the head and control its movements, as well as protect the spinal cord [5]. The anatomical components of the human neck include vertebral bones, intervertebral discs, nerves, muscles, ligaments, and tendons. Stability of the human head and stability within the neck is achieved through complex vertebral joints and musculature.

Oftentimes the position of the human head is described relative to the Frankfurt plane. This plane passes through the inferior margin of the left orbit and the superior margin of the auditory canals (Figure 2.1).

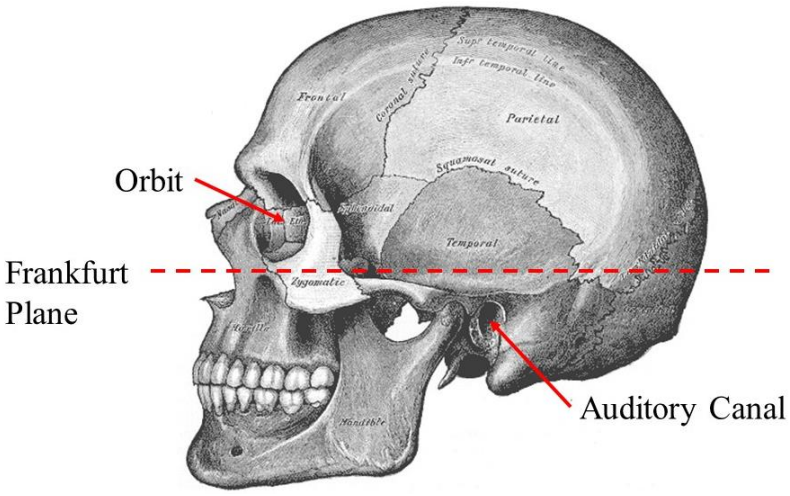

Figure 2.1: Annotated schematic of the human skull detailing the orbit cavity, auditory canal, and Frankfurt plane
Image modified from H. Vandyke Carter, *Temporal Line*, 1858. Accessed June 21, 2018 from https://commons.wikimedia.org/wiki/File:Gray188_-_Temporal_lines.png. This image is licensed under the Creative Commons Public Domain Mark 1.0.

The craniocervical junction is located at the most superior aspect of the human cervical spine [6]. This junction encompasses three bony structures, namely, the occipital bone at the base of the skull, the atlas (the first cervical vertebra), and the axis (the second cervical vertebra) [6] (Figure 2.2). The occipital condyles (OC) are ridges at the base of the occiput that articulate with the atlas [5]. The atlanto-occipital (AO) joint lies between the occiput and the atlas, and the atlano-axial (AA) joint lies between the atlas and the axis. The coupled movements between these two joints are quite complex and they offer the most motion in head rotational movements [6].

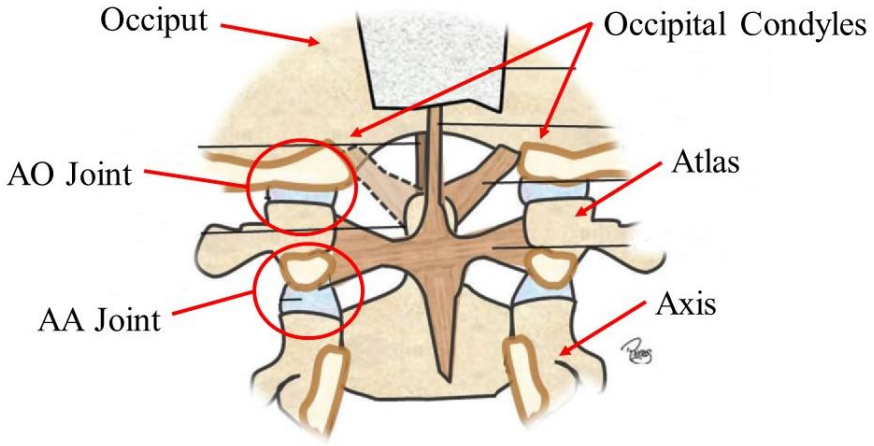

Figure 2.2: Annotated schematic of atlanto-occipital and atlanto-axial joints at the superior end of the human cervical spine
Image modified from R. Riascos, E. Bonfante, C. Cotes, et al., RadioGraphics, 2015, vol. 35, pp. 2121-2134, with permission of RSNA.

Each vertebra within the human cervical spine consists of three basic components, including: the vertebral body, the vertebral arch, and the articular process [5] (Figure 2.3). Vertebral bodies are primarily composed of porous cancellous bone [7], and the structural function of these components is to transfer the weight of the human head along the axis of the vertebral column [5]. The vertebral arch is formed around the spinal cord, which consist of the pedicle that attaches to the vertebral body [5]. The transverse processes are lateral projections of the vertebral body, which are muscle attachment sites and may articulate in extreme bending movements [5]. The superior articular process of one vertebra will articulate with the inferior articular process of the vertebra superior to it [5]. This junction forms the facet joint between two consecutive vertebral bodies [5]. The movements of the vertebral bodies within the human spine are mechanically coupled such that the rotation of one vertebra will initiate movement of the vertebral body inferior or superior to it.

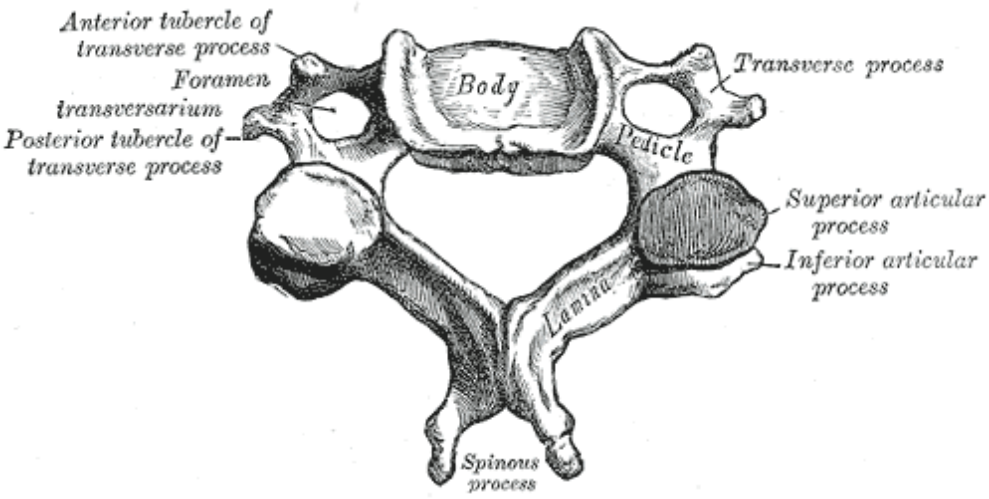

Figure 2.3: Annotated superior view of the human vertebral body
Image from H. Vandyke Carter, *A Cervical Vertebra*, 1858. Accessed June 21, 2018 from https://en.wikipedia.org/wiki/Vertebra#/media/File:Vertebra_Superior_View-en.svg. This image is licensed under the Creative Commons Public Domain Mark 1.0.

Consecutive vertebrae are connected through a series of ligaments and musculature, and are separated by intervertebral discs [5]. The human intervertebral disc is a composite structure, with gel-like properties at the core, more rigid annulus structure surrounding the core, and even more rigid and fibrous outer layer [5] (Figure 2.4). The superior and inferior ends of the discs are covered by vertebral endplates, which are adhered to the adjacent vertebral bodies [5].

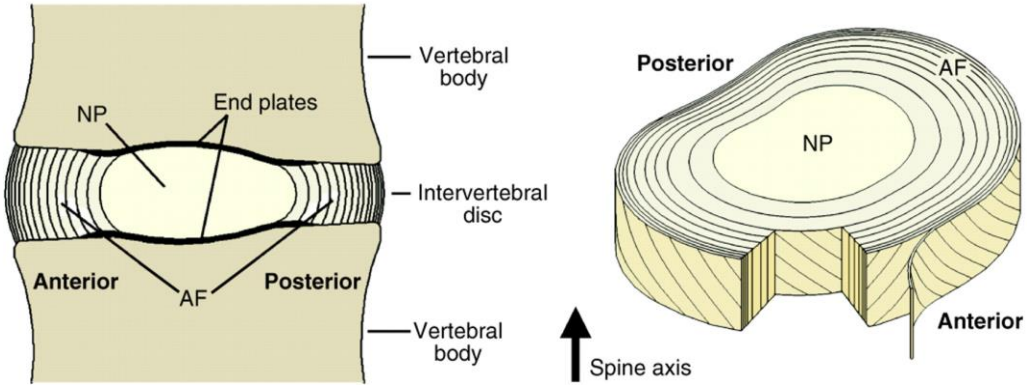

Figure 2.4: Annotated image detailing the layers of a human intervertebral disc
L. Smith et al., "Degeneration and regeneration of the intervertebral disc: lessons from development," *Journal of Disease Models & Mechanisms,* vol. 4, pp. 31-41, 2011. DOI: 10.1242/dmm.006403. This image is licensed under the Creative Commons Attribution 4.0 International.

2.1.1 Limitations of Human Impact Response Models

Data regarding realistic impact response of the human is critical when developing human protective equipment, however, there are limitations to consider when using human models in protective equipment testing. In many cases, impact speeds in human protection certification criteria exceed biological tissue limitations, therefore severe head and/or neck injury would likely occur [8]. To comply with ethic protocol, studies of direct human head impact responses at these speeds are limited to PMHS models. However, the flexibility of each spinal segment, head and neck injuries, head kinematics, and upper neck kinetics are not consistent in each replicated PMHS experiment, resulting in a high degree of variability in the data. Furthermore, PMHS models are expensive to obtain, are often limited to one-time use, and are scarce to come by. PMHS experimentation must be completed shortly after death, as the mechanical properties of the subject become less realistic to the living human as time goes on. For these reasons, PMHS are not ideal to use in helmet certification and assessment methods.

2.1.2 Human Quasi-Static Bending Response Corridors

Quasi-static bending of human cervical spine segments offers valuable data regarding realistic flexibility and ROM in the human spine, and allows for accurate characterization of surrogate neck models [9]. Often, quasi-static bending experiments include cyclic loading of 50th percentile human male cervical spine segments, with extraneous soft tissue removed, to a maximum moment within the elastic range of motion in a given bending plane [9]–[11]. By

removing the extraneous soft tissue from the cervical spine segments, researchers can track and calculate angular displacements of vertebral bodies about their joint center of rotation.

2.1.3 Human Impact Response Corridors

Direct head impact tests of PMHS provides three-dimensional (3D) head kinematic and upper neck response corridors and allows for realistic characterization of mechanical surrogate neck models. Many PMHS data sets include direct head impacts ranging from 1.5 m/s to 7 m/s to different impact locations of a 50th percentile human male head [8], [12], [13]. Either whole PMHS or human head-neck segments fixed at the T1 vertebra are used in most PMHS direct head impact experiments.

2.2 Current ATD Mechanical Surrogate Neck Models

ATDs were developed by the automotive industry to serve as a mechanical surrogate of the human to aid in evaluating the installed restraint systems in simulated vehicle collision scenarios [14]. At the time of ATD inception, the purpose of the neck component was to bend and mimic the response of a human, based on inertial effects in vehicle collisions. These neck models were not validated against human quasi-static flexibility bending responses, therefore, these models are thought by many to be too mechanically stiff in bending to be considered a biofidelic model for use in direct head impact and helmet certification.

The development of many ATD surrogate neck components include the comparison of the head and neck segment, fixed to a rigid structure, to the whole body response of human volunteer sled data collected from the Naval Biodynamics Laboratory (NBDL) [15]. These test results have the potential to be misleading, as the ATD data includes the attachment of the head-neck segment to a rigid structure, whereas the NBDL data is subjectively influenced by the response of the human torso [15]. Other ATD developments include a comparison of the dummy head-neck segment fixed to the dummy torso compared to the NBDL data [15]. While these tests are more comparable to the NBDL data, there are still variables such as the dummy thoracic and restraint system responses that continue to make the tests incomparable [15]. Additionally, the validity of using the NBDL data as a baseline for the ATD neck component has been brought to question due to factors including, but not limited to, the stature and mechanical properties of personnel in the study are unknown, as well as unknown muscle activation in the necks of the participants.

Although ATD neck components are known to be too stiff in bending during direct head impacts, the material properties of these components were specifically chosen to reduce fabrication costs and increase durability, which adds to the appeal of using these models in helmet certification methods and assessment metrics [16]. Since the currently available ATD neck models are designed to be durable and repeatable, there has been little interest to further develop these components, or to manufacture a new neck component specific for direct head impact for a more biofidelic response.

2.2.1 The Hybrid III ATD Neck

The Hybrid III neck is one of the most commonly used neck models in the automotive industry, the Department of Transportation, the Department of Defense [17], and the helmet certification industry. General motors initiated the development of the midsize adult male ATD, the Hybrid III, in 1974 [14]. At the time, the human response in frontal vehicle collisions was the focus for the automotive industry, hence the Hybrid III neck was validated in flexion and extension motion only [15].

The Hybrid III neck consists of five 6061-T6 aluminum plates; three representing vertebral bodies and one at both the superior and inferior end of the neck as attachment surfaces [16] (Figure 2.5). The aluminum plates are separated by four 75 durometer butyl elastomer discs [16]. To closer match frontal collision biomechanics data, horizontal slits on the anterior side of the Hybrid III neck reduces resistance to extension motion, but does not affect flexion motion [16]. A steel cable runs through the center of the neck to achieve axial strength [16]. The nodding joint allows for fixation to the upper neck load cell of the Hybrid III headform, which approximates the OC in the human [16]. The nodding blocks are pressed against the load cell of the Hybrid III headform to measure axial and sheer loads, as well as moments about the approximated OC [16].

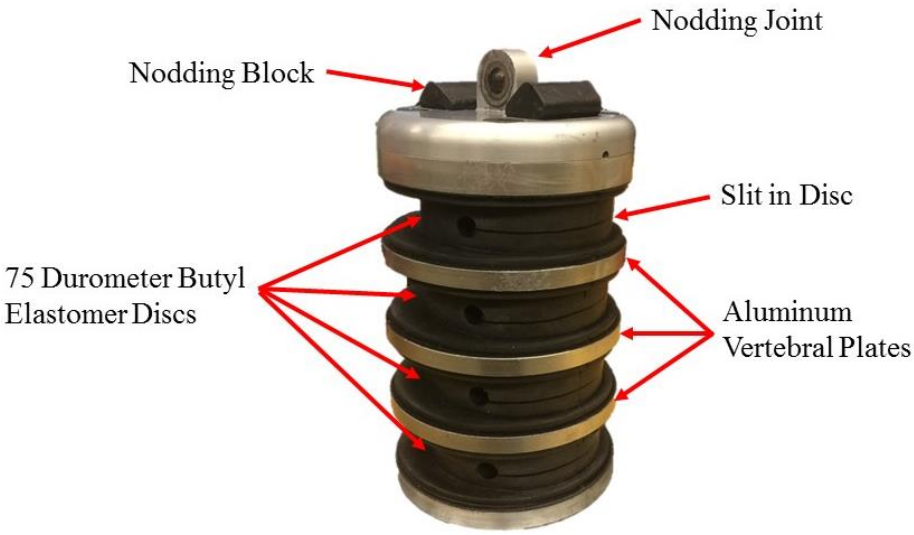

Figure 2.5: Annotated image of Hybrid III neck model (photo credit: author)

2.2.2 Standardized Performance of ATD Neck Models

Specific dynamic flexion and extension performance requirements have been defined by Mertz, Neathery, and Culver which detail dynamic loading corridors that ATD mechanical neck models must exhibit [18]. The test procedure of the dummy is similar to that of the NBDL sled tests, such that the chest of the restrained, seated test dummy is reclined 15 degrees to the vertical, and the anterior-posterior axis of the dummy headform (approximating the Frankfurt Plane) is horizontal [18]. The dynamic loading corridor requirements include:

1. Flexion: Accelerate the sled by 19 g (19 times the acceleration due to gravity, 1 g = 9.81 m/s^2). The chest is to experience a change in velocity of 32 ft/sec (9.75 m/s) and a peak moment at the approximated OC of the dummy headform to be at least 120 ft.-lbs (162.70 Nm) [18].
2. Extension: Accelerate the sled to 9 g. The chest is to experience a change in velocity of 22 ft/sec (6.71 m/s) and a peak moment at the approximated OC of the dummy headform to be at least 40 ft.-lbs (-54.23 Nm) [18].

The moment-angle corridors of the dynamic sled tests defined by Mertz et al. can be found in Figure 2.6. The corridors in this figure were amalgamated from static volunteer, non-injurious dynamic volunteer, and injurious PMHS data, and were assumed to represent a tensed individual [18].

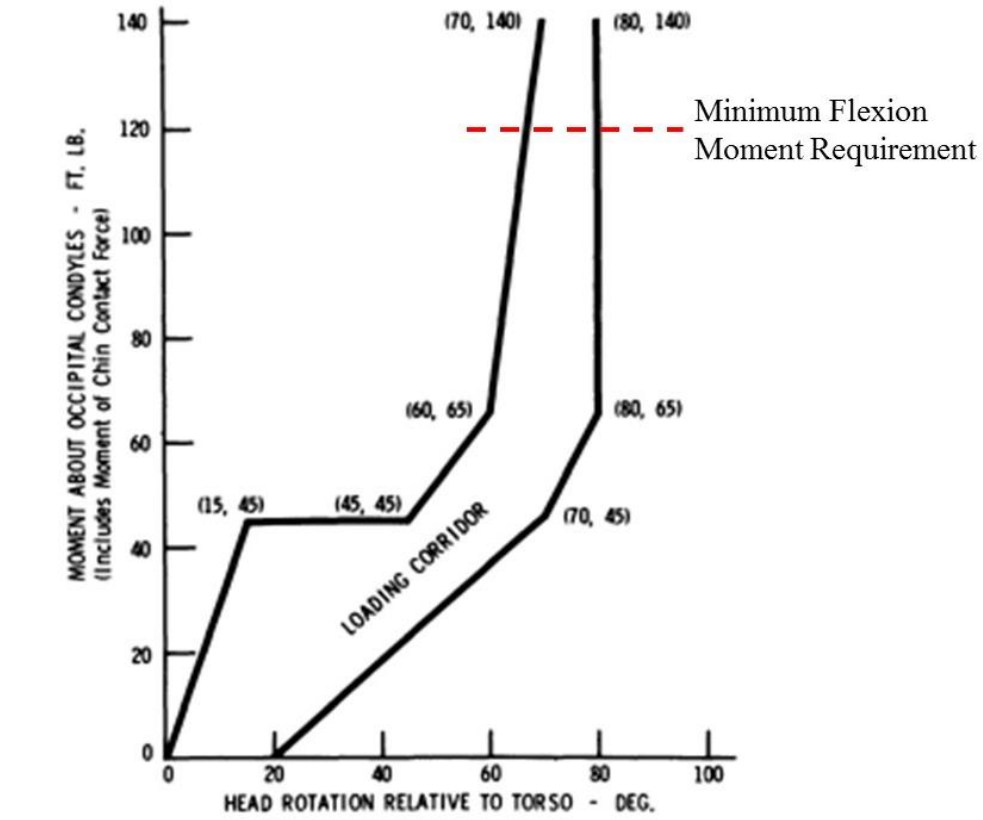

(a)

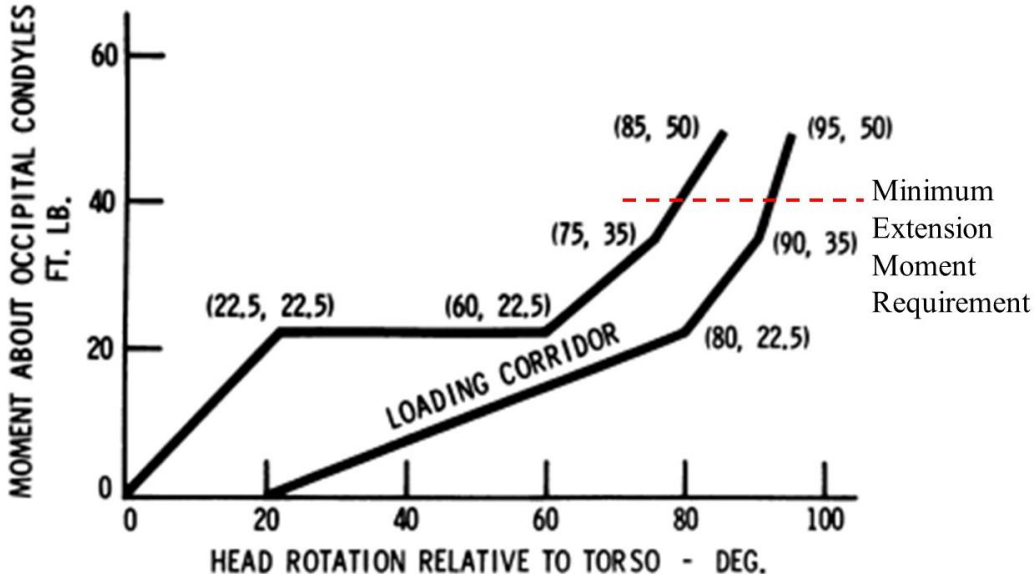

(b)

Figure 2.6: Moment-angle loading corridors defined by Mertz et al. [18], (a) Flexion response, (b) Extension response

A study by Foster et al. found the Hybrid III neck response did fall within the corridors prescribed by Mertz et al., however, the peak flexion and extension moments fell below the prescribed minimums [16]. This study did not conclude what affects these deficient responses would have on automotive crash test results. However, the study did conclude that overall, the Hybrid III neck flexion and extension responses closer matched the defined corridors presented in by Mertz et al. than the preceding Hybrid II neck model [16].

The Code of Federal Regulations (CFR) generated design and performance criteria of ATDs to be used in testing of motor vehicle equipment [19]. This criteria was intended to describe tools to measure the performance of occupant protection in vehicles, as well as to become a part of test procedures specified in vehicle safety standards [19]. There are multiple tests that the CFR defines for the Hybrid III components. One flexion and extension test procedure for the Hybrid III neck is defined as follows:

1. Mount the Hybrid III head and neck on a rigid pendulum so the midsagittal plane of the Hybrid III headform is vertical and coincides with the plane of motion [19].
2. Release the pendulum and allow it to fall freely from a height such that the tangential velocity at impact is 23.0 ± 0.4 ft/s (7.01 ± 0.12 m/s) for flexion and 19.9 ± 0.4 ft/s (6.07 ± 0.12 m/s) for extension, measured at the headform COG [19].
3. Allow the neck to flex without impact of the head or neck with any object other than the pendulum arm [19].

When testing flexion, the Frankfurt plane of the Hybrid III headform is to rotate between 64 and 78 degrees at 57 to 64 ms post-impact, and the peak moment about the OC must be 65 to 80 lbs-ft (88.13 to 115.24 Nm) [19]. When testing extension, the Frankfurt plane of the headform is to rotate 81 to 106 degrees at 72 to 82 ms from impact, and the peak moment about the OC is to be -39 to -59 lbs-ft (52.88 to 79.99 Nm) [19]. It is important to note that it is the pendulum, not the Hybrid III headform, which is impacted, therefore, the resulting rotations experienced by the Hybrid III head and neck are due to inertial reactions of the impacted pendulum. The remaining design performance procedures of flexion and extension of the Hybrid III neck (frontal collision dummy), or lateral bending of the SID neck (side impact dummy) defined by the CFR are also the result of pendulum impacts.

2.2.3 Gaps Between Hybrid III Neck Model and the Human Neck

As stated at the beginning of Section 2.2, the geometries and material properties of the ATD neck models were specifically chosen to reduce fabrication costs and increase durability. The Hybrid III neck contains three simplified vertebral bodies rather than a total of seven, as in the human cervical spine. In addition, the intervertebral discs are much thicker than found in the human spine. The nodding joint and nodding blocks of the Hybrid III neck are not realistic representations of the AO and AA joints in the human because the nodding joint of the Hybrid III neck allows for flexion and extension rotations only, and the nodding blocks reduce this movement at the approximated OC. This design was likely chosen because the Hybrid III ATD was developed for frontal vehicle collisions, therefore, only flexion and extension responses were collected. Also, the nodding blocks hold the Hybrid III headform in the correct position prior to the vehicle collision.

The response of the Hybrid III neck model may be considered biofidelic when compared to volunteer sled impact data, however, discrepancies in peak resultant linear and/or angular accelerations of the headform COG, upper neck forces, and/or upper neck moments may be present when compared to direct head impact PMHS literature. An example of this is noted in experiments conducted by Rizzetti et al. [8]. These tests included forehead and occipital head impact experiments of PMHS and the Hybrid III dummy. In these tests, the percent difference in peak resultant linear acceleration at the Hybrid III headform COG was found to be up to 54% greater than PMHS data in forehead impacts, and up to 138% greater than PMHS in occipital impacts, relative to the PMHS peak resultant linear acceleration [8]. Additionally, the percent difference in angular acceleration about the rotational axis of the Hybrid III headform was found to be up to 40% greater than PMHS data in forehead impacts and up to 239% greater than PMHS in occipital impacts, relative to the PMHS peak angular acceleration [8]. These considerable differences in peak resultant linear and angular accelerations at the headform COG are due to differences in material properties and geometries within the Hybrid III neck model. Considering some helmet certification methods and assessment metrics use the Hybrid III head and neck to evaluate helmet performance, these percent differences in peak values are concerning because the results presented by Rizzetti show that the Hybrid III head-neck segment does not behave in a biofidellic manner in direct head impact.

Although the Hybrid III was not validated in quasi-static bending, quasi-static bending tests of the Hybrid III neck model were completed by Spittle [17]. In the quasi-static bending tests, pure bending moments were applied to the superior end of the Hybrid III neck, while the inferior end was held stationary [17]. Potentiometers measured the angular displacement and a torque sensor measured the resistive torque of the neck model [17]. Spittle applied moments 1000 times larger in magnitude [17] to attain comparable angular displacement values presented in PMHS literature [9]–[11]. This is not surprising, as the rubber described in Section 2.2.1 used in the Hybrid III neck is substantially more stiff than soft tissue of the human neck.

2.2.4 Other ATD Neck Models

Steps have been taken to improve the biomechanical biofidelity of the Hybrid III neck for lateral vehicle impact and rollover testing [15], as well as other applications such as motorcycle crash testing [20]. Other available ATD surrogate necks include the BioRID for use in rear vehicle simulations, the Euro SID and the WorldSID for use in side-impact vehicle collisions, and the THOR for frontal vehicle impacts. However, the focus of these efforts remain in automotive testing and not direct head impact testing.

Instead, a surrogate neck component that is specifically developed and characterized to similarly match direct head impact response, relative to the human cadaver, while also remaining durable and repeatable, could then be used as a surrogate neck model for helmet certification applications that would offer more realistic head kinematics and upper neck kinetics than currently available surrogate neck models.

2.3 Helmet Certification Standard and Assessment Metric Experimental Protocol Development

The brain is one of the most important and complex organs in the human body. This roughly three-pound mass defines an individual's personality, generates and controls movement of the body, serves as a sensory information processing center, is the autonomic regulator of other critical organs in the body, and controls higher cognitive function [5]. These operations are crucial for day-to-day function, and damage to any part of the brain could result in a considerable consequence to an individual's quality of life.

Head and brain injury are categorized to focal and diffuse. The occurrence of both brain injury types is not disjointed, and both injuries can involve life-threatening symptoms. Additionally, neurodegenerative diseases can be the result of progressive damage to different areas of the brain, whether traumatic or mild, and can worsen with age [21].

TBI and mTBI occur when the human head is subjected to loads that exceed the biological protection limitations of the brain [22]. Athletes of contact sports, such as hockey and football, are at greater risk of suffering head and brain injuries due to the high-speed collisions between athletes, and the resulting accelerations or decelerations translated to their heads from these collisions. It is estimated that 1.6-3.8 million of all reported TBI cases worldwide are sport related [23].

Helmets are not currently marketed as brain protectors, but rather head protectors, and are developed under the assumption that its ability to attenuate energy transfer to the surrogate headform is an indicator the helmet can reduce head injury severity in the living human. Specific to sport, many standard organizations have developed certification experimental protocol for helmets as an attempt to reduce TBI occurrence. Many brain injury-related injuries and fatalities in the 1960's were due to focal injuries, such as cerebral contusions and intracerebral hemorrhages, therefore reduction in peak linear acceleration in direct head impact was the focus for early helmet development.

Although most sports require different helmet types, many are developed to add additional protection to the frontal, temporal, parietal, and occipital bones of the human skull over the human scalp and hair. Often, helmets include a hard outer shell and one or more soft liners (Figure 2.7). The hard outer shell protects against penetration of sharp objects and distributes the load across the soft liner layer underneath. The soft liner absorbs and further dissipates the impact energy to reduce the impact energy to the headform as much as possible. Whether the helmet is intended for single impact use, such as cycling helmets, or multi use, such as hockey and football helmets, the materials and design generally differ.

Figure 2.7: Annotated image of hockey helmet detailing the hard shell and soft liner layers (photo credit: author)

Currently, a multitude of sport helmet standards and assessment metrics are available for many different applications, all developed in an attempt to reduce the probability of focal injury. Each one includes distinct impact velocities and impact locations of the helmeted headform, collection of specific headform COG kinematic variables and acceptable thresholds of these variables, unique experimental setups, and different head-neck components. The American hockey helmet standard includes a guided linear drop of a helmeted magnesium headform (EN960 Half Headform Magnesium K1A, Cadex Inc., Saint-Jean-sur-Richeliu, QC) fixed to a rigid metal rod, onto a horizontal anvil to measure peak linear acceleration [24] (Figure 2.8a). The anvil surface is a one-inch, flat modular elastic programmer (MEP) pad (MEP Pad, Model 345_08_MP60, Cadex Inc., Saint-Jean-sur-Richeliu, QC), which is a 60 durometer rubber on the Shore A hardness scale [24]. The required MEP pad is used to approximate an impact onto an ice surface. This standard can be considered one of the most extreme, rigid boundary conditions of the test headform, as this test method does not allow for any head rotation kinematics whatsoever.

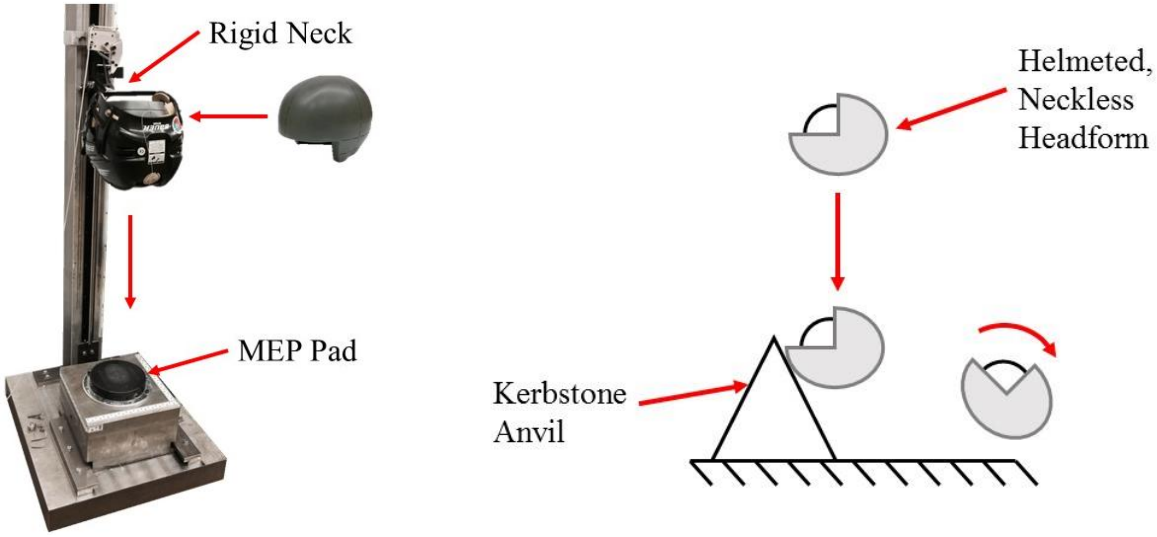

(a) **(b)**

Figure 2.8: Annotated example of sport helmet certification experimental setups, (a) ASTM standard with a linearly guided, helmeted magnesium headform and rigid neck striking a MEP pad (photo credit: Biomedical Instrumentation Lab at University of Alberta), (b) annotated schematic of European neckless, helmeted headform vertically dropped onto an angled kerbstone anvil, adapted from Halldin et al. [25]

Alternatively, the European motorcycle helmet standard can be considered the most extreme, no boundary condition case. This standard includes a vertically dropped, neckless helmeted headform onto an angled kerbstone anvil [26] (Figure 2.8b). This test metric does allow for, and measures, rotational acceleration, however, the fact that the headform is not tethered to any neck model at all could raise questions related to the overall biofidelity of the certification method.

Other helmet certification and assessment metrics utilize human surrogate head and neck components to measure rotational head motion. For example, the NOCSAE football helmet standard certifies helmets using a pneumatic ram which impacts the helmeted NOCSAE headform fixed to a 50th percentile Hybrid III neck [27]. The standard is based on pass/fail criteria for injury severity index, rotational acceleration, and other measures [27]. Another example is the STAR rating system, which is not a certification but rather a proposed method to assess helmet performance and provide the public with performance data. The Hockey STAR is a performance metric formula that combines the probability of the head impact type in a single hockey season, and brain injury probability as a function of linear and angular acceleration [28]. The Hockey STAR experimental setup also uses a 50th percentile Hybrid III neck in pendulum impacts directly to the surrogate headform [28] (Figure 2.9).

Figure 2.9: Example of Hockey STAR helmet assessment metric setup of forehead pendulum impact tests
Image from B. Rowson, S. Rowson, & S.M. Duma, Ann Biomed Eng (2015) 43: 2429. https://doi.org/10.1007/s10439-015-1278-7. This image is licensed under the Creative Commons license (Attribution-Noncommercial).

While all the above helmet standards have proven to effectively reduce the probability of TBI from focal injury, discussions on how helmet testing protocol could change to include criteria to reduce probability of both focal and diffuse injury, as well as use of equipment that offers realistic response when compared to the human, have surfaced. Currently, there are no biofidelic neck models that have been characterized for direct head impact experimentation. In helmet assessment, realistic equipment, specifically head-neck models, are crucial for accurate collection of surrogate head kinematics when compared to human response and injury predictions of the helmet test protocol.

2.4 Thesis Scope

The overarching objective of this thesis is to design and characterize a Phase 1 neck prototype for use in helmet assessment applications. The purpose of this novel neck design is to fill the gaps between currently available ATD neck models and PMHS data in direct head impact. The ideal neck component would offer realistic flexural stiffness, head COG kinematics, and upper neck

kinetics when compared to PMHS data. Any pitfalls in the proposed design could give a future direction to acquire a realistic neck model, relative to PMHS.

Table 2.1 defines the design specifications for this research project, which have been arranged into separate categories including: 1.0 Physical Design, 2.0 Functional Design, and 3.0 Other Design Considerations. Additionally, the importance of each design specification were rated from 1 to 5, where 1 is the least important and the 5 is the most important.

Table 2.1: Phase 1 mechanical surrogate neck prototype research project design specification matrix

Item	Design Specification	Specification Description	Importance (1-5)
1.0 Physical Design			
1.1	Compatible with Equipment	The Phase 1 mechanical surrogate neck prototype must be compatible with equipment available in the accessible laboratories at the University of Alberta campus. Testing and characterization of the neck model cannot be completed without this compatibility.	5
1.2	Anatomical Measurements of 50^{th} Percentile Male	The Phase 1 mechanical surrogate neck prototype must contain similar overall anatomical measurements to the 50^{th} percentile human male.	5
1.3	Anatomical Components of Human Cervical Spine	The Phase 1 mechanical surrogate neck prototype must contain similar anatomical components, such as vertebral bodies, intervertebral discs, and soft tissue, to the 50^{th} percentile human male.	4
2.0 Functional Design			
2.1	Compare Angular Vertebral Movement to PMHS Data	The quasi-static bending response of the Phase 1 mechanical surrogate neck prototype will be compared to PMHS data at the same maximum applied bending moments in the same bending planes. It is desired that the peak bending response of the Phase 1 neck match the PMHS peak bending response within 20%.	5
2.2	Compare Head Kinematics and Neck Kinetics to an ATD Neck Model	The Hybrid III headform impact response when fixed to the Phase 1 mechanical surrogate neck prototype will be compared to the Hybrid III headform response when fixed to the Hybrid III neck at the same impact speeds and the same impact locations to the surrogate headform. It is desired that the difference in peak biomechanical magnitudes of the Phase 1 neck response exceed 20% when compared to the Hybrid III neck response.	5

2.3	Compare Head Kinematics and Neck Kinetics to PMHS Data	The Hybrid III headform COG impact response when fixed to the Phase 1 mechanical surrogate neck prototype will be compared to PMHS data at the same impact speeds and the same impact locations. It is desired that the peak biomechanical measures of the Hybrid III headform when fixed to the Phase 1 neck match the PMHS peak bending response within 20%.	5
2.3	Durability	The Phase 1 mechanical surrogate neck prototype must survive multiple impact tests without failure. Additionally, the prototype must survive impact speeds commonly used for helmet certification methods.	4
2.4	Repeatability	The Phase 1 mechanical surrogate neck prototype must contain a CV of 20% or less in all data sets. Using simple linear regression models, the R2 value of the obtained impact biomechanical data must be 0.7 or greater.	4
3.0 Other Design Considerations			
3.1	Cost of Manufacturing	The Phase 1 mechanical surrogate neck prototype must cost under $1000.	1
3.2	Ease of Assembly	The number of components and complexity of design must be limited for ease of assembly.	3

The scope of this study focuses on the characterization of a Phase 1 neck by comparing quasi-static bending and impact responses to published PMHS data and an available ATD neck model. This characterization analysis cannot be completed without the compatibility of the Phase 1 neck with test equipment available in laboratories at the University of Alberta campus. As many PMHS data sets focus on the analysis of 50th percentile male, the overall measurements and components that make up the Phase 1 neck shall also similarly match that of a 50th percentile human male.

In this study, the quasi-static bending response characterization will be limited to the sagittal plane for the Phase 1 comparison, which will include the summation of peak flexion and peak extension vertebral body angular displacements from the C1 to C7 levels. The collected quasi-static bending data of the Phase 1 neck will be compared to PMHS data presented by Camacho et al. [9], Nightingale et al. [10], and Wheeldon et al. [11]. It is desired that the peak flexion and extension vertebral body angular displacements from C1 to C7 of the final version of the mechanical surrogate neck component matches within 20% of the peak response reported in PMHS

literature. From data adapted from the chosen PMHS literature, the maximum CV in peak flexion angular displacement was approximately 40% and in peak extension angular displacement was approximately 30%, respectively [9]–[11]. By matching the peak angular displacement of the mechanical surrogate neck to within 20% of the reported PMHS values, the mechanical surrogate neck data should then fall within PMHS values majority of the time. If this specification is not met when testing the Phase 1 neck, documentation of design alterations necessary to achieve peak differences in flexion and extension angular displacements less than or equal to 20% must be given.

The Hybrid III headform COG kinematics and upper neck kinetics when fixed to the Phase 1 neck will be compared to the same biomechanical measures of the Hybrid III headform when fixed to the Hybrid III neck. It is desired that the difference in peak biomechanical measures observed exceed 20%. This will prove that majority of the time the peak biomechanical values of the two surrogate neck models do not fall within a range to be considered similar. This is a desired quality in the Phase 1 neck, because the purpose of this thesis is to develop a novel surrogate neck prototype for use in direct head impact. By proving the obtained peak biomechanical measures are different between the two neck models in direct headform impacts, the conclusions of the how surrogate neck compliancy affects biomechanical data can be drawn.

In addition, the peak biomechanical measures obtained from the impact tests of the Phase 1 neck will be compared to PMHS data published by Advani et al. [12], Rizzetti et al. [8] and Yoganandan et al. [13]. It is desired that the peak biomechanical measures of the final version of the mechanical surrogate neck component to fall within 20% of the peak response reported in PMHS literature. CV values obtained in dynamic PMHS literature can range from 20% to 140% [29], therefore, by matching peak biomechanical data from the mechanical surrogate neck experiments to fall within 20% of the reported PMHS data, the mechanical surrogate neck data should then fall within PMHS values majority of the time. If this specification is not met when testing the Phase 1 neck, documentation of design alterations necessary to achieve peak differences biomechanical measures less than or equal to 20% must be given.

The Phase 1 neck should be a repeatable component that can withstand multiple impact tests without damage. Small values of CV, such as 20%, identify that the Phase 1 neck responses are stable and little variation of peak values between tests are present [29]. CV analyses will be performed on both the quasi-static bending and impact data of the Phase 1 neck to assess the

repeatability and variance. To obtain a repeatable neck model, the CV values from these analyses should be less than or equal to 20%.

Simple linear regression models of the impact data will be used to describe the correlation between biomechanical variables and impact speed. The coefficient of determination (R^2) of these simple linear regression models will be used to determine this correlation. Large R^2 values, such as 0.70 or greater, indicate impact speed explains approximately 70% or more of the variation in the observed biomechanical measures. R^2 values of 0.70 or greater are regarded as satisfactory in early phases of research [30].

At this stage of the project, a characterized durable prototype is the most important requirement. Cost reduction and design optimization may be included in future work if these specifications are not met in this phase.

3 DEVELOPMENT OF A PHASE 1 MECHANICAL SURROGATE NECK PROTOTYPE

The development of the Phase 1 mechanical surrogate neck prototype to be compared to PMHS data and a currently available ATD neck model is detailed in this chapter. A decision matrix to justify chosen materials and component geometries is also presented.

3.1 Methods

In this study, a novel Phase 1 neck prototype was designed to be characterized when compared to PMHS data and the Hybrid III neck. By comparing the Hybrid III headform COG kinematic and upper neck kinetic data when fixed to the Phase 1 neck to PMHS data, a representation of how closely the Phase 1 design matches realistic human response may be defined. Any gaps between PMHS neck response and the Phase 1 neck could give insight for a future direction in optimizing the design. Additionally, comparing the biomechanical data of the Hybrid III headform when fixed to the Phase 1 neck to these measures when fixed to the Hybrid III neck offers the ability to quantify how neck compliancy affects the impact response of the headform.

The Phase 1 neck was designed to contain similar components to the human neck, such as vertebral bodies, intervertebral discs, facet joints, and soft tissue, while achieving durability and repeatability. Measurements of neck length and neck circumference were based off a study conducted by Vasavada et al. whose study objectives were to quantify head and neck anthropometry of a 50^{th} percentile male [31]. Figure 3.1 describes the external anthropometry

measurements of a human neck, and Table 3.1 compares these measurements between the Phase 1 neck and the values obtained from a 50th percentile human male. The Hybrid III headform does not contain detailed ears, therefore the neck length was measured to an approximated Frankfurt plane. Additionally, Table 3.1 compares the mass of the Phase 1 neck to the mass of a 50th percentile male from a study conducted by Armstrong [32].

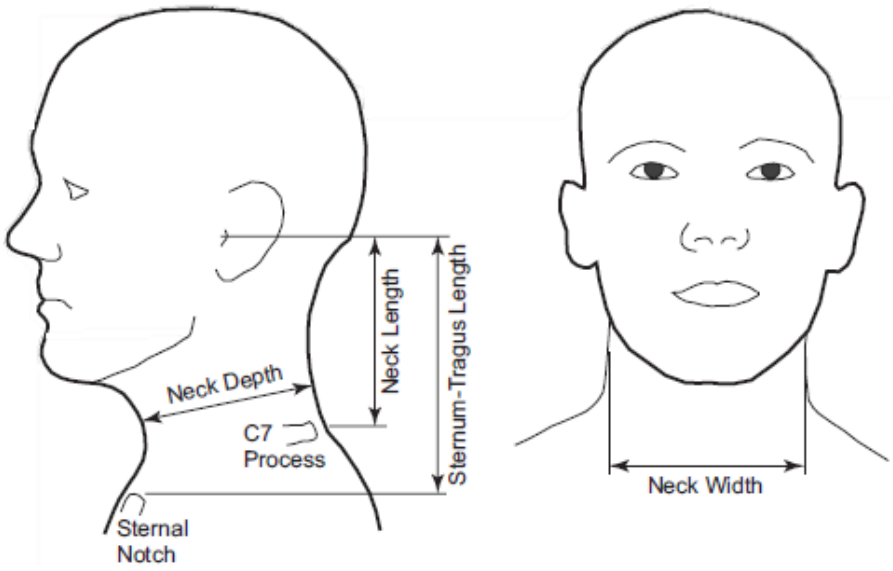

Figure 3.1: External anthropometric measurements of a human neck
Reprinted from Journal of Biomechanics, Vol. 41, A. Vasavada, J. Danaraj, and G. Siegmund, Head and neck anthropometry, vertebral geometry and neck strength in height-matched men and women, Pages 114-121, Copyright 2008, with permission from Elsevier

Table 3.1: External anthropometry of 50th percentile neck

External measurement	50th percentile male	Phase 1 neck
Neck Length (Frankfurt plane to C7)	108 mm [31]	115 mm
Neck Depth	123 mm [31]	100 mm
Neck Width	117 mm [31]	100 mm
Neck Circumference	394 mm [31]	314 mm
Neck Weight	1.10 kg [32]	1.01 kg

A detailed computer model of the Phase 1 neck can be found in Figure 3.2. The nodding joint was manufactured from aluminum 6061-T6 with a similar design to the Hybrid III neck nodding joint. The vertebral bodies were simplified and waterjet cut from 1/4" aluminum 6061-T6 sheet stock. TangoBlack 3D printed rubber-like material (TangoBlack – FullCure®970, 3D Printers Canada, Vaughan, ON) was chosen for the intervertebral discs. The entire spinal column of the

Phase 1 neck was encased in silicone rubber (Ecoflex® 00-30, Smooth-On Inc., Macungie, PA). The chosen silicone rubber was suggested by Sparks et al. whose study objective was to evaluate the ability of silicone materials to mimic stress in muscular tissue [33]. Prior to pouring the silicone rubber into the neck mold, the liquid was degassed in a vacuum chamber to remove the air bubbles formed when preparing the silicone rubber. Stability of the Phase 1 neck was accomplished via three tensioned 1/8" diameter steel cables, one that passed through the center of each vertebral body, and one through each transverse process. The clamping collars (6436K500 Two-Piece Shaft Collars, McMaster-Carr, Cleveland, OH) at the base of the Phase 1 neck dictated tension in the steel cables. The facet joints were approximated with dual-stacked square profile O-rings (4061T111 Square-Profile Oil-Resistant Buna-N O-Rings, McMaster-Carr, Cleveland, OH). The base plate served as a fixed T1 vertebral body in experiments.

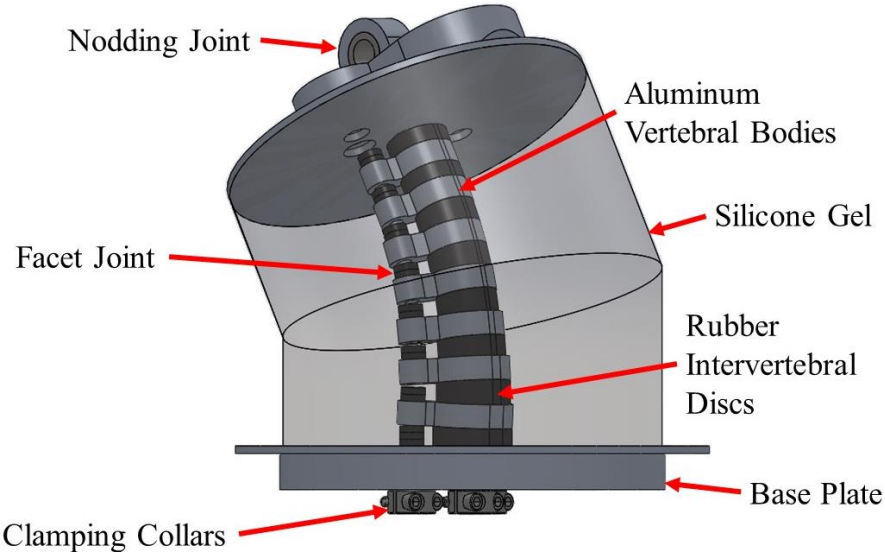

Figure 3.2: Annotated CAD model of Phase 1 mechanical surrogate neck prototype

Table 3.2 compares the material properties chosen to manufacture the Phase 1 neck and human tissue. Specifically, Table 3.2 compares the yield strength, σ_y, the ultimate tensile strength, σ_u, the Young's modulus, E, the hardness, the elongation at break, and the shear modulus, G. As can be seen from the table, the aluminum vertebral bodies can withstand approximately 400 times more axial force than human vertebral bodies before failure. This shows the aluminum vertebrae of the Phase 1 neck are more durable than human vertebrae. The ultimate tensile strength of the TangoBlack material is less than that of a human intervertebral disc, however, the rubber-like discs were not adhered to the aluminum vertebral bodies, therefore axial tension experienced in the

Phase 1 neck will be transferred to the silicone rubber and steel cables. The Ecoflex silicone rubber suggested by Sparks et al. can withstand approximately 2.5 more axial force than human muscle tissue. This shows the silicone rubber used to simulate soft tissue is more durable than human muscle tissue.

Table 3.2: Comparison of materials properties used to design Phase 1 mechanical surrogate neck prototype to material properties of human tissue

Material	σ_y (MPa)	σ_u (MPa)	E (GPa)	Hardness	Elongation at Break (%)	G (GPa)
Aluminum 6061-T6	270	310	69.0	60 (Rockwell)	12.0	26.0
Vertebral cancellous bone [34]	-	-	0.17	-	-	-
TangoBlack 3D printed rubber	-	2.00	-	61 (Shore A)	48.0	-
Intervertebral disc [35]	-	8.80	3.61e-3	-	-	-
Ecoflex 00-30 Silicone	-	1.38	6.9e-5	00-30 (Shore)	900	-
Relaxed muscle tissue	-	-	2.7e-5 [36]	-	-	4.6e-6 - 23.8e-6 [33]

An example of the aluminum vertebral body structure and 3D printed rubber-like intervertebral disc structure can be found in Figure 3.3. The pedicle lengths, ℓ, were 7.20 mm for all seven vertebral bodies to achieve simplicity. The transverse process angles, α, vertebral body widths, w, vertebral body depths, d, and inclinations of the intervertebral discs, Θ, were based on dimensions observed by Panjabi et al. whose study objectives were to quantify the anatomy of vertebral parts of the middle and lower cervical regions [37]. The measurements for all Phase 1 neck vertebral bodies and intervertebral discs can be found in Table 3.3. Each intervertebral disc width, w, and depth, d, were identical to the widths and depths of the vertebral body inferior to it. The intervertebral heights, h, were all 4.50 mm before the additional angled material was added. This initial height of the intervertebral disc was chosen to be 1.25 mm larger than defined by Gilad and Nissan [38] to make up for the lost height from the simplified vertebral bodies. Additional

height to the anterior side of the intervertebral discs were added to achieve the lordotic curvature of the Phase 1 neck spinal column.

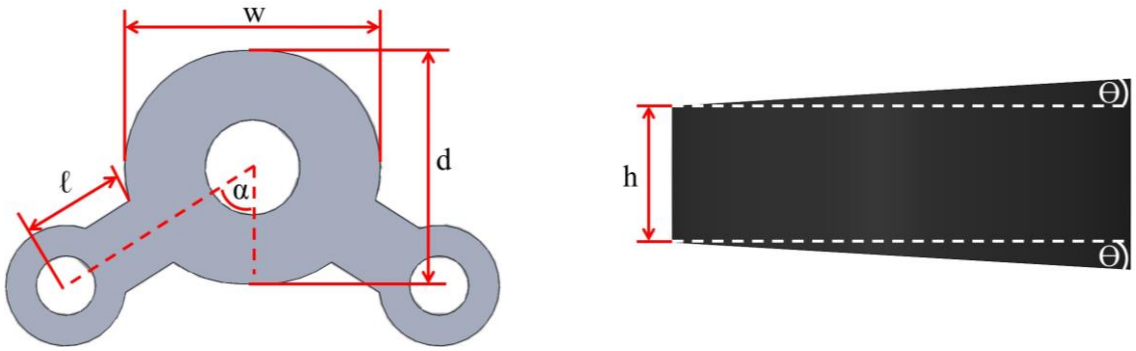

(a) **(b)**

Figure 3.3: Annotated CAD models of Phase 1 mechanical surrogate neck prototype spinal elements, (a) top view of vertebral body, (b) side view intervertebral disc

Table 3.3: Spinal element measurements of the Phase 1 mechanical surrogate neck prototype

Vertebral Body Measurements			
Vertebral Body	**α (deg)**	**w (mm)**	**d (mm)**
C1	57.76	16.91	15.45
C2	57.76	16.91	15.45
C3	56.45	16.51	15.25
C4	57.68	17.00	15.50
C5	56.58	18.50	16.50
C6	56.06	20.50	17.50
C7	54.46	22.50	17.50
Intervertebral Disc Measurements			
Intervertebral Disc			**Θ (deg)**
O-C1			0.00
C1-2			0.00
C2-3			3.50
C3-4			3.75
C4-5			2.00
C5-6			3.75
C6-7			2.50
C7-T1			1.80

3.2 Discussion

As seen in Table 3.1, the Phase 1 neck contains lesser external anthropometry measurements when compared to the 50th percentile male, except for the neck length. The additional 7.00 mm in height is due to simplifying the geometry of the Phase 1 neck. The height of all seven vertebral bodies were 1/4", as they were all waterjet cut from the same aluminum 6061-T6 sheet stock. To make up for the lost height of the vertebral bodies, all eight intervertebral discs began at 4.50 mm, approximately 1.25 mm larger than prescribed by Gilad and Nissan [38]. To achieve the resting vertebral body angular inclinations, additional material was added to the anterior side of the intervertebral discs. The neck depth and neck width measurements of the Phase 1 neck were simplified so the muscle tissue was a circular column, rather than the ovular shape seen in a human.

As expected, common engineering materials encompass different material properties than the human neck. In most cases, the chosen materials were shown to be more durable than human tissue. These materials were chosen for their availability, durability, and repeatability features, which were required design specifications outlined in Table 2.1.

3.2.1 Phase 1 Neck Design Evaluation

The Phase 1 neck design is evaluated according to the decision matrix shown in Table 3.5. In the development stage of the Phase 1 neck, all components could have either been designed to be anatomically identical to human cervical components, labeled as the Complex Design in Table 3.5, or the components could have been simplified, labeled as the Simple design, to achieve ease of assembly and manufacturability. The following decision matrix was constructed based on the Physical Design category of the design specification matrix in Table 2.1. Table 3.4 details the meaning of the numerical scores in the decision matrix.

Table 3.4: Decision matrix legend

Score	Description
5	Meets expectation
3	Meets expectation (second best relative ranking)
1	Meets expectation (third best relative ranking)
0	Does not meet expectation

Table 3.5: Phase 1 mechanical surrogate neck prototype decision matrix

Category	Desire and Weight Reasoning	Weight	Complex Design	Simple Design	Reasoning
AO Joint	AO joint is replicated	3	5	3	Although the AO joint would be better approximated with a complex design, the simpler design would make the overall manufacture process of the Phase 1 neck much easier. This joint was not a crucial feature for the Phase 1 neck design.
AA Joint	AA joint is replicated	3	5	3	Admittedly, the AA joint would be better approximated with a complex design; however, the simpler design would make the overall manufacture process of the Phase 1 neck much easier. This joint was not a crucial feature for the Phase 1 neck design.
Compatibility with the Hybrid III Headform	The neck can be fixed to the Hybrid III headform	5	1	5	A simple nodding joint that similarly matches the Hybrid III neck design will allow compatibility of the Phase 1 with the Hybrid III heaform. This requirement was deemed more important than a realistic AO joint at this stage of the project.
Vertebra	Overall geometry, structures, and structural function are included in component design	5	5	3	The vertebra structures and geometries would be exactly replicated with a complex design; however, the simpler design is achieves greater manufacturability and was desired for the Phase 1 neck.
Intervertebral Disc	Overall geometry and structural function are included in component design	5	5	3	Despite an exact replication of the intervertebral disc with a complex composite design, the simpler homogenous design was desired for the Phase 1 neck.

Simple Mechanical Coupling	Simplistic mechanical coupling between vertebral levels is achieved	5	3	5	Simple mechanical coupling was deemed adequate for Phase 1. Based on the Phase 1 neck performance, more complex designs could be investigated if required.
Soft Tissue	Ligaments, tendons, and musculature are included in the design	5	5	3	Though an exact replication of soft tissues within the neck would be achieved with a complex composite design, the simpler homogenous design was desired for the Phase 1 neck.
Tension of Steel Cables	Stability of the neck model can be achieved	5	5	3	A permanent fixture at the inferior end of the neck would allow for the most repeatable neck design. However, the durability of the Phase 1 neck was unknown prior to quasi-static bending and impact testing, therefore a simple cable collar design was chosen to achieve tension in the steel cables. This would allow the Phase 1 neck to be easily disassembled and reassembled, should a component break.
Ease of Fabrication	The components must be easy to manufacture, and to assemble	5	0	5	The manufacturability and ease of assembly were paramount design features in Phase 1.
Total Score			150	**153**	

The AO and AA joints of the human cervical spine (described in Section 2.1) are very complex. Replicating these geometries would require an intricate vertebral design, which would reduce the overall manufacturability and ease of assembly in the Phase 1 neck. Additionally, the nodding joint allowed the Phase 1 neck to be rigidly fixed to the Hybrid III head in impact experiments. A rigid connection with the Hybrid III heaform was deemed more important than an exact replication of the AO and AA joints in the Phase 1 stage. The extra intervertebral disc at the superior end of the Phase 1 neck (Figure 3.2) offers some, but not all, of the required compliancy at this level.

The vertebra design included transverse process elements to achieve mechanical coupling between vertebral levels. It was decided these simplified transverse elements were sufficient for the Phase 1 neck design. Aluminum 6061-T6 was chosen for the vertebral bodies as this light, rigid material offered durability and rigidity, appropriately approximating the structural function of vertebral bodies in the human spine.

TangoBlack 3D printed rubber-like material was chosen for the vertebral bodies as it offers compliancy, durability, and can be easily printed into complex shapes. The intervertebral disc design in the Phase 1 neck is homogeneous, such that it is a single component disc. This design simplified the manufacture process. However, the human intervertebral disc is a composite structure, with gel-like properties at the core, more rigid annulus structure surrounding the core, and even more rigid and fibrous outer layer [5]. Although the more complex, composite disc design would closer match the intervertebral disc of the human described in Section 2.1, a simple, homogeneous rubber intervertebral disc was desired or Phase 1. The chosen rubber offers compliancy while remaining durable. Additionally, the angled design attained the lordotic curvature of the Phase 1 neck spinal column.

Mechanical coupling in the spinal column is a fundamental response characteristic in the human spine, therefore, this coupling must be achieved in the Phase 1 neck for the most realistic response. As this is a Phase 1 attempt to characterize a novel neck design, it was decided that a simple cable design was adequate.

A composite soft tissue design that included ligaments, tendons, and musculature would better represent the human neck, however, a homogenous design was considered sufficient for Phase 1. The chosen silicone rubber proved to be strong in shear, which increased the durability of the Phase 1 neck and was a desirable feature.

Clamping collars at the base of the neck offered a simple, non-permanent method for tensioning the steel cables. The overall durability of the Phase 1 neck was unknown at the design phase; therefore, the clamping collars could be easily removed to disassemble and reassemble the Phase 1 neck should a component require replacing.

The simple component designs scored higher than the more complex designs for the categories outlined in Table 3.5. Simplicity, manufacturability, and ease of assembly proved to be important deciding factors. While the more complex designs would better represent the human neck segment, simplistic designs were found to satisfy the physical design requirements outlined in Table 2.1. If, in the following three characterization chapters, the response of the simplified Phase 1 neck prototype did not meet the functional requirements outlined in Table 2.1, deficiencies in the Phase 1 physical designs may be investigated, and future directions may be suggested.

4 COMPARISON OF PHASE 1 MECHANICAL SURROGATE NECK PROTOTYPE TO PMHS NECK – QUASI-STATIC BENDING RESPONSE

The purpose of this chapter is to quantify how closely the flexural bending response of the Phase 1 neck matches published PMHS data, and to assess the degree of repeatability in the Phase 1 neck quasi-static bending tests. The evaluation of flexural compliance is completed by applying a series of moments in the sagittal plane that match the maximum magnitudes in the published PMHS data to the Phase 1 neck. Additionally, variation within the Phase 1 neck results are examined.

4.1 Background

Camacho et al. stated that any model of the human cervical spine in impact loading must include meaningful cervical stiffness data [9]. Better understanding of quasi-static bending of surrogate neck models allows for unambiguous conclusions concerning relative stiffness within these neck models when compared to PMHS data. The flexural stiffness characteristics of the neck segment include the angular displacement of the vertebra in a given bending direction with respect to applied moment.

In Chapter 4, multiple moments will be applied to the Phase 1 neck to simulate flexural bending in the sagittal plane. At this stage of the Phase 1 neck characterization, the overall neck flexibility results will be compared to previously published literature containing results of PMHS flexural limits in the sagittal plane [9]–[11]. Using PMHS data as a baseline, rather than live human

data, as well as analysis in a single bending plane, allows for an initial assessment of the overall flexural stiffness of the Phase 1 neck when compared to PMHS data. Based on these results, future methods such as analysis of rotations at individual vertebral levels, flexural assessment in multiple bending planes, and comparisons to live human data may be suggested. Additionally, the repeatability of the Phase 1 neck quasi-static bending results are analyzed.

4.2 Materials and Methods

4.2.1 Experimental Equipment

Quasi-static bending tests included a six-degree of freedom (DOF) robotic platform (Model R2000 Rotopad, Mikrolar Inc., Hampton, NH). While one end of the neck was held stationary, the opposing end was fastened to a six-axis load cell (MC3A Force/Torque Sensor, AMTI Inc., Watertown, MA) (Figure 4.1). A 3D printed displacement wedge was secured via double-sided tape between the Phase 1 neck and the rigid test frame to attain a horizontal starting position of the robotic platform. This maximized the possible ROM in the robotic platform, as the prescribed limits of rotation of the platform were ±15 degrees from horizontal. The applied moment and robotic platform angular displacement were collected and saved at 20 Hz using LabVIEW software (LabVIEW v8.5, National Instruments, Austin, TX). All quasi-static bending tests were video recorded at 60 frames per second for post-hoc vertebral body angular motion analysis (SONY HDR-XR160 Camcorder, Sony Electronics Inc., San Diego, CA).

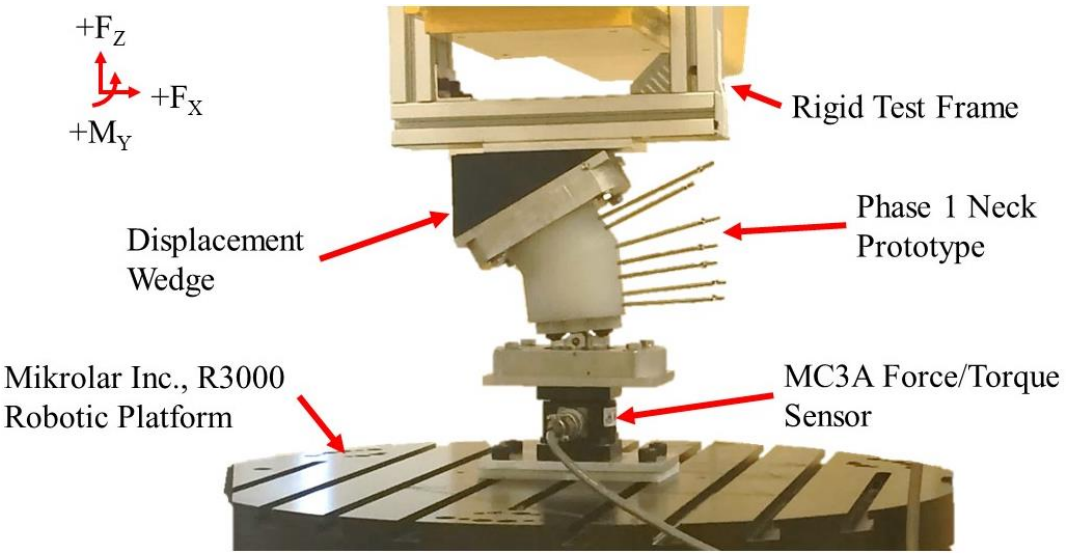

Figure 4.1: Annotated image of Phase 1 mechanical surrogate neck prototype mounted to Mikrolar 6 DOF robotic platform

Metal rods were threaded into the aluminum vertebral bodies and extended out of the silicone. Markers that resembled a Secchi disc were adhered to the metal rods, which allowed the Kinovea motion tracking software to track the translational displacement of the metal rods (Kinovea v.0.8.15). From this software, the translational displacements were collected and saved at 14 Hz. The resulting translational maker displacements were input into a MATLAB code for processing (MATLAB R2016b, MathWorks, Natick, MA).

4.2.2 Experimental Protocol

Multiple PMHS literature sources presenting quasi-static bending data were considered. Table 4.1 details the literature considered, and the reasoning for acceptance or rejection when forming the Phase 1 neck quasi-static bending experimental protocol. A total of three PMHS quasi-static bending data sets were accepted. The data presented by Camacho et al. [9], Nightingale et al. [10], and Wheeldon et al. [11] offered a range of testing methods and data collection that allowed for initial quasi-static bending characterization of the Phase 1 neck in the sagittal plane.

Table 4.1: PMHS literature considered to form the Phase 1 mechanical surrogate neck prototype quasi-static bending experimental protocol

Citation	Accepted or Rejected	Reasoning
Camacho et al. [9]	**Accepted**	This conference paper was accepted to develop the Phase 1 neck quasi-static bending test protocol because the authors generated sagittal plane flexibility data from whole cervical spine segments.
GESAC Inc. [39]	Rejected	This report generated sagittal plane flexibility data from only the AO-C2 joints rather than the whole cervical spine segment and was therefore rejected.
Ishii et al. [40]	Rejected	This journal paper generated flexibility data from only the C1 and C2 vertebral bodies and was therefore rejected.
Myers et al. [41]	Rejected	This conference paper generated torsional flexibility data. At this phase of the neck development, torsional flexibility was not considered.
Nelson and Cripton [42]	Rejected	This journal paper generated sagittal flexibility data for a surrogate neck model designed by the authors. At this phase of the neck development, only PMHS data was considered.
Nightingale et al. [10]	**Accepted**	This journal paper was accepted to develop the Phase 1 neck quasi-static bending test protocol because the authors generated sagittal plane flexibility data from cervical spine segments that could be summed into a whole cervical spine segment.
Wheeldon et al. [11]	**Accepted**	This journal paper was accepted to develop the Phase 1 neck quasi-static bending test protocol because the authors generated sagittal plane flexibility data from whole cervical spine segments.

The quasi-static bending test matrix is shown in Table 4.2. A total of 12 tests were conducted, with applied moments in the sagittal plane ranging ±1.5 Nm and ±2.0 Nm, encompassing moments within the flexion/extension elastic range of a human cervical spine specified in previous work. The objectives of these studies were to observe flexibility corridors of PMHS cervical spine segments [9]–[11]. The load protocol was moment controlled, with the center of rotation (COR) positioned at the mid-height of the prototype neck.

Table 4.2: Distribution of quasi-static bending tests in sagittal plane of Phase 1 mechanical surrogate neck

Stationary End	Applied Moment (Nm)		Total
	±1.5	±2.0	
Inferior	3	3	6
Superior	3	3	6
All	6	6	**12**

Prior to each test, the robotic platform was automatically positioned such that 0 Nm moments were experienced in the x-, y-, and z-directions. The robotic platform rotated at 0.1 to 0.3 deg/sec until the maximum desired moments were achieved. A single test included three repeated moment cycles of the prototype neck. A sample of the moment time history can be found in Figure 4.2. The positive moments resulted in flexion bending and the negative moments resulting in extension bending of the Phase 1 neck.

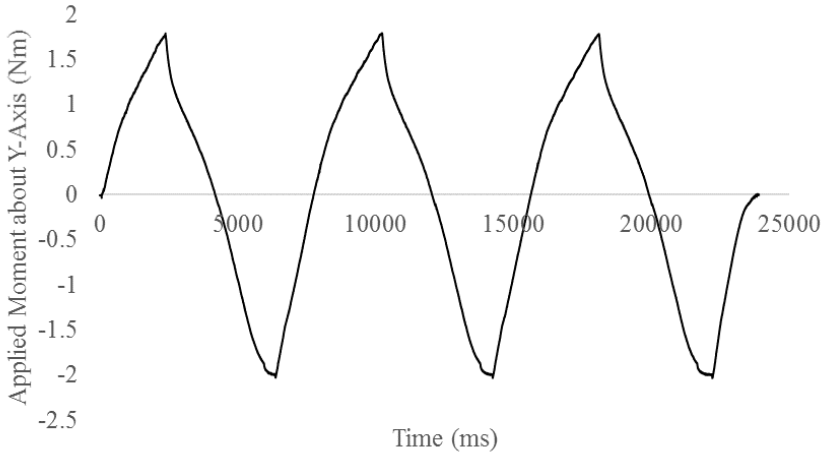

Figure 4.2: Sample ±2.0 Nm applied moment time history of superiorly fixated Phase 1 mechanical surrogate neck prototype from C1-C7

4.2.3 Application of Motion Tracking Software

Cinematography and motion tracking techniques are common practices used to analyze kinematic parameters in biomechanic laboratories. Using rigid body theory, it was assumed the angular displacement of the marker was the same as the vertebral body in which the metal rod was threaded into. The determination of angular displacement may be broken into three steps:

1. Perform quasi-static bending test.
2. Post-hoc analysis of quasi-static bending videos.
3. Calculate angular displacement.

In motion tracking software, a two-dimensional (2D) coordinate system can be used to describe the position of a given point. The coordinates are dictated by the pixel size of the collected videos. A scaling factor calibration converts the pixel coordinates to known physical coordinates of a Cartesian reference frame. In the Kinovea software, the origin is chosen to be the starting point of the object to be tracked. The scaling factor was chosen to be the 7" plate between the displacement wedge and the end of the neck that was held stationary, as seen in Figure 4.3. This plate was chosen as the scaling factor because it was large enough in the frame to reduce errors in calibration.

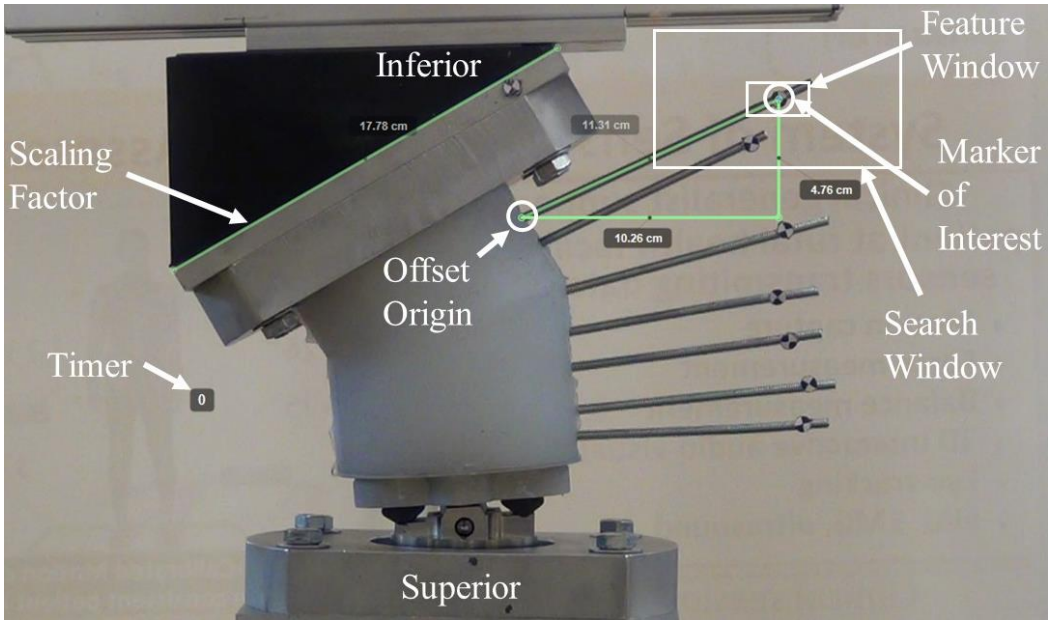

Figure 4.3: Annotated Kinovea user interface of inferiorly fixated Phase 1 mechanical surrogate neck prototype

Figure 4.3 shows an example of the first frame of an inferiorly fixed, Phase 1 neck with the C7 marker to be tracked in the Kinovea software. The inner rectangle surrounding the C7 marker is called the Feature Window, which defines the feature of interest. The larger rectangle surrounding the Feature Window is the Search Window, in which the Kinovea software searches for the image of the marker. The motion tracking was a semi-automatic process, such that the Kinovea software compared the position of the marker between two consecutive frames, relative to the starting point. If, at any point, the automatic tracking feature did not track the correct point, the motion tracking was completed manually. This same process was repeated for all seven markers of each quasi-static bending test.

From the Kinovea motion tracking software, the x- and y-coordinates of each marker were exported to separate Microsoft Excel Sheets with a scale relative to the chosen scaling factor. The coordinates of each marker were offset such that the origin was shifted to the silicone-metal rod interface (depicted in above in Figure 4.3). Due to the slow movements and the application of moments about the y-axis of the Phase 1 neck, it was assumed the motions of the silicone-metal rod interface were negligible.

4.2.4 Quasi-static bending MATLAB Processing Code

The position of the Feature Window is limited to the size of the pixel. If the center of the feature of interest falls between two pixels, the tracking software must choose a pixel at a location to the left, right, above, or below of the feature of interest. This skipping to and from the center of feature of interest introduces a low frequency noise component in the displacement data. To remove the noise component in the tracked data, the x- and y-coordinates of the seven markers were first filtered with a 2^{nd} order low pass Butterworth filter at a cutoff frequency of 0.01 Hz in the MATLAB software. A Butterworth filter was chosen over other digital filter options, such as Elliptic or Chebyshev, because this filter type has a magnitude response that is maximally flat in the passband and is a monotonic filter. Additionally, Butterworth filters are commonly used in human surrogate instrumentation standards, such as SAE Standard J211 [43].

Figure 4.4 compares the raw and filtered C1 marker data of a superiorly fixed Phase 1 neck, with a maximum applied moment of ±2.0 Nm. As can be seen in Figure 4.4a), the output from tracking software resembles a stepwise function where the Feature Window moved between pixels.

The path of the C1 marker was considerably smoother after the filtering techniques were applied, as can be seen in Figure 4.4b).

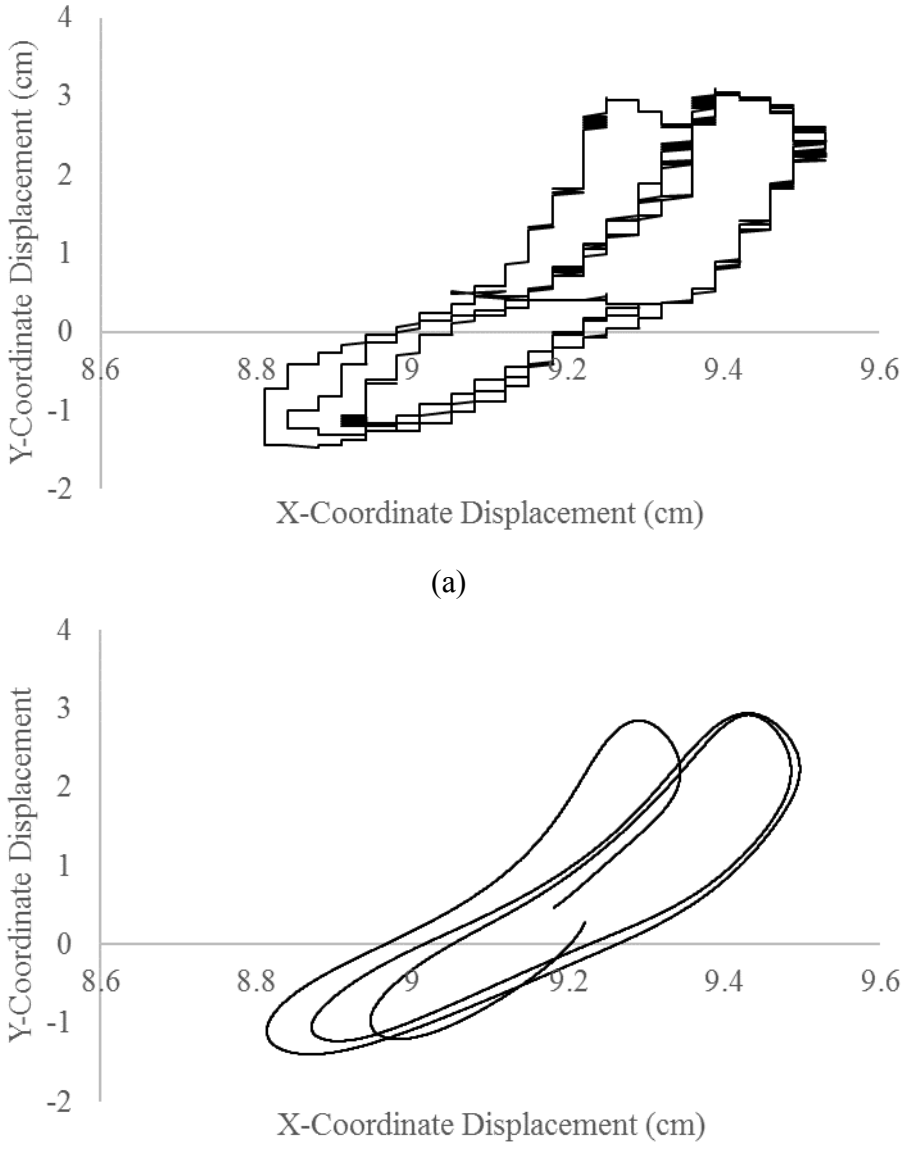

Figure 4.4: C1 marker displacement in superiorly fixed Phase 1 neck with an applied moment of ±2.0 Nm, (a) raw marker displacement, (b) filtered marker displacement

Once the filtering techniques were completed, the angular displacements of the metal rods were calculated. The following calculations will allow for angular displacements of individual vertebral bodies to be observed in future iterations of the Phase 1 neck model. However, for the

purpose of this study, the overall angular displacements of all vertebral bodies combined were compared to cadaver literature.

The initial angle of the metal rods with respect to the horizontal were calculated using Equation 4.1, where $C_{n,i}$ represents the initial x and y position of the marker of interest relative to the COR as seen in Figure 4.5. The angle with respect to the horizontal of the remaining frames, $\Delta\Theta_n$, was calculated using Equation 4.2, where $C_{n,d}$ represents the change in x and y positions of the marker of interest relative to the silicone-metal rod interface. Finally, the angular displacement of the metal rod over time, Θ_n, was calculated using Equation 4.3, which is the difference of Equation 4.1 and 4.2.

$$\theta_{n,i} = \tan^{-1}\left(\frac{C_{n,i,y}}{C_{n,i,x}}\right) \tag{4.1}$$

$$\Delta\theta_n = \tan^{-1}\left(\frac{C_{n,d,y}}{C_{n,d,x}}\right) \tag{4.2}$$

$$\theta_n = \Delta\theta_n - \theta_{n,i} \tag{4.3}$$

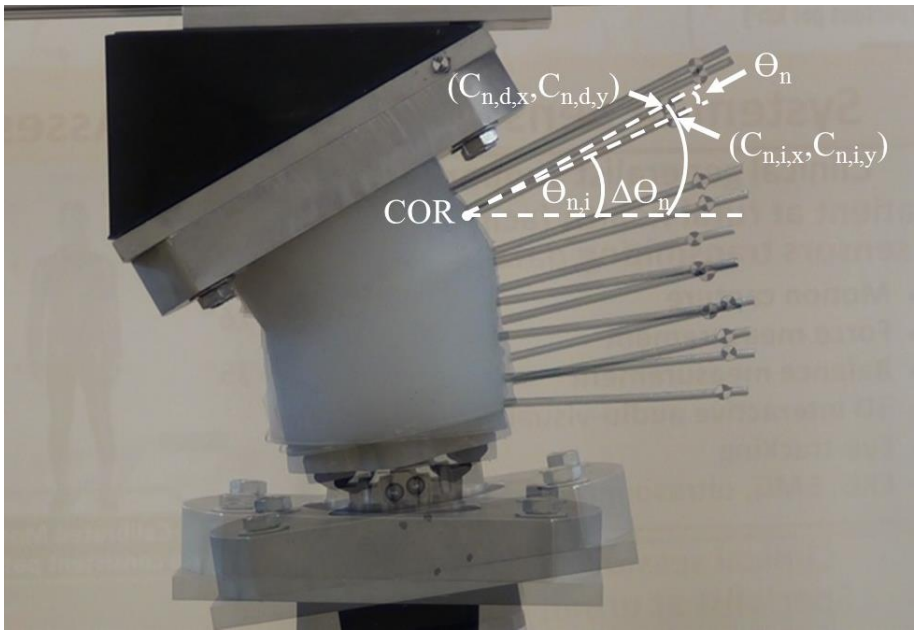

Figure 4.5: Annotated overlay of starting position and maximum flexion position of first moment cycle of the Phase 1 mechanical surrogate neck prototype

The angular displacement between two consecutive vertebral bodies, as seen in Figure 4.6, was calculated using Equation 4.4, where Θ_{n-1} is the change of angle over time of the metal rod inferior to Θ_n. All angular displacements between vertebral bodies were then summed using

Equation 4.5 to determine the overall angular displacement, Θ_T, of the Phase 1 neck in quasi-static bending (Figure 4.7).

$$\theta_{n,n-1} = \theta_n - \theta_{n-1} \tag{4.4}$$

$$\theta_T = \sum_{1}^{7} \theta_{n,n-1} \tag{4.5}$$

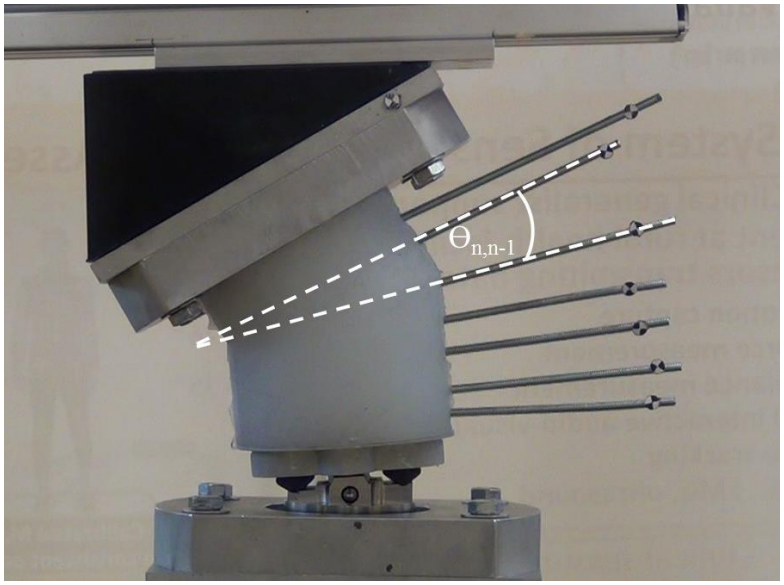

Figure 4.6: Annotated image of angular displacement between two consecutive vertebral bodies

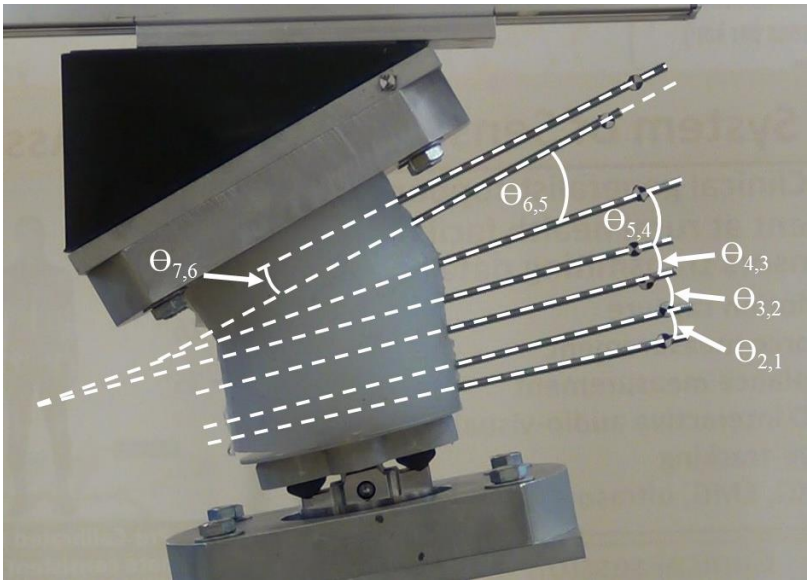

Figure 4.7: Annotated image of summed angular displacement from C1-C7

The raw moment data was filtered with a 2nd order low pass Butterworth filter at a cutoff frequency of 0.125 Hz, as a low frequency noise component from the load cell was present. The filtered moment data was then resampled to match the slower acquisition rate of the Kinovea tracking software. The sum of inter-vertebral angular displacements from C1-C7 were then plotted against the applied moment and compared to literature.

4.2.5 Comparison to PMHS Literature

To compare the overall flexion/extension ROM from the Phase 1 neck to the data presented in the chosen literature by Camacho et al. [9], Nightingale et al. [10], and Wheeldon et al. [11], the presented angular displacements and variances in these literature sources were summed and contrasted to the Phase 1 neck results. At this Phase 1 characterization stage of the Phase 1 neck, it was desired to determine whether the overall neck flexibility was within the reported corridors in PMHS literature. Total vertebral rotations, as opposed to rotation at each vertebral level, were quantified. The percent difference in flexion or extension angle was calculated using Equation 4.6.

$$\frac{Cadaver\ Peak - Phase\ 1\ Peak}{Cadaver\ Peak} \times 100\% \tag{4.6}$$

4.2.6 Variability Analysis

To determine the variation in the collected quasi-static bending data of the Phase 1 neck, the CV for each test group was calculated (Equation 4.7). The CV is a ratio that compares the standard deviation, σ, to the mean, μ, of the collected data between three repeated tests. Again, since this is an initial attempt to characterize the Phase 1 neck, the average peak flexion and extension angles and standard deviations at these points were used to calculate the CV.

$$CV = \frac{\sigma}{\mu} \times 100\% \tag{4.7}$$

4.3 Results

A summary of flexion and extension angular displacements of the Phase 1 neck summed from C1-C7 are reported in Table 4.4. The percent differences between angular displacements of the Phase 1 neck compared to PMHS literature are presented in Table 4.5. The CV values for the Phase

1 neck data are given in Table 4.6. As this is an initial characterization of the Phase 1 neck, the results are reported as peak angular displacement values of flexion and extension inducing applied moments.

4.3.1 Experimental Observations

The load cell recorded forces and moments in the x-, y-, and z-directions. The intention was to apply pure moments about the y-axis, however, forces in the y-direction and moments about the x- and z-directions were still detected. Table 4.3 outlines maximum loads and moments for all 12 tests conducted. The maximum magnitude of force in the y-direction, F_y, is 2.59 N, the maximum moment about the x-axis, M_x, is 0.59 Nm, and the maximum moment about the z-axis, M_z, is 0.07 Nm. These values correspond to less than 30% of the variables of interest, therefore these loads were considered negligible. Additionally, due to the ROM limitations of the rotating robotic platform, the maximum applied moment fell below the intended ±2.0 Nm in all superiorly fixed Phase 1 neck tests (labeled Base_2.0_Test# in Table 4.3), and in one of the inferiorly fixed Phase 1 neck tests (labeled Top_2.0_Test# in Table 4.3).

Table 4.3: Maximum loads and moments recorded by the MC3A Force/Torque Sensor

Test ID	Fx (N)	Fy (N)	Fz (N)	Mx (Nm)	My (Nm)	Mz (Nm)
Base_1.5_Test1	6.66	0.70	22.31	0.36	1.50	0.04
Base_1.5_Test2	6.56	0.79	21.95	0.35	1.50	0.04
Base_1.5_Test3	6.60	0.80	22.76	0.35	1.50	0.04
Base_2.0_Test1	8.46	1.06	43.48	0.56	**1.80**	**0.07**
Base_2.0_Test2	8.51	1.15	39.46	0.58	**1.80**	**0.07**
Base_2.0_Test3	8.56	1.20	39.28	**0.59**	**1.80**	**0.07**
Top_1.5_Test1	9.61	**2.59**	24.72	0.30	1.51	0.03
Top_1.5_Test2	10.29	2.30	24.42	0.32	1.51	0.04
Top_1.5_Test3	10.33	2.28	25.13	0.32	1.51	0.04
Top_2.0_Test1	11.59	2.07	35.11	0.23	2.00	0.05
Top_2.0_Test2	13.21	2.18	33.54	0.30	**1.85**	0.05
Top_2.0_Test3	13.36	1.89	33.42	0.27	2.00	0.05

Examples of maximum extension, neutral, and maximum flexion rotations of an inferiorly fixated Phase 1 neck at an applied moment of ±2.0 Nm are shown in Figure 4.8. Peak flexion and extension angles of the 12 quasi-static bending tests can be found in Table 4.4. Over the 12 trials, the maximum summation of the angular displacement in flexion is 13.58 degrees and in extension is -9.88 degrees.

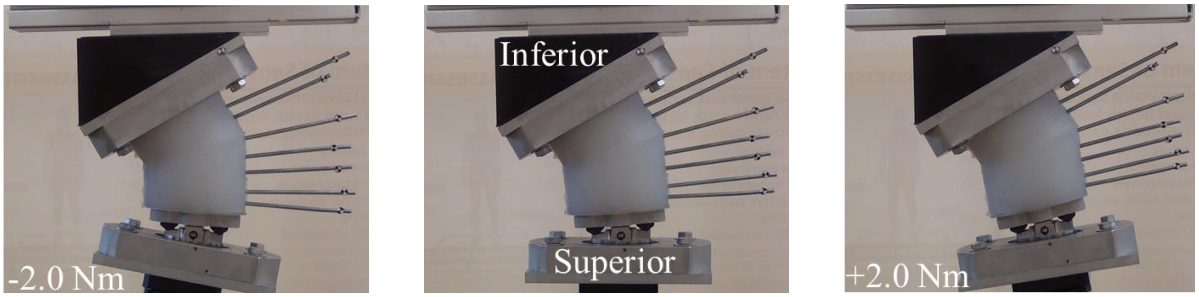

(a) (b) (c)

Figure 4.8: Sample images from the recorded experimental videos of maximum extension, neutral, and flexion positions of an inferiorly fixed Phase 1 neck with ±2.0 Nm applied moment

Table 4.4: Peak flexion and extension angles of the 12 quasi-static bending tests

Test ID	Max. Flexion Angle (deg)	Max. Extension Angle (deg)
Base_1.5_Test1	10.85	-5.86
Base_1.5_Test2	9.29	-6.30
Base_1.5_Test3	9.84	-6.10
Base_2.0_Test1	**13.58**	-7.39
Base_2.0_Test2	13.53	-7.33
Base_2.0_Test3	13.69	-7.36
Top_1.5_Test1	8.06	-6.98
Top_1.5_Test2	7.19	-5.16
Top_1.5_Test3	8.17	-5.76
Top_2.0_Test1	12.01	-9.48
Top_2.0_Test2	11.57	**-9.88**
Top_2.0_Test3	13.17	-9.58

4.3.2 Comparison to PMHS Literature

Figure 4.9 presents sample inferiorly and superiorly loaded quasi-static flexibility comparisons of the Phase 1 neck at an applied moment of ±2.0 Nm to averaged PMHS data presented in literature [9]–[11]. A sample, rather than an average, of the Phase 1 neck data set is chosen to convey how the rotations change over three flexion-extension cycles. The arrows indicate which peak data points were used for the flexion/extension comparisons.

Table 4.5 summarizes the percent differences between the Phase 1 neck peak flexion and extension rotations to data presented by Camacho et al. [9], Nightingale et al. [10], and Wheeldon et al. [11]. Over the 12 trials, the maximum percent difference in overall peak flexion angle and peak extension angle between the Phase 1 neck to data published by Camacho et al. is 80.24% and

84.95%, data published by Nightingale et al. is 76.95% and 81.72%, and data published by Wheeldon et al. is 83.74% and 78.56%, respectively.

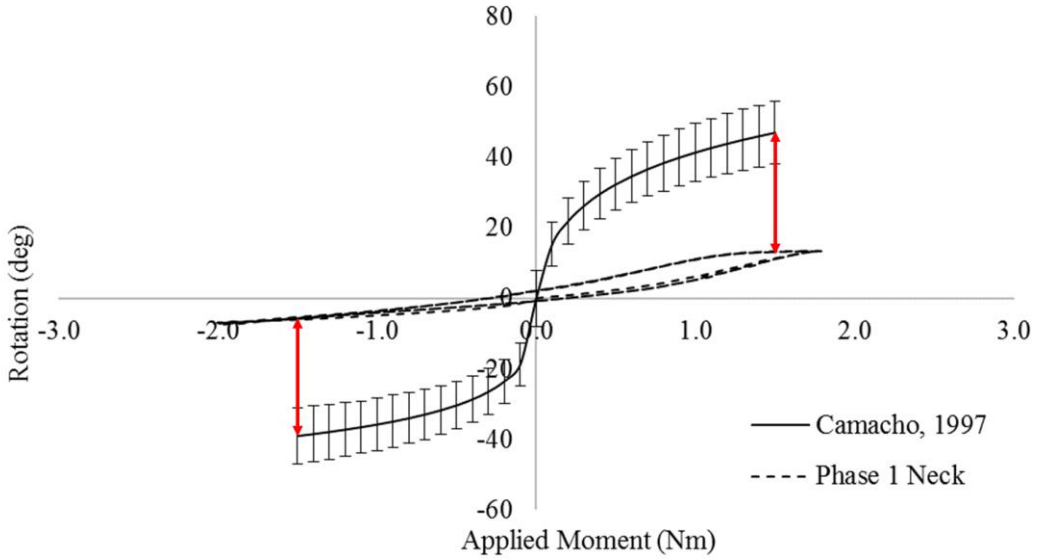

(a)

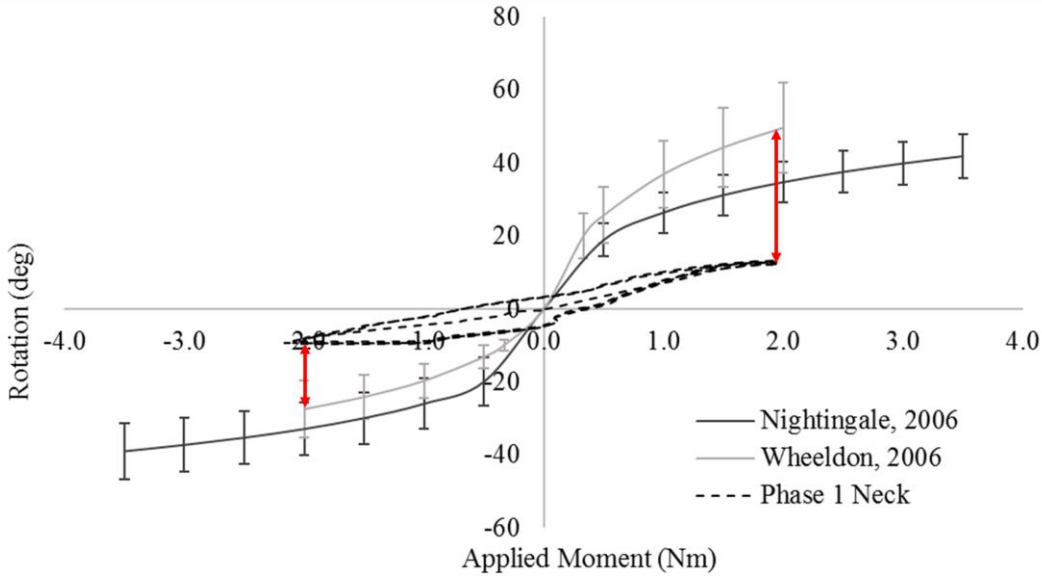

(b)

Figure 4.9: Summated angular displacements from C1-C7; (a) superior end of Phase 1 mechanical surrogate neck prototype held stationary compared to adapted data presented by Camacho et al. [9], (b) inferior end of Phase 1 mechanical surrogate neck prototype held stationary compared to adapted data presented by Nightingale et al. [10] and Wheeldon et al. [11]

Table 4.5: Percent differences in peak flexion and extension values between Phase 1 mechanical surrogate neck prototype to published PMHS data

Test ID	% Difference of Phase 1 neck to Camacho		% Difference of Phase 1 neck to Nightingale		% Difference of Phase 1 neck to Wheeldon	
	Flex.	Ext.	Flex.	Ext.	Flex.	Ext.
Base_1.5_Test1	76.88	**84.95**	-	-	-	-
Base_1.5_Test2	**80.24**	83.84	-	-	-	-
Base_1.5_Test3	79.08	84.34	-	-	-	-
Base_2.0_Test1	71.13	81.04	-	-	-	-
Base_2.0_Test2	71.23	81.18	-	-	-	-
Base_2.0_Test3	70.88	81.11	-	-	-	-
Top_1.5_Test1	-	-	74.17	76.65	81.78	71.01
Top_1.5_Test2	-	-	**76.95**	**81.72**	**83.74**	**78.56**
Top_1.5_Test3	-	-	73.81	80.73	81.53	76.08
Top_2.0_Test1	-	-	72.86	60.62	61.52	68.27
Top_2.0_Test2	-	-	62.93	66.92	73.85	58.94
Top_2.0_Test3	-	-	57.81	67.94	70.24	60.20

4.3.3 Variability Analysis

Figure 4.10 presents a sample average (solid line) and one standard deviation (greyed areas) of a superiorly fixed Phase 1 neck at applied moments ranging ±2.0 Nm. This test group is labeled Base_2.0 in Table 4.6, which summarizes the averaged overall peak flexion angular displacement, μ_f, the standard deviation at peak flexion, σ_f, averaged overall peak extension angular displacement, μ_e, and the standard deviation at peak extension, σ_f. The maximum CV in flexion is 44.29% and in extension is 70.70%. It is important to note that the camera shifted in one of the inferiorly fixated, ±2.0 Nm tests (labeled Top_2.0 in Table 4.6), therefore this test was removed from the CV analysis as test is to be considered erroneous. The resulting average peak flexion and extension angles and standard deviations of the Top_2.0 group was estimated using the remaining two data sets.

It was decided to remove, instead of replacing, the erroneous data because the peak flexion and extension angles and the respective CV values were gleaned from each cycle of the tests. That is, a total of nine data points were used to calculate the peak average and standard deviation of the flexion and extension angular displacements. Therefore, by removing the erroneous data set, the CV of the test group labeled Top_2.0 was calculated using six peak angular displacement data

points. The six data points still offered meaningful average and standard deviation values for this exploratory study.

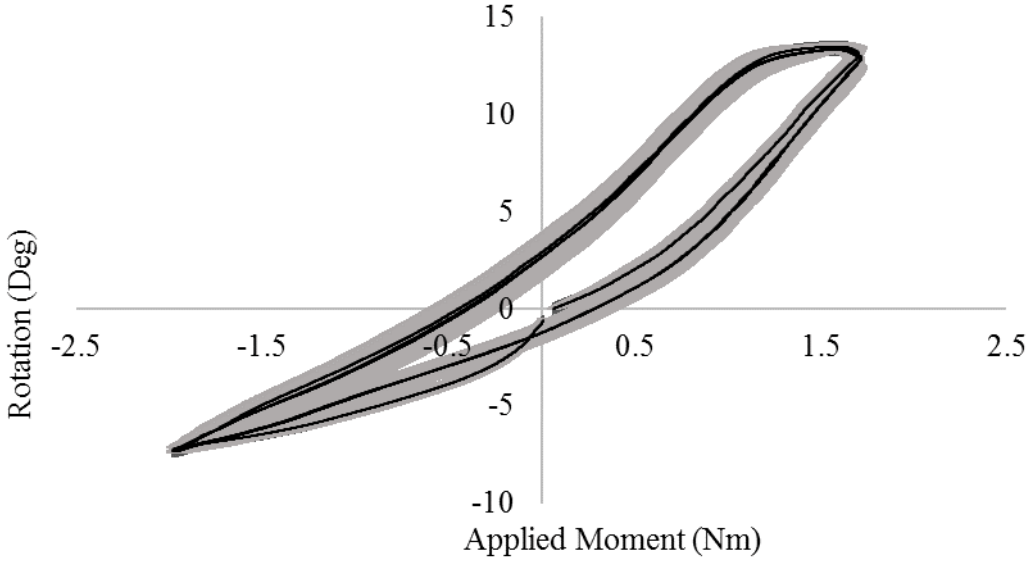

Figure 4.10: Sample averaged summation of angular displacement of superiorly fixed Phase 1 mechanical surrogate neck prototype from C1-C7 versus ±2.0 Nm moment
Note: Greyed areas are ±1 SD of three averaged tests (solid)

Table 4.6: Coefficient of variation analysis of Phase 1 mechanical surrogate neck prototype quasi-static bending tests

Test ID	μ_f	σ_f	CV_f (%)	μ_e	σ_e	CV_e (%)
Base_1.5	8.68	3.84	**44.29**	-5.03	3.56	**70.90**
Base_2.0	12.93	0.71	5.46	-7.25	0.15	2.04
Top_1.5	7.21	1.27	17.66	-5.21	0.80	15.31
Top_2.0	9.79	2.73	27.93	-5.96	3.27	54.95

4.4 Discussion

This method of quasi-static testing is an initial observation of the ROM of the Phase 1 neck. By comparing the collected peak values to published PMHS data, one is able to quantify how much more stiff the Phase 1 neck is compared to the human cadaver, and use this information to further develop the Phase 1 neck prototype.

The data presented by Camacho et al. [9], Nightingale et al. [10], and Wheeldon et al. [11] offered a range of testing methods and data collection that offered an initial characterization of the Phase 1 neck in quasi-static bending when compared to PMHS data. The published data sets

encompassed moments and angular displacements within the elastic flexion/extension ROM of a human cervical spine. Additionally, the presented data could be summed to compare the peak angular displacement of the whole cervical spine segment. At this Phase 1 stage, it was desired to determine whether the overall neck flexibility was within the reported corridors in PMHS literature, therefore, total vertebral rotations were quantified as opposed to rotation at each vertebral level. In future iterations of the Phase 1 neck, once the total rotation of the surrogate neck model is optimized to fall within a realistic range of the human, next steps to analyze whether angular rotations at each vertebral level are realistic can be investigated.

Pure flexion and extension moment cycles were repeated three times in a single test. This was done to observe how much or how little the rotations change over the moment cycles. Each test type (i.e. inferior fixation and superior fixation, ±1.5 Nm and ±2.0 Nm) was applied three times, offering meaningful average and standard deviation calculations of peak values for the initial CV analysis.

In the Phase 1 analysis, the maximum CV of all peak flexion angular displacement was approximately 44% and peak extension angular displacement was approximately 71%, as shown in Table 4.6. Although the CV of the quasi-static bending data exceeds the 20% target to achieve repeatability, data adapted from the chosen PMHS literature shows the maximum CV in peak flexion angular displacement was approximately 40% and in peak extension angular displacement was approximately 30%, respectively [9]–[11]. This shows that the CV of the Phase 1 neck is comparable to the CV of PMHS data in quasi-static bending. Coupled with the fact the Phase 1 neck is a reusable component, these findings could be interpreted to convey the Phase 1 neck is a first step towards a reusable model to be used in a controlled laboratory setting that could mimic PMHS response.

4.4.1 PMHS Comparisons

The summation of vertebral rotations from the Phase 1 neck are smaller, by approximately 80%, than those reported in PMHS literature [9]–[11]. One contributor to this could be the fact the Phase 1 neck has no neutral zone, where the stiffness of the human spine is very low and considerable vertebral rotations occur at small-scale applied moments (Figure 4.9a, between 0 Nm and 0.25 Nm). This is a phenomena that has been observed for the osteoligamentous cervical spine [44].

The quasi-static bending experimental method was limited to published PMHS data in the sagittal plane. This is because minimal PMHS data exists in the remaining two anatomic planes. It is likely that the cervical spine segment of a PMHS with the musculature removed behaves differently than the quasi-static bending of a living human. Even if refined to match the behavior of a PMHS neck, the Phase 1 neck model may not match the flexural stiffness of a living human. A possible solution could be employment of 3D magnetic resonance imaging (MRI) scans of each vertebral body motion such as the methods presented by Ishii et al. [40]. This method would give the best representation of a realistic ROM of the living human to characterize the Phase 1 neck.

4.4.2 Modified Human PMHS Comparisons

To observe the affects of the neutral zone in the human spine, the neutral zone was manually removed from the PMHS data. The percent differences in peak flexion and extension angles were then recalculated. Figure 4.11 presents sample inferiorly and superiorly loaded quasi-static flexibility comparisons of the Phase 1 neck at an applied moment of ±2.0 Nm to averaged PMHS data presented in literature [9]–[11] with the neutral zones removed.

Table 4.7 summarizes the percent differences between the Phase 1 neck peak flexion and extension rotations to modified PMHS data presented by Camacho et al. [9], Nightingale et al. [10], and Wheeldon et al. [11]. Over the 12 trials, the maximum percent difference in peak flexion angle and peak extension angle between the Phase 1 neck to data published by Camacho et al. is 63.01% and 62.24%, data published by Nightingale et al. is 35.42% and 44.44%, and data published by Wheeldon et al. is 69.99% and 63.93%, respectively.

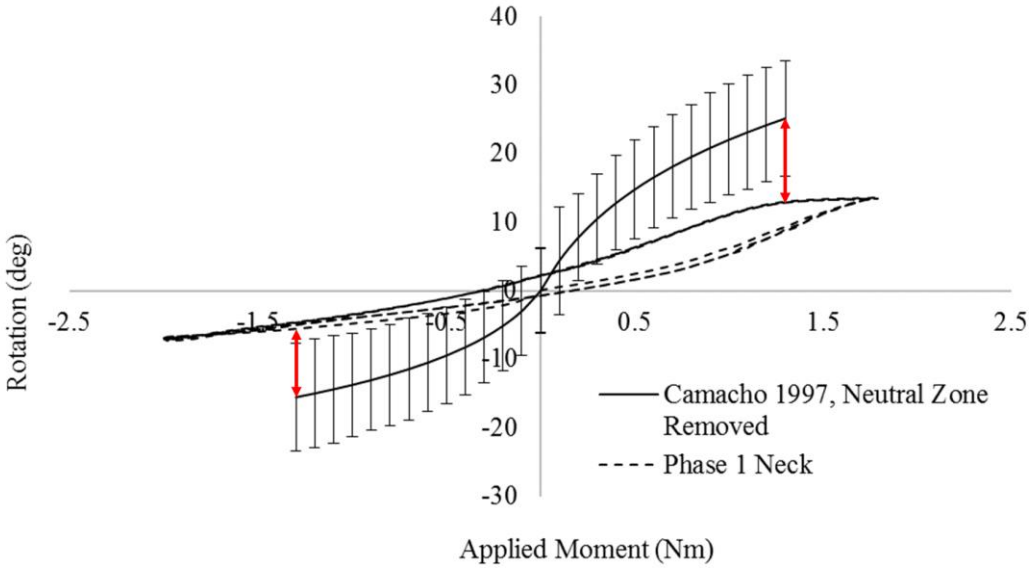

(a)

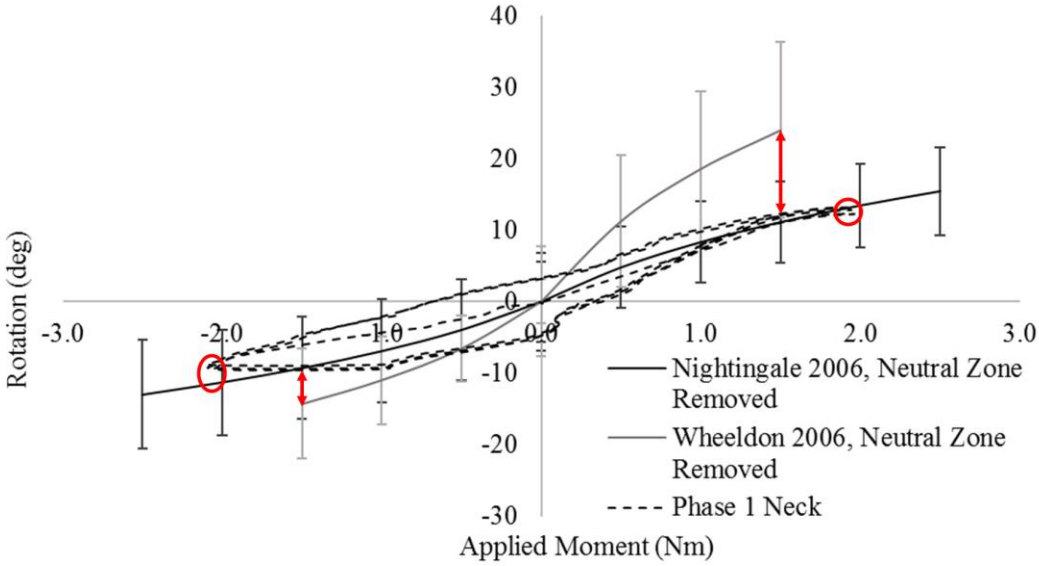

(b)

Figure 4.11: Summated angular displacements from C1-C7; (a) superior end of Phase 1 mechanical surrogate neck prototype held stationary compared to modified, adapted data presented by Camacho et al. [9], (b) inferior end of Phase 1 mechanical surrogate neck prototype held stationary compared to modified, adapted data presented by Nightingale et al. [10] and Wheeldon et al. [11]

Table 4.7: Percent differences in peak flexion and extension values between Phase 1 mechanical surrogate neck prototype to modified published PMHS data

Test ID	% Difference of Phase 1 neck to Camacho		% Difference of Phase 1 neck to Nightingale		% Difference of Phase 1 neck to Wheeldon	
	Flex.	Ext.	Flex.	Ext.	Flex.	Ext.
Base_1.5_Test1	56.71	**62.24**	-	-	-	-
Base_1.5_Test2	**63.01**	59.46	-	-	-	-
Base_1.5_Test3	60.85	60.72	-	-	-	-
Base_2.0_Test1	45.96	52.43	-	-	-	-
Base_2.0_Test2	46.14	52.79	-	-	-	-
Base_2.0_Test3	45.49	52.62	-	-	-	-
Top_1.5_Test1	-	-	27.63	24.90	66.37	51.25
Top_1.5_Test2	-	-	**35.42**	**44.44**	**69.99**	**63.93**
Top_1.5_Test3	-	-	26.63	38.03	65.91	59.77
Top_2.0_Test1	-	-	22.27	27.08	49.90	33.77
Top_2.0_Test2	-	-	25.12	23.96	51.73	30.94
Top_2.0_Test3	-	-	14.77	33.06	45.07	33.06

By removing the neutral zone in the PMHS data, the percent difference between Phase 1 neck peak flexion and extension values were reduced by approximately 20% when compared to the modified Camacho data, approximately 40% when compared to the modified Nightingale data, and approximately 10% when compared to the modified Wheeldon data. These results suggest that by including components within the Phase 1 neck model to simulate the neutral zone of the human spine, the Phase 1 neck would closer match human flexibility results in the sagittal plane. In future iterations of the Phase 1 neck, lateral bending should also be investigated to determine if these results are true in the coronal plane.

4.4.3 Limitations

There are essential limitations in the quasi-static bending data presented in this thesis that are important to note. One limitation of the quasi-static bending setup of the Phase 1 neck is that the rotating end of the neck occurred at the same point where the moments were measured. The data published by Camacho et al. included superior fixation of the inverted halo-T2 spine segment to a load cell, and an eccentric force couple loaded the inferior end to observe the individual inter-vertebral angular displacements [9]. Nightingale et al. sectioned cervical spine segments from O-C3, C4-C5, and C6-C7 to observe flexural stiffness differences in the upper, middle, and lower cervical spine [10]. The inferior end of the spinal segments were rigidly fixed to a load cell, and

pneumatic pistons loaded the superior end of the spinal segments to generate a force-couple [45]. Wheeldon et al. observed the individual angular displacements of C2-T1 spinal columns by applying pure moments to the superior end while rigidly fixing the inferior end to a load cell [11]. Intuitively, the vertebral body closest to the rotating equipment will experience the largest angular displacement. Contrarily, the vertebral body farthest away from the rotating equipment will experience the smallest angular displacement. These differences in experimental setups and the resulting vertebral angular displacements may be considered too great to make a reasonable comparison of peak values.

One solution to ensure an exact comparison of flexural stiffness between PMHS cervical spine segment and the Phase 1 neck would be to undertake in-house or partnered lab PMHS cervical spine segment quasi-static bending tests to a greater number of test cases than presented in this chapter. Alternatively, employment quasi-static bending methods presented by Ishii et al. [40], as described in Section 4.4.1, would allow comparisons of flexural stiffness in the living human to the Phase 1 neck.

In addition, the musculature of the neck segments was removed in all three PMHS data sets. In many PMHS quasi-static bending tests, the musculature of the human neck is removed so the 3D position of each vertebra can be recorded. For all Phase 1 neck quasi-static bending tests, the simulated musculature remained intact, and only the 2D displacement of the vertebral bodies were recorded. Since the silicone rubber was held intact, this material could have influenced the rotations of the vertebral bodies within the Phase 1 neck. However, at this stage of the Phase 1 neck development, it was desired to complete the characterization process between the two experimental protocol (quasi-static bending and impact) without changing the neck model. In future iterations of the Phase 1 neck, employment of stereo photogrammetry to ascertain vertebral motions in a manner that more closely matches previous efforts will be required [9]–[11].

In the proposed experimental protocol, the robotic platform was moment controlled and fixed the COR of the robotic platform at the mid-height of the Phase 1 neck, with no post-hoc force or moment translation to the vertebral bodies. The fact forces in the x- and z-directions were recorded suggests that the COR was not stationary, as it was originally assumed. The forces in the x- and z-directions that were offset from the COR would also result in moments about the y-axis, which would contribute to the overall M_y magnitude. The deviation of the COR in the x- and z-directions may be a contributing factor to the abnormal saw-tooth shape of the moment time history plot

presented in Figure 4.2. Furthermore, this shifting COR could be a contributing factor to the CV values exceeding 40% presented in Table 4.6.

The angular displacement calculations of the vertebral bodies assumed an instantaneous center of rotation (ICR) as a stationary extension of the metal rods relative to the horizontal. This simplified the test protocol and demonstrated an initial analysis of the ROM of the Phase 1 neck in the sagittal plane. However, in the human spine, the ICR for each vertebral body is located at the superior aspect of the vertebral body inferior to the body of interest [46] (Figure 4.12). Additionally, the ICR translates when changing from flexion to extension bending. If the applied moments were translated to the ICR of each vertebral body, as well as translation of the COR of the robotic platform to be located at the over ICR of the surrogate neck prototype, the quasi-static experimental protocol could more thoroughly characterize future iterations of the Phase 1 neck ROM.

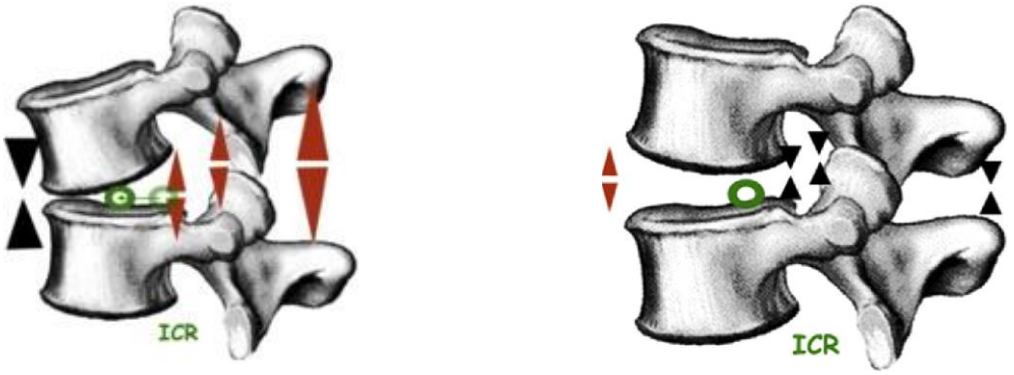

(a) (b)

Figure 4.12: Schematic of ICR of vertebral body in human cervical spine, (a) in flexion, (b) in extension
Reprinted from European Journal of Radiology, Vol. 84, G. Bonaldi, C. Brembilla, A. Cianfoni, Minimally-invasive posterior lumbar stabilization for degenerative low back pain and sciatica. A review, Pages 789-798, Copyright 2015, with permission from Elsevier.

Additionally, as a safety protocol of the equipment used, the angular ROM of the robotic platform was limited to ±15 degrees from horizontal. In some ±2.0 Nm tests, the peak recorded moment was less than 2.0 Nm due to the limited motion of the platform. Accordingly, the peak flexion and extension angular displacements of the Phase 1 neck of the 2.0 Nm tests are likely greater than what was recorded. Alternative equipment options that closer match the experimental protocol found in the selected PMHS literature described above could mitigate this limitation.

The applied moment in simulated cervical spine flexibility and injury must be an accurate representation of the biological viscoelastic response. Human spinal segments can be deformed at rates between 0.5-5.0 deg/sec with negligible viscoelastic effects, however, rates slower than 0.5 deg/sec may introduce effects of creep [47]. A study conducted by Busscher et al. found that creep effects did result in an increase in ROM by an average of 36%, meaning the flexibility is also increased after 30 minutes of 2 Nm creep loading [48]. However, a study by Meij et al. observed canine cadaver spinal segments cyclically loaded 5 times up to a maximum of ±3 Nm at a loading rate of 0.3 deg/sec, and creep effects were neglected [49]. Creep for silicone rubber is so small in magnitude that it was assumed negligible, therefore, the loading rate of 0.1-0.3 deg/sec of the prototype neck model would not cause significant creep or error in the cycled results. However, to keep the results as realistic as possible, the angular velocity of the robotic platform should be increased to 0.5 deg/sec in future quasi-static bending experiments.

The duration of repeated tests were not identical, which resulted in shifts between peak flexion and extension inducing moments. When calculating the average and standard deviation of peak flexion and extension angular displacements in the Phase 1 neck, the shifts in peak values had to be manually aligned. These manual alignment methods could be contributors of the 40% and 70% CV values presented in Table 4.6. Ensuring the rotations of the robotic platform are consistent between all quasi-static bending tests (i.e. 0.5 deg/sec) would reduce the manual alignments in the data, and therefore reduce the human error introduced in the experiments.

Finally, some of the quasi-static bending tests caused slippage of the clamping collars that dictated the tension in the steel cables. Clamping collars manufactured at the University of Alberta Machine Shop and the purchased two-piece shaft collars from McMaster Carr (6436K500 Two-Piece Shaft Collars, McMaster-Carr, Cleveland, OH) were tested in the quasi-static bending experimental protocol. The McMaster Carr shaft collars proved to perform better between the two. However, these collars were manufactured to clamp to a shaft for power transmission. Since these collars were used in tension on cables rather than power transmission on shafts, the collars still slipped under the quasi-static testing conditions. The slipped collars could change the ROM between repeated tests. It is possible that because the angular displacements in the Phase 1 neck are so small, changes in cable tension could have an affect on the variation results. In future iterations of the Phase 1 neck, a redesign at the base of the neck model to hold the tension within the steel cables consistent between tests would reduce this error in variation.

5 COMPARISON OF PHASE 1 MECHANICAL SURROGATE NECK PROTOTYPE IMPACT RESPONSE TO HYBRID III CRASH TEST DUMMY NECK

Presented in this chapter is the comparison of Hybrid III headform COG kinematic and upper neck kinetic impact responses when fixed to the Phase 1 neck and the Hybrid III crash test dummy neck. This information offers insight about how biomechanical impact responses might change if the Phase 1 neck prototype were to replace the Hybrid III neck model in helmet certification experimental methods.

5.1 Background

Currently available ATD neck models are thought by many to be too mechanically stiff to be considered a biofidelic model for use in direct head impact and helmet certification experimental methods. Quantifying the biomechanical differences between an available ATD surrogate neck and the Phase 1 neck will lead to valuable characterization techniques of the Phase 1 neck, and will offer beneficial implications of how surrogate neck compliancy affects biomechanical impact results. In Chapter 5, Hybrid III headform COG kinematic and upper neck kinetic results in impact when fixed to both the Hybrid III neck and the Phase 1 neck are compared.

5.2 Materials and Methods

5.2.1 Experimental Equipment

The experimental setup for impact testing included a custom designed, adjustable linear impact tower to guide an un-helmeted 50th percentile Hybrid III ATD headform. Although the goal of this thesis is to characterize a neck model to be used in helmet certification applications, the PMHS literature presented in Chapter 6 are results of un-helmeted tests. The Hybrid III neck and Phase 1 neck comparisons were also un-helmeted for consistency in all impact experiments. The Hybrid III headform was fixed to a surrogate neck and impacted onto a MEP (Figure 5.1). This impact surface allowed for un-helmeted impacts while ensuring the test equipment was not damaged.

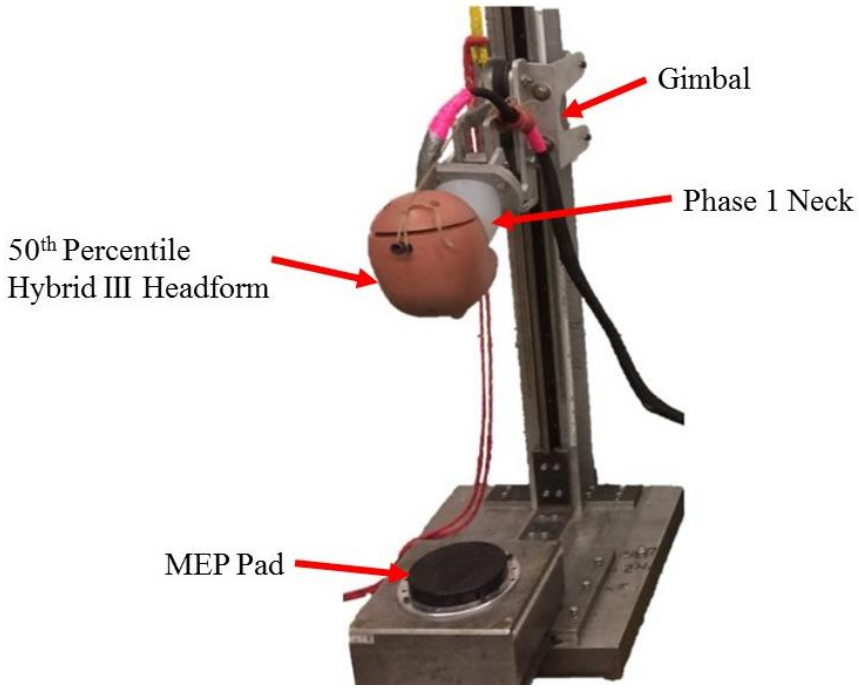

Figure 5.1: Guided linear drop tower with 50th percentile Hybrid III headform and Phase 1 mechanical surrogate neck prototype mounted to a custom gimbal with MEP impact surface (photo credit: author)

The Hybrid III headform was instrumented with nine uniaxial accelerometers (model 64C-2000-360, Measurement Specialties Inc., Hampton, VA) arranged in a 3-2-2-2 array (Figure 5.2). Accelerator mounting blocks with two accelerometers were located at the left side, front, and top inner surfaces of the Hybrid III headform. An accelerometer-mounting block with three accelerometers was located at the Hybrid III heaform COG. This accelerometer array allows for

Hybrid III COG linear acceleration measurement and post-hoc angular acceleration measurement using equations presented by Padgaonkar [50]. Although some researchers have found angular velocity of the headform is a better predictor of brain strain than angular acceleration, the chosen cadaver literature detailed in Chapter 6 report angular accelerations only, therefore only the angular accelerations of the Hybrid III heaform will be compared. The upper neck forces and moments were measured using a six-axis upper neck load cell (model N6ALB11A, mg sensor GmbH, Iffezheim, Germany). The location of the upper neck load cell within the Hybrid III headform approximated the OC in the human (Figure 5.2). Impact speeds were measured using a purpose-built velocity gate. The coordinate system used in the Hybrid III headform can be found in Figure 5.3, which was prescribed in SAE Standard Method J211 [43].

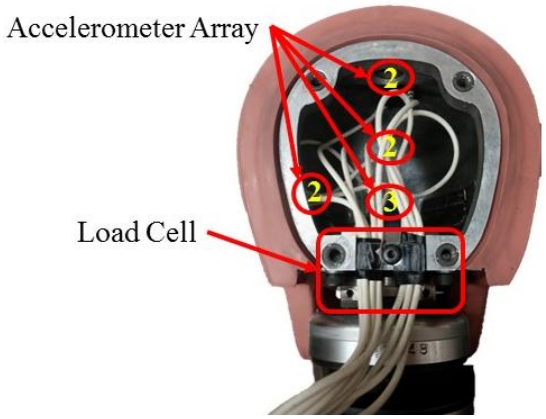

Figure 5.2: Annotated image of instrumentation locations of 50th percentile Hybrid III headform (photo credit: Biomedical Instrumentation Lab at University of Alberta)

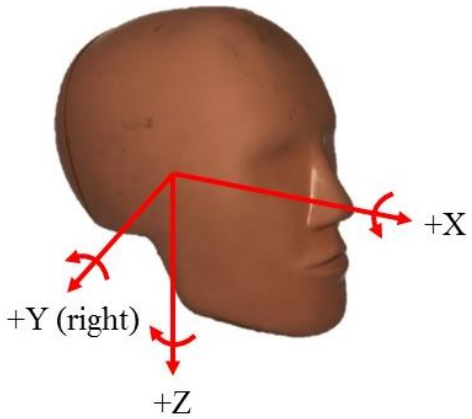

Figure 5.3: Annotated image of 50th percentile Hybrid III headform showing positive coordinate system (photo credit: Biomedical Instrumentation Lab at University of Alberta)

The Hybird III headform linear acceleration and upper neck kinetics were collected and saved at 100 kHz using National Instruments software (PXI 6251 and LabVIEW v8.5, Austin TX). The linear acceleration and upper neck kinetic data was filtered with a hardware anti-aliasing filter with a cut-off frequency of 4 kHz prior to post-hoc CFC software filtering methods in MATLAB guided by SAE standard instrumentation measurement techniques for impact testing ATDs [43].

Due to the compliancy of the Phase 1 neck, the Hybrid III headform was held in place using breakaway cables. These cables were used to hold the Hybrid III in approximately the correct position before impact, and to break away at impact to reduce the influence on post-impact biomechanical results. The impact tests were recorded with dual high-speed video cameras at 1000 frames per second for post-hoc observation of impacts (Phantom v611, Vision Research Inc., Wayne, NJ).

5.2.2 Experimental Protocol

The Hybrid III neck-Phase 1 neck impact test matrix can be found in Table 5.1. A total of 24 tests were conducted at an impact velocity of 1.5 m/s and impact locations to the front, rear, side, and crown of the Hybrid III ATD headform. These impact locations are common in helmet certification experimental protocol. The Hybrid III headform COG kinematics and upper neck kinetics between the Hybrid III neck and Phase 1 neck were then compared. It was assumed the kinematic and kinetic differences observed at the minimum impact speed of the cadaveric comparison (described in Chapter 6) would be similarly, or more drastically, scaled at higher impact speeds.

Table 5.1: Distribution of 1.5 m/s impact comparison of Hybrid III ATD headform fixed to Hybrid III neck and Phase 1 mechanical surrogate neck prototype, categorized by Hybrid III ATD headform impact location

Impact Location	Hybrid III Neck	Phase 1 Neck	Total
Forehead	3	3	6
Rear	3	3	6
Side	3	3	6
Crown	3	3	6
All	12	12	**24**

5.2.3 MATLAB Impact Test Processing Code

Following the impact tests, the collected data was processed in a MATLAB code to meet SAE Standard J211 recommended practice when using ATD components [43]. The head COG linear accelerations and upper neck forces were filtered with a 4th order low pass Butterworth filter at a cutoff frequency of 1,650 Hz. A 4th order low pass Butterworth filter with a cutoff frequency of 1,000 Hz was used to filter the upper neck moments. The angular accelerations about the Hybrid III headform COG were calculated using methods presented by Padgaonkar et al. [50].

5.2.4 Hybrid III Neck and Phase 1 Neck Comparison

To compare the Phase 1 neck to the Hybrid III neck, the percent difference in peak resultant Hybrid III headform COG kinematic and upper neck kinetic data were calculated using Equation 5.1. Since this is an initial attempt to characterize the Phase 1 neck, only the peak values were compared.

$$\frac{HybridIII\ Neck\ Peak - Phase\ 1\ Neck\ Peak}{HybridIII\ Neck\ Peak} \times 100\% \tag{5.1}$$

5.3 Results

A summary of peak headform COG kinematics and upper neck kinetics of the Hybrid III headform fixed to the Phase 1 neck and Hybrid III neck are reported in Table 5.2. The percent difference in peak biomechanical values are presented in Table 5.3. As this is an initial characterization of the Phase 1 neck, the results are reported as peak resultant biomechanical measures upon direct impacts to the Hybrid III headform.

Figure 5.4 compares high-speed images of the Hybrid III headform response just before impact, just after impact, and at rest, when fixed to the Hybrid III neck and when fixed to the Phase 1 neck. Both tests are at an impact speed of 1.5 m/s to the forehead of the Hybrid III headform. When comparing Figure 5.4b) to Figure 5.4e), the Phase 1 neck appears to experience more extension rotation than the Hybrid III neck in freefall. Additionally, the rest position of the Hybrid III headform is more externally rotated when fixed to the Phase 1 neck than when fixed to the Hybrid III neck, as seen in Figure 5.4c) and Figure 5.4f).

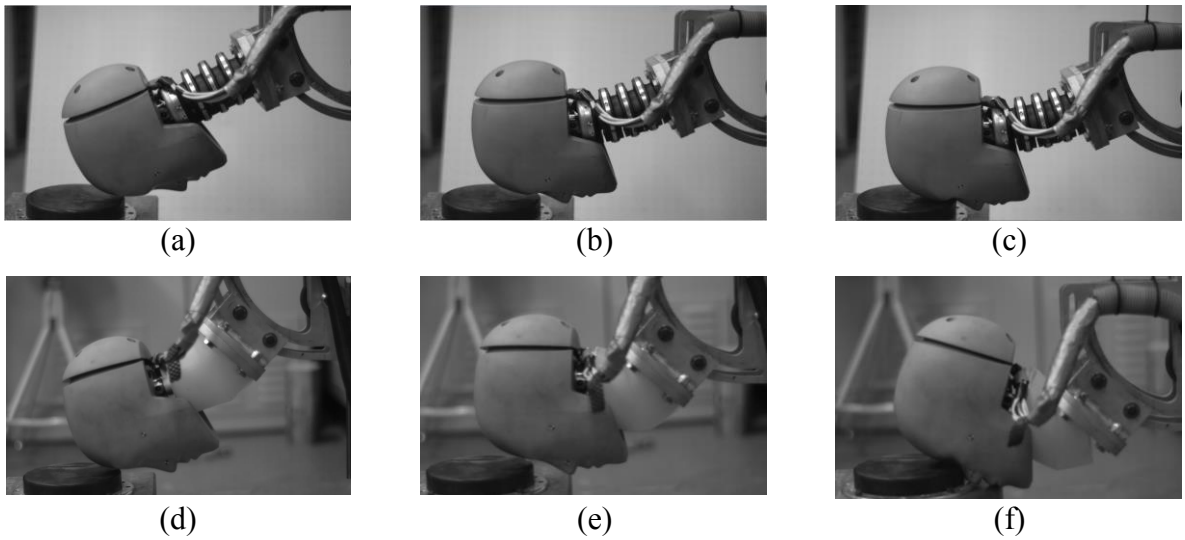

(a) (b) (c)

(d) (e) (f)

Figure 5.4: High-speed images of 1.5 m/s forehead impacts to Hybrid III headform, (a) fixed to Hybrid III neck just before impact, (b) fixed to Hybrid III neck just after impact, (c) fixed to Hybrid III neck at rest, (d) fixed to Phase 1 mechanical surrogate neck prototype just before impact, (e) fixed to Phase 1 mechanical surrogate neck prototype just after impact, (f) fixed to Phase 1 mechanical surrogate neck prototype at rest

Figure 5.5 compares the average resultant Hybrid III headform COG kinematics and upper neck kinetics at 1.5 m/s forehead impacts between the Phase 1 neck and the Hybrid III neck. The total time duration of these plots are set to 40 ms to highlight the initial response after the Hybrid III headform impacted the MEP pad. For all biomechanical variables in forehead impacts, the Phase 1 neck exhibited lesser magnitudes than the Hybrid III neck (Table 5.2).

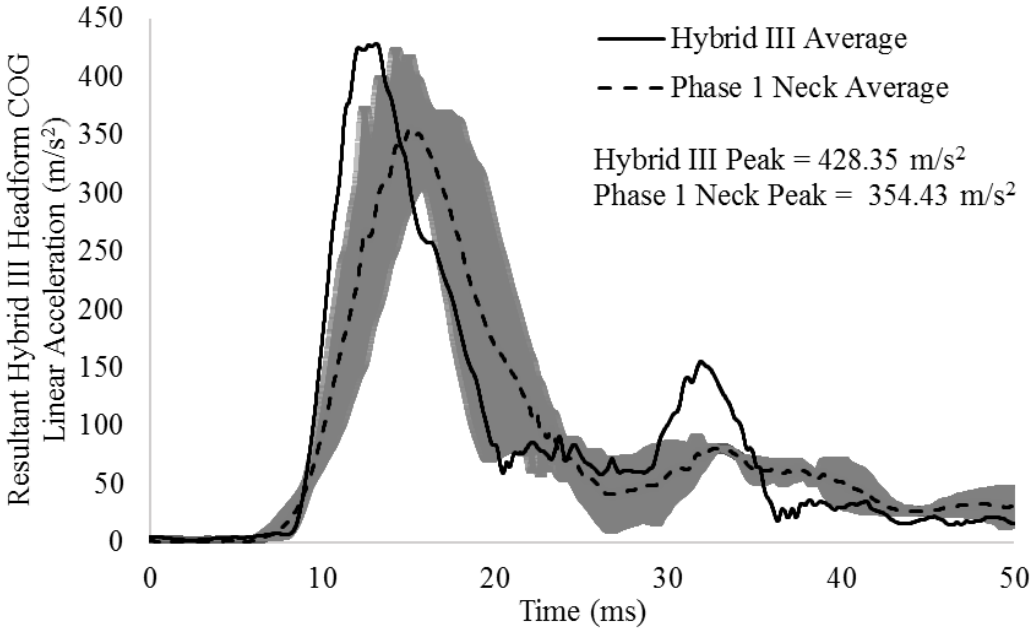
Hybrid III Average
Phase 1 Neck Average
Hybrid III Peak = 428.35 m/s²
Phase 1 Neck Peak = 354.43 m/s²
Resultant Hybrid III Headform COG Linear Acceleration (m/s²)
Time (ms)
0
50
100
150
200
250
300
350
400
450
0
10
20
30
40
50

(a)

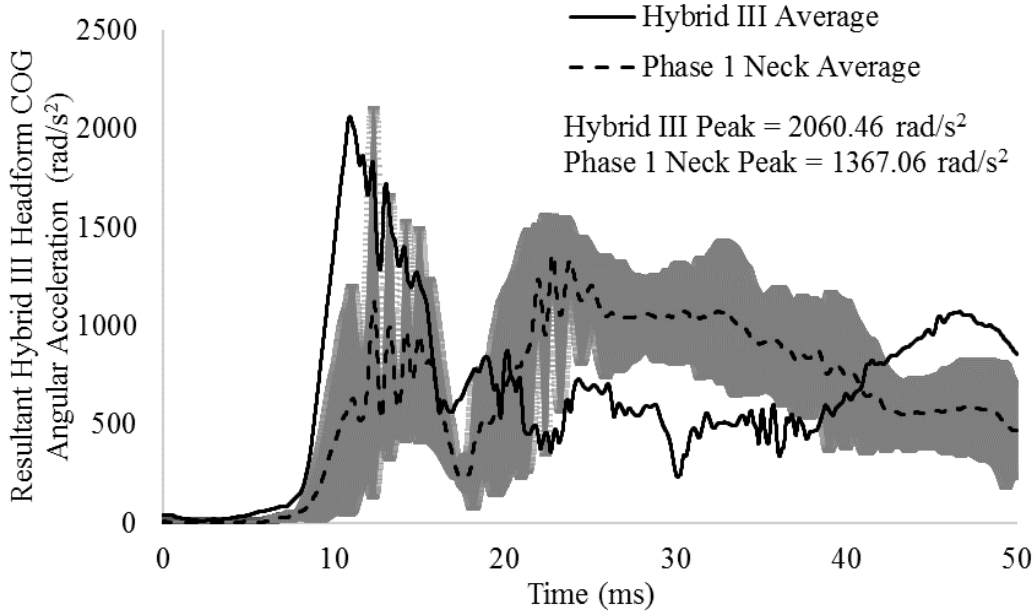
Hybrid III Average
Phase 1 Neck Average
Hybrid III Peak = 2060.46 rad/s²
Phase 1 Neck Peak = 1367.06 rad/s²
Resultant Hybrid III Headform COG Angular Acceleration (rad/s²)
Time (ms)
0
500
1000
1500
2000
2500
0
10
20
30
40
50

(b)

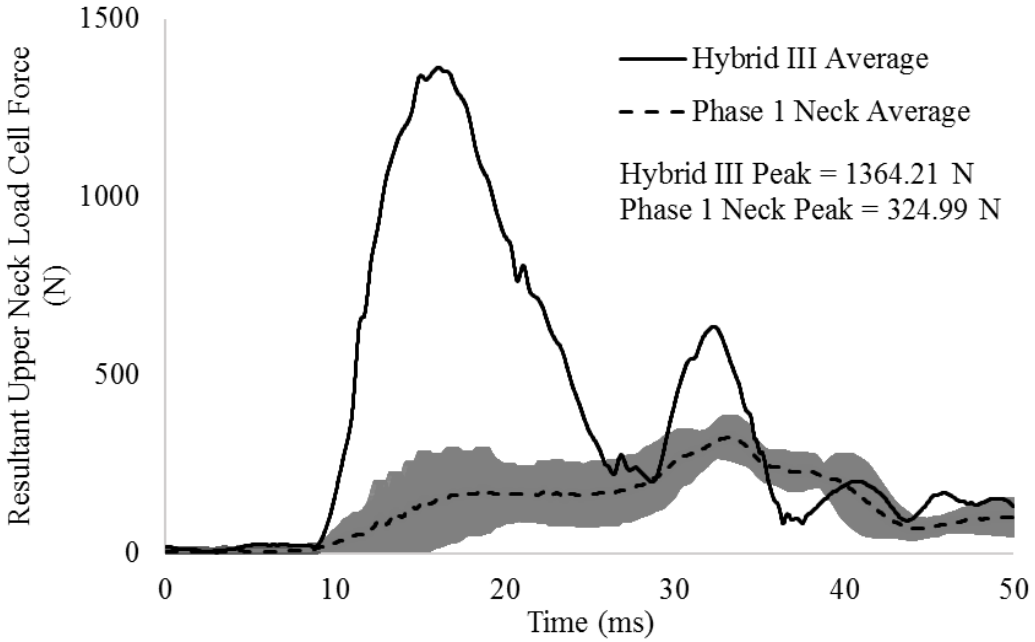

(c)

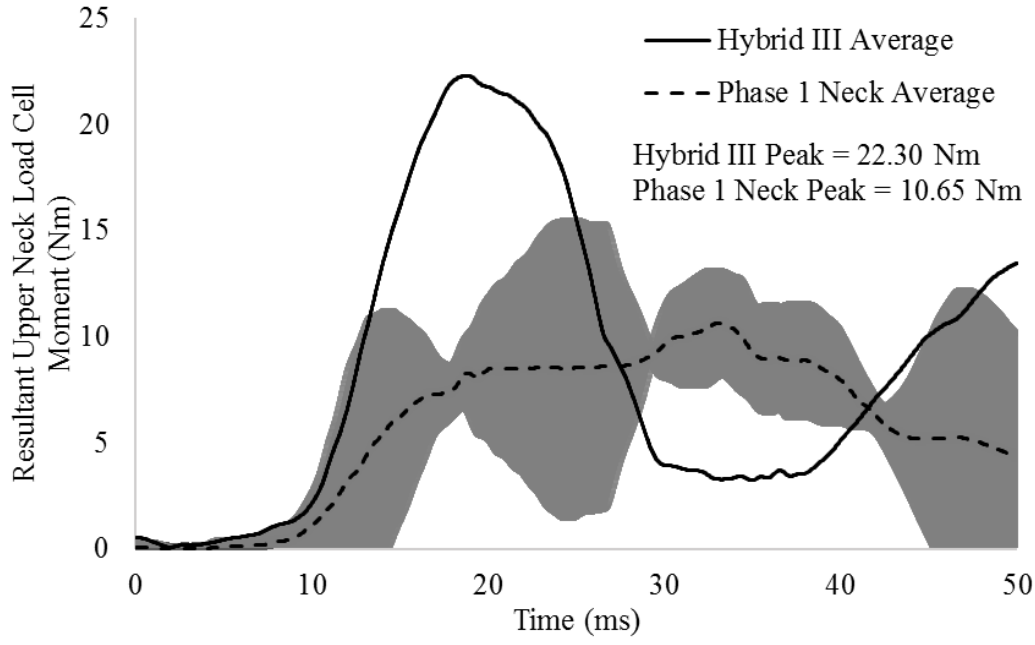

(d)

Figure 5.5: Averaged impact comparison of Hybrid III ATD neck model and Phase 1 mechanical surrogate neck prototype at 1.5 m/s forehead impact, (a) resultant linear acceleration of Hybrid III headform COG, (b) resultant angular acceleration of Hybrid III headform COG, (c) resultant upper neck forces, (d) resultant upper neck moments Note: Greyed areas show ±1 SD of three averaged Phase 1 neck tests

Table 5.2: Average ± 1 SD peak resultant Hybrid III headform COG kinematics and upper neck load cell kinetics

(a) when fixed to Hybrid III neck

Impact Location	Front	Side	Rear	Crown
Impact Speed (m/s)	1.57 ± 0.10	1.52 ± 0.61	1.57 ± 0.08	1.59 ± 0.16
Peak Resultant COG Linear Acceleration (m/s^2)	428.35 ± 142.51	584.78 ± 29.74	522.40 ± 27.10	493.39 ± 54.71
Peak Resultant COG Angular Acceleration (rad/s^2)	2060.46 ± 791.61	4995.47 ± 392.58	3217.32 ± 470.94	1846.72 ± 380.65
Peak Resultant Upper Neck Force (N)	1364.21 ± 144.81	1478.03 ± 26.28	1049.12 ± 20.33	2968.86 ± 145.16
Peak Resultant Upper Neck Moment (Nm)	22.30 ± 1.65	5.58 ± 0.69	25.02 ± 0.73	33.17 ± 4.73

(b) when fixed to Phase 1 mechanical surrogate neck prototype

Impact Location	Front	Side	Rear	Crown
Impact Speed (m/s)	1.74 ± 0.04	1.82 ± 0.16	1.59 ± 0.09	1.89 ± 0.16
Peak Resultant COG Linear Acceleration (m/s^2)	354.43 ± 63.15	535.24 ± 86.42	458.22 ± 26.34	605.88 ± 64.35
Peak Resultant COG Angular Acceleration (rad/s^2)	1367.06 ± 198.74	3598.78 ± 441.06	2877.13 ± 241.87	2676.02 ± 529.65
Peak Resultant Upper Neck Force (N)	324.99 ± 60.58	271.16 ± 12.88	440.65 ± 10.50	414.41 ± 23.04
Peak Resultant Upper Neck Moment (Nm)	10.65 ± 2.25	4.93 ± 0.55	4.63 ± 0.22	8.39 ± 0.34

The percent differences in peak resultant biomechanical values can be found in Table 5.3. The positive values indicate the peak resultant biomechanical measure was greater when the Hybrid III headform was fixed to the Hybrid III neck than when fixed to the Phase 1 neck. Alternatively, the negative values indicate the peak resultant biomechanical measure was greater when the Hybrid III headform was fixed to the Phase 1 neck than when fixed to the Hybrid III neck. To summarize, focusing on angular acceleration, the Hybrid III neck yielded peak resultant angular accelerations that were 34%, 28%, and 11% greater than the Phase 1 neck in forehead, lateral, and rear impacts, respectively. The Phase 1 neck yielded peak resultant angular accelerations that were 45% greater than the Hybrid III neck in crown impacts. For all impact locations, the percent difference in Hybrid III headform COG linear accelerations are within 23%, whereas the maximum upper kinematic data percent difference exceeds 80%.

Table 5.3: Percent difference between average peak resultant Hybrid III headform COG kinematics and upper neck load cell kinetics between the Hybrid III neck and Phase 1 mechanical surrogate neck prototype in impact

Impact Location	Front	Side	Rear	Crown
Peak Resultant COG Linear Acceleration (%)	+17.26	+8.47	+12.28	-22.81
Peak Resultant COG Angular Acceleration (%)	**+33.65**	**+28.96**	**+10.57**	**-44.91**
Peak Resultant Upper Neck Force (%)	+76.18	+81.65	+58.00	-86.04
Peak Resultant Upper Neck Moment (%)	+52.23	+11.76	+81.50	-74.69

5.4 Discussion

Many helmet certification standards include different neck models in the experimental setup, such that the flexural stiffness range from rigid metal rods, to ATD neck models, to no neck whatsoever [24], [26]–[28]. One reason no standardized neck model exists for helmet certification is the assumption the neck model has no effect on the headform COG kinematic and upper neck kinetic results. This method of comparing identical Hybrid III headform impact experiments when fixed to the Hybrid III neck model and the Phase 1 neck offers an initial understanding of how neck compliancy affects peak resultant biomechanical responses in head impact.

The experimental protocol included three 1.5 m/s impacts to the forehead, crown, side, and rear cap of the Hybrid III headform when fixed to the Hybrid III neck and the Phase 1 neck. These impact locations are common in current helmet certification experimental protocol. It was then

assumed the peak biomechanical differences observed at the minimum impact speed of the cadaveric comparison test protocol, later described in in Chapter 6, would be similarly, or more drastically, scaled at higher impact speeds. The impacts to the Hybrid III headform were repeated three times to achieve acceptable mean and standard deviation calculations of the impact data.

Specific to Hybrid III headform COG kinematic data, the maximum percent differences in peak resultant headform linear acceleration exceeds 20% and in peak resultant headform angular acceleration exceeds 40% in all impact locations. Additionally, the maximum percent differences in peak resultant upper neck kinetic data exceeds 80%.

These are important findings, because the results presented in Section 5.3 imply neck compliancy does in fact make a difference in recorded biomechanical data. This refutes the conventional assumption that surrogate neck compliancy has no effect on the data. Further, the presented results suggest that headform acceleration thresholds prescribed in helmet certification standards and assessment metrics may not be realistic to more compliant human head-neck models. In the future, if a more compliant neck model is implemented into helmet certification and assessment experimental methods, new linear and angular acceleration thresholds may be required to ensure these test protocols are realistic to human limits.

6 COMPARISON OF PHASE 1 MECHANICAL SURROGATE NECK PROTOTYPE TO PMHS NECK – IMPACT RESPONSE

In this chapter, the resulting head COG kinematic and upper neck kinetic responses at multiple impact speeds and multiple impact locations to the head are compared between documented PMHS data and the Phase 1 neck. The purpose of this chapter is to quantify how closely the biomechanical results match published PMHS data, and to assess the degree of repeatability in the Phase 1 neck direct head impact tests.

6.1 Background

To achieve biofidelity of a mechanical surrogate neck component, the impact responses must be comparable to the human. Characterizing a surrogate neck model in direct head impacts offers conclusions concerning how realistic the impact response within the surrogate model is compared to PMHS data. The kinematic characteristics of the head-neck segment include the translational and rotational motions of the headform COG with respect to time [15]. The kinetic characteristics include the forces and moments of the head-neck segment with respect to time [15]. The combination of these two characteristics will allow for a more biofidelic head-neck segment that represents realistic responses to given loading conditions [15].

In Chapter 5, the peak biomechanical impact response of the Phase 1 neck was compared to the Hybrid III neck model. In Chapter 6, the Hybrid III headform COG kinematic and upper neck kinetic results when fixed to the Phase 1 neck will be compared to published PMHS data. At this

stage of the Phase 1 neck characterization, the peak biomechanical magnitudes will be compared to previously published literature containing results of PMHS direct head impact [8], [12], [13]. Using peak PMHS data as a baseline allows for an initial evaluation of the overall impact response of the Phase 1 neck. Based on these results, future experimental methods such as analysis of whole time histories of biomechanical data, a broader PMHS data set, and comparisons to live human data may be suggested. Additionally, the repeatability of the Phase 1 neck impact results are analyzed.

6.2 Materials and Methods

6.2.1 Experimental Equipment

Please refer to Section 5.2.1 and Section 5.2.3 of Chapter 5 for details of experimental equipment, instrumentation, data collection, and post-hoc data processing methods. These components were identical for this chapter.

6.2.2 Experimental Protocol

Multiple PMHS literature sources presenting impact data were considered. Table 6.1 details the papers considered, and the reasoning for acceptance or rejection when forming the Phase 1 neck direct head impact experimental protocol. A total of three PMHS impact papers were accepted. The data presented by Advani et al. [12], Rizzetti et al. [8], and Yoganandan et al. [13] offered a range of head impact locations and speeds that allowed for initial impact response characterization of the Phase 1 neck.

Table 6.1: PMHS literature considered to base the Phase 1 mechanical surrogate neck prototype impact experimental protocol

Citation	Accepted or Rejected	Reasoning
Advani et al. [12]	**Accepted**	This paper was accepted to develop the Phase 1 neck impact test protocol because the authors generated forehead, occipital, and lateral direct head impact data from whole PMHS.
Alem et al. [51]	Rejected	This report generated compression impact data. At this phase of the neck development, impact compression response was not considered.
Camacho et al. [52]	Rejected	This journal paper generated compression impact data of a finite element model. At this phase of the neck development, impact compression response was not considered. Additionally, only PMHS data was considered.
GESAC Inc. [39]	Rejected	This report generated forehead flexion response thresholds the THOR surrogate neck model based on sled impact data. This was not adequate data to compare in direct head impact response.
Nelson and Cripton [42]	Rejected	This journal paper generated compression data for a surrogate neck model designed by the authors. At this phase of the neck development, impact compression response was not considered. Additionally, only PMHS data was considered.
Nusholtz and Huelke [53]	Rejected	This conference paper generated compression impact data. At this phase of the neck development, impact compression response was not considered.
Nusholtz et al. [54]	Rejected	This conference paper generated compression impact data. At this phase of the neck development, impact compression response was not considered.

Pintar et al. [55]	Rejected	It was determined that a proper comparison of the biomechanical data obtained from this journal paper was unattainable due to the differences in experimental setups in this paper to what was available at the University of Alberta, and was therefore rejected.
Rizzetti et al.[8]	**Accepted**	This conference paper was accepted to develop the Phase 1 neck impact test protocol because the authors generated forehead, occipital, and lateral direct head impact data from whole PMHS.
Toomey et al. [56]	Rejected	This journal paper generated compression data for the Hybrid III surrogate neck model. At this phase of the neck development, impact compression response was not considered. Additionally, only PMHS data was considered.
VanIngen-Dunn and I. Kaleps [15]	Rejected	This report generated forehead flexion response thresholds the Hybrid III surrogate neck model based on sled impact data. This was not adequate data to compare in direct head impact response.
Yoganandan et al. [57]	Rejected	This journal paper generated compression impact data. At this phase of the neck development, impact compression response was not considered.
Yoganandan et al. [58]	Rejected	This conference report generated rear sled impact extension response of PMHS head-neck segments. This was not adequate data to compare in direct head impact response.
Yoganandan et al. [13]	**Accepted**	This paper was accepted to develop the Phase 1 neck impact test protocol because the authors generated lateral direct head impact data from whole PMHS.
Yoganandan et al. [59]	Rejected	This journal generated lateral sled impact response of PMHS head-neck segments. This was not adequate data to compare in direct head impact response.

The Phase 1 neck impact test matrix can be found in Table 6.2. A total of 72 tests were conducted, with impact speeds ranging from 1.5 m/s to 5.0 m/s, and impact locations to the front, side, and rear of the un-helmeted Hybrid III headform. As described in Chapter 5, the Hybrid III headform was un-helmeted to allow for a closer comparison of the Hybrid III headform COG kinematic and upper neck kinetic results to the PMHS data presented by Advani et al. [12], Rizzetti et al. [8], and Yoganandan et al. [13].

Table 6.2: Distribution of impact tests to Hybrid III ATD headform fixed to Phase 1 mechanical surrogate neck prototype, categorized by impact speed and impact location

Impact Location	Impact Speed								Total
	1.5	2.0	2.5	3.0	3.5	4.0	4.5	5	
Forehead	3	3	3	3	3	3	3	3	24
Side	3	3	3	3	3	3	3	3	24
Rear	3	3	3	3	3	3	3	3	24
All	9	9	9	9	9	9	9	9	**72**

6.2.3 Comparison to PMHS Literature

To compare the peak head kinematics and upper neck kinetics of the Phase 1 neck to data presented in literature by Advani et al. [12], Rizzetti et al. [8], and Yoganandan et al. [13], the presented impact histories in the chosen literature sources were digitized and adapted to excel, and contrasted against the Phase 1 neck results. Because this is an initial attempt to characterize the Phase 1 neck, only the percent difference of peak biomechanical magnitudes were compared rather than comparison of whole time histories of the data. The percent difference in peak magnitudes were calculated using Equation 6.1.

$$\frac{Cadaver\ Peak - Phase\ 1\ Peak}{Cadaver\ Peak} \times 100\% \tag{6.1}$$

6.2.4 Variability Analysis

The CV was used to describe the variation in the Phase 1 neck data (Equation 6.2). The CV is a ratio that compares the standard deviation, σ, to the mean, μ, of the collected data between three repeated tests. Again, since this is an initial attempt to characterize the Phase 1 neck, the average peak magnitudes and standard deviations at these points were used to calculate the CV.

$$CV = \frac{\sigma}{\mu} \times 100\% \tag{6.2}$$

6.2.5 Simple Linear Regression

Simple linear regression models comparing peak resultant Hybrid III headform COG kinematics and upper neck kinetics of the Phase 1 neck impacts to increasing impact speed were observed. The R^2 was considered, as this value would indicate if increasing impact speed predicts the variation in the data. A high R^2 value, such as 0.70 or greater, indicates the simple linear model predicts the variation in the data [30].

6.3 Results

A summary of peak Hybrid III headform COG kinematics and upper neck kinetics in all experiments are presented in Table 6.3. The percent differences between peak biomechanical measures of the PMHS data and the Phase 1 neck may be found in Table 6.4. The CV values for the Phase 1 neck data are given in Table 6.6. Finally, a summary of the R^2 values for the Phase 1 neck impact tests can be found in Table 6.7. As this is an initial characterization of the Phase 1 neck, the results are reported as peak resultant biomechanical measures upon direct impacts to the headform.

6.3.1 Experimental Observations

Table 6.3 summarizes the peak average (μ) and standard deviation (σ) of the Hybrid III headform COG kinematics and upper neck kinetics of all Phase 1 neck tests. Each test group (i.e. P1_(impact location)_(impact speed)) includes the averaged data of the Hybrid III headform fixed to the Phase 1 neck at the same impact location and same impact speed.

Table 6.3: Peak average resultant Hybrid III headform COG kinematics and upper neck kinetics of all Phase 1 mechanical surrogate neck prototype impact tests

Test Group ID	Impact Velocity (m/s)	Peak Resultant COG Linear Acceleration (m/s^2)		Peak Resultant COG Angular Acceleration (rad/s^2)		Peak Resultant Upper Neck Force (N)		Peak Resultant Upper Neck Moment (Nm)	
		μ	±σ	μ	±σ	μ	±σ	μ	±σ
P1_F_1.5	1.74	354.43	63.15	1367.06	198.75	324.99	60.58	10.65	2.25
P1_F_2.0	1.82	762.21	57.70	4263.44	225.32	311.55	6.43	9.87	0.65
P1_F_2.5	2.42	957.83	79.99	5973.64	1492.16	369.25	27.45	11.16	0.46
P1_F_3.0	2.87	1178.72	13.19	6215.85	841.20	523.82	48.95	12.23	0.30
P1_F_3.5	3.62	1307.90	18.32	5988.89	227.31	1107.43	53.35	18.28	1.09
P1_F_4.0	4.07	1594.82	196.29	5536.77	357.89	1286.40	110.55	20.28	0.40
P1_F_4.5	4.46	1995.60	51.74	4867.89	418.29	1802.08	46.08	17.79	0.62
P1_F_5.0	5.02	2314.83	63.71	5520.00	813.62	1784.20	84.25	21.04	0.94
P1_S_1.5	1.82	535.24	47.42	3598.78	441.06	271.16	12.88	4.93	0.19
P1_S_2.0	2.34	1164.34	15.96	5991.32	419.30	464.04	14.00	10.69	0.44
P1_S_2.5	2.63	1452.87	112.93	5417.47	522.13	581.77	56.61	14.87	2.04
P1_S_3.0	3.17	1687.03	138.00	8794.00	574.06	640.68	35.17	14.42	0.90
P1_S_3.5	3.66	1704.07	89.11	11368.99	884.89	621.95	45.47	15.40	2.05
P1_S_4.0	4.16	2023.44	160.41	11694.91	884.89	719.06	104.42	18.24	1.86
P1_S_4.5	4.75	2235.10	156.90	16040.96	2527.96	816.66	68.21	19.49	1.86
P1_S_5.0	5.30	29988.60	144.81	16480.81	1063.20	1107.66	55.46	23.52	1.62
P1_R_1.5	1.59	458.22	26.34	2877.16	241.87	440.65	10.50	4.63	0.22
P1_R_2.0	2.25	1136.62	37.73	4281.91	595.19	450.46	23.59	12.15	0.40
P1_R_2.5	2.61	1381.63	26.64	5802.92	460.25	449.78	24.26	13.92	0.47
P1_R_3.0	3.08	1667.36	8.53	6359.21	453.67	763.99	241.06	16.00	0.69
P1_R_3.5	3.58	1640.46	77.78	2726.14	1027.22	650.38	6.72	20.16	0.33
P1_R_4.0	4.26	2150.24	94.90	4042.66	798.71	791.21	17.64	23.14	0.60
P1_R_4.5	4.68	2561.44	24.03	5459.19	1326.40	1180.81	283.85	28.25	2.51
P1_R_5.0	5.16	2962.18	110.27	7180.93	1349.06	1226.88	219.20	32.24	0.56

6.3.2 Comparison to PMHS Literature

PMHS data presented by Advani et al. included the x-component of the acceleration response of the specimen head COG in a 2.87 m/s impact to the forehead [12]. Figure 6.1 compares the averaged x-component of the Hybrid III headform COG linear acceleration at 3.0 m/s forehead impact when fixed to the Phase 1 neck to data presented by Advani et al. [12]. The PMHS data includes head COG linear accelerations calculated by differentiation from high-speed videos [12].

The percent difference in peak values between the Phase 1 neck and PMHS data is -34.74%. The negative value indicates the averaged peak x-component of linear acceleration in the Phase 1 neck tests was larger in magnitude than the data presented by Advani et al. Figure 6.2 is a high-speed image of the Hybrid III headform fixed to the Phase 1 neck in a forehead impact orientation.

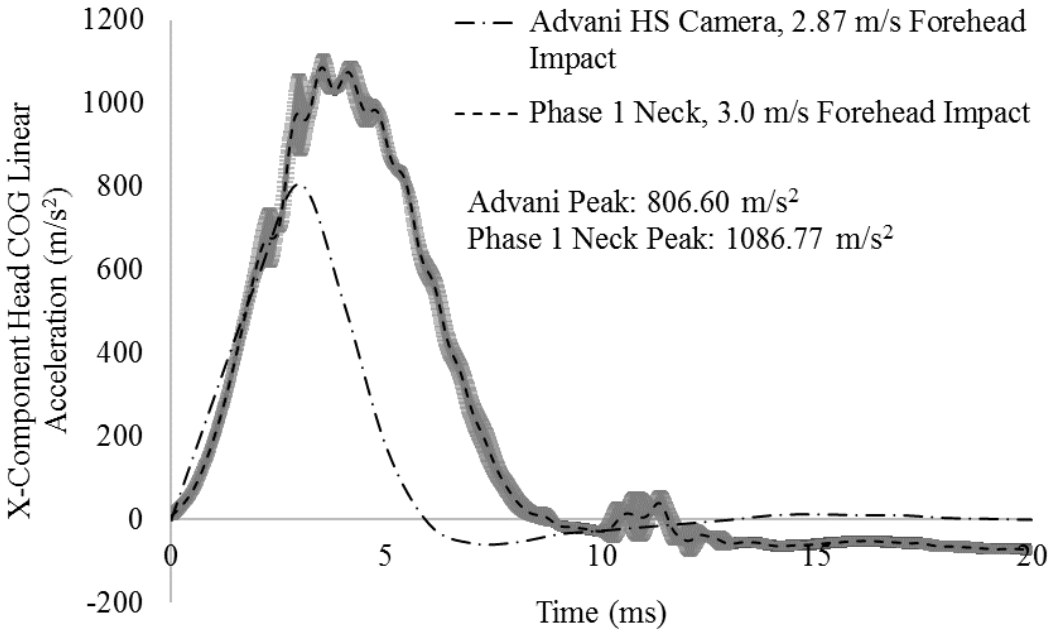

Figure 6.1: Comparison of three averaged x-component linear accelerations at Hybrid III headform COG at 3.0 m/s forehead impact when fixed to Phase 1 mechanical surrogate neck prototype and adapted 2.87 m/s PMHS forehead impact data presented by Advani et al. [12]
Note: Greyed areas show ±1 SD of three averaged Phase 1 neck tests.

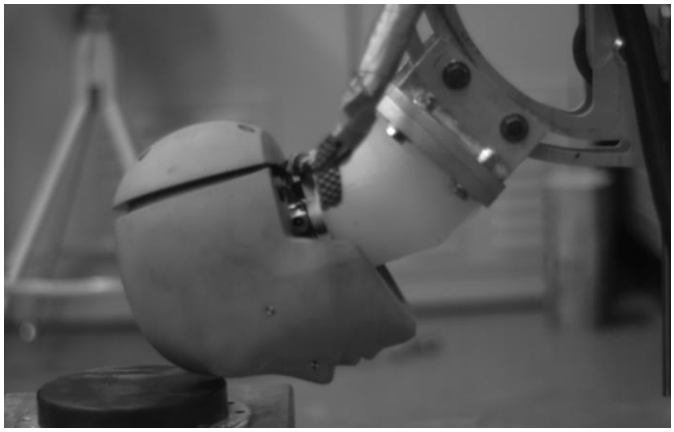

Figure 6.2: High-speed image of Hybrd III headform fixed to Phase 1 mechanical surrogate neck in forehead impact

PMHS data presented by Rizzetti et al. included the resultant linear acceleration and angular acceleration about the y-axis of the specimen head COG in a 5.56 m/s occipital impact [8]. Figure 6.3 compares averaged 5.0 m/s impacts to the rear cap of the Hybrid III headform when fixed to the Phase 1 neck to occipital impact data presented by Rizzetti et al. [8]. Figure 6.3a) compares the resultant linear acceleration and Figure 6.3b) compares angular accelerations about the y-axis of head COG. The total time duration of the Phase 1 neck linear acceleration data is set to 20 ms and the angular acceleration data is set to 16 ms to highlight the initial response after the Hybrid III headform impacted the MEP pad.

The percent difference in peak resultant linear acceleration between the Phase 1 neck and data presented by Rizzetti et al. is -83.64%, and in rotational acceleration about the y-axis is 36.75%. The negative value indicates the averaged peak resultant linear acceleration in the Phase 1 neck test is larger than the peak magnitude presented by Rizzetti et al. Figure 6.4 is a high-speed image of the Hybrid III headform fixed to the Phase 1 neck in a rear impact orientation. The breakaway cables are visible in this image.

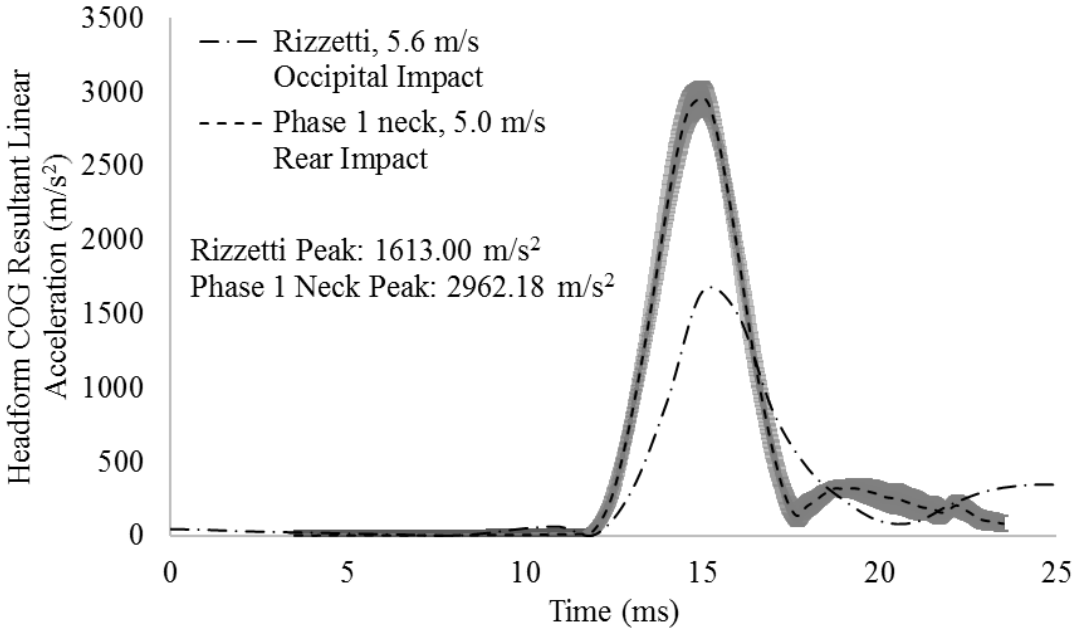

(a)

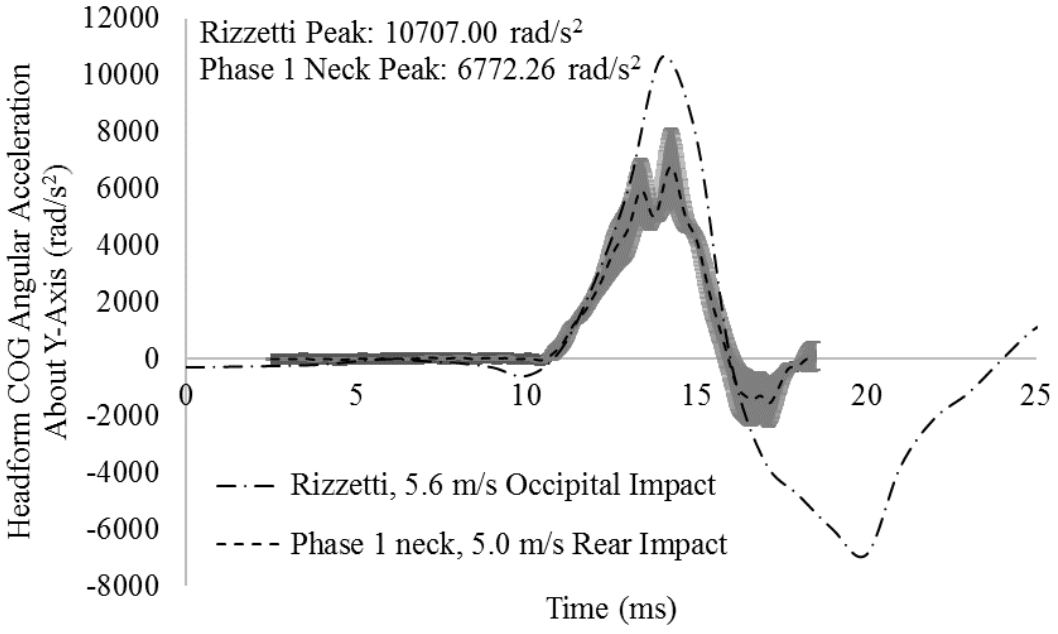

(b)

Figure 6.3: Comparison of three averaged Hybrid III headform COG kinematics at 5.0 m/s impacts to rear cap when fixed to Phase 1 mechanical surrogate neck prototype to adapted 5.6 m/s PMHS occipital impact data presented by Rizetti et al. [8], (a) resultant linear acceleration, (b) angular acceleration about y-axis
Note: Greyed areas show ±1 SD of three averaged Phase 1 neck tests

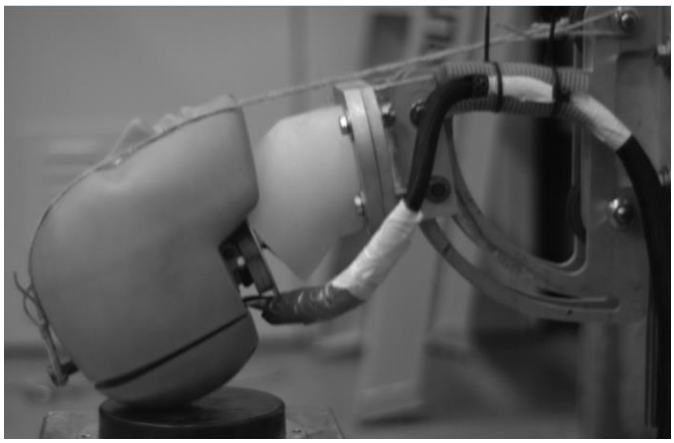

Figure 6.4: High-speed image of Hybrd III headform fixed to Phase 1 mechanical surrogate neck in rear impact

PMHS data presented by Yoganandan et al. included upper neck x-, y-, and z-force and moment responses in a 7.0 m/s lateral impact [13]. The data was adapted into excel, and the resultant force and moment time histories were obtained. Figure 6.5 compares the averaged resultant force and moment responses of 5.0 m/s lateral impacts to the Hybrid III headform fixed to the Phase 1 neck to data presented by Yoganadan et al. [13]. The total time duration of the Phase 1 neck upper neck kinetic data is set to 20 ms to highlight the initial response after the Hybrid III headform impacted the MEP pad. At impact speeds greater than 5.0 m/s, noticeable damage was observed in the Phase 1 neck model, therefore the impact speeds to the Phase 1 neck were limited to 5.0 m/s. This resulted in a 2.0 m/s difference between the Phase 1 neck experiments and the lateral PMHS literature. However, even at the lower impact speed, it was found that the peak resultant upper neck force and moment magnitudes were greater within the Phase 1 neck data than found in literature, suggesting the Phase 1 neck is stiffer than the PMHS neck model.

The percent difference in peak resultant upper neck forces between the Phase 1 neck and data presented by Yoganandan et al. data is -157.74%, and peak resultant upper neck moments is 72.89%. Again, the negative value indicates the averaged peak resultant upper neck force in the Phase 1 neck test is larger than the peak magnitude presented by Yoganandan et al. Figure 6.6 is a high-speed image of the Hybrid III headform fixed to the Phase 1 neck in a lateral impact orientation. The breakaway cables are visible in this image.

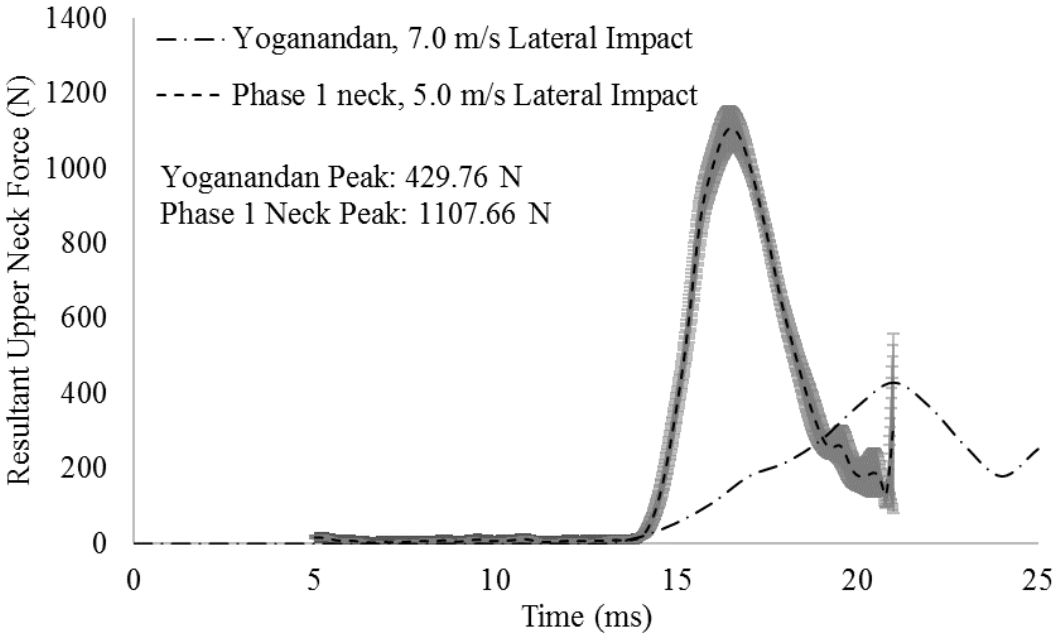

(a)

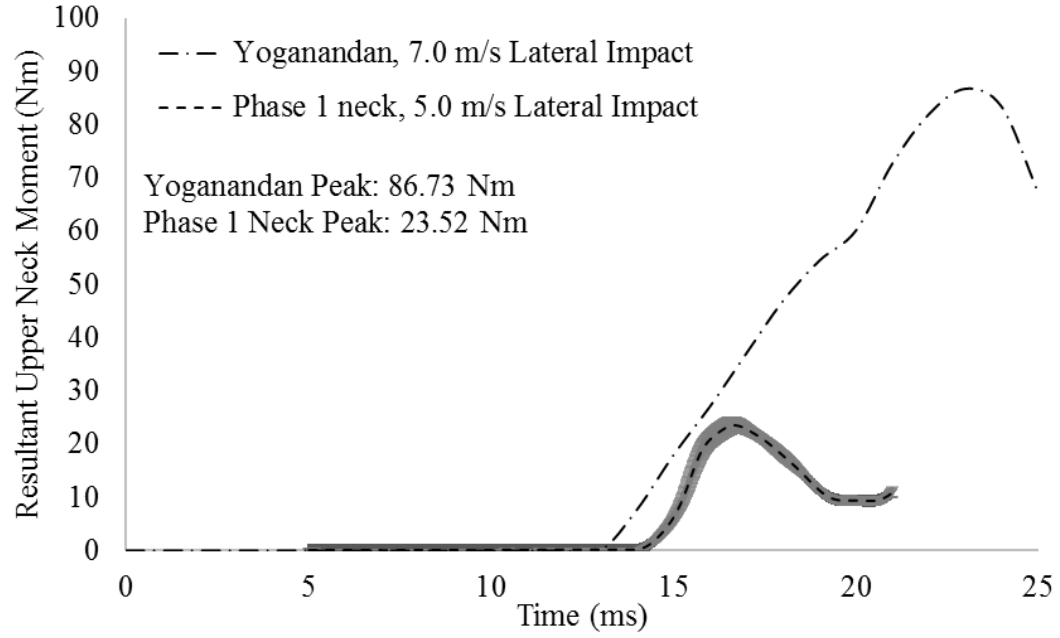

(b)

Figure 6.5: Comparison of three averaged resultant upper neck kinetics of 5.0 m/s lateral impact to Hybrid III headform when fixed to Phase 1 mechanical surrogate neck prototype to adapted 7.0 m/s PMHS lateral impact data presented by Yoganandan et al. [13], (a) resultant upper neck forces, (b) resultant upper neck moments
Note: Greyed areas show ±1 SD of three averaged Phase 1 neck tests

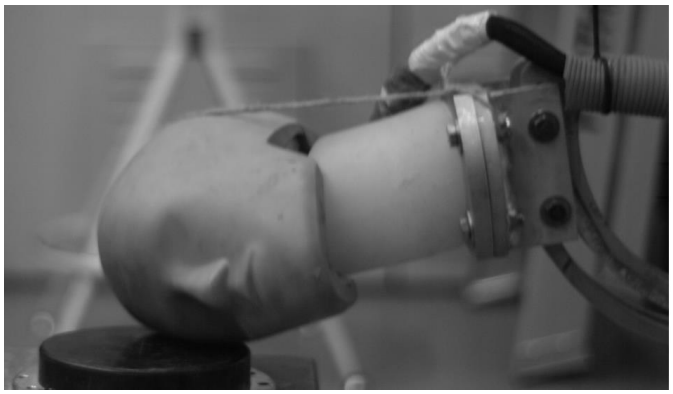

Figure 6.6: High-speed image of Hybrd III headform fixed to Phase 1 mechanical surrogate neck in lateral impact

Table 6.4 summarizes the percent differences between peak headform COG kinematics and upper neck kinetics of the Phase 1 neck and all reported data values presented by Advani et al. [12], Rizzetti et al. [8], and Yoganandan et al. [13]. Specifically, the x-component of the linear acceleration, a_x, the peak angular acceleration about the y-axis, α_y, the peak resultant linear acceleration about the heaform COG, a, the peak resultant upper neck force, and the peak upper neck moments are compared. In all cases, the percent differences in peak biomechanical magnitudes exceed 30%.

Table 6.4: Percent differences in peak head COG kinematic and upper neck kinetic magnitudes between Phase 1 mechanical surrogate neck prototype and published PMHS data

Test Group ID	% Diff. of Phase 1 Neck to Advani et al. [12]	% Diff. of Phase 1 Neck to Rizetti et al. [8]			% Diff. of Phase 1 Neck to Yoganandan et al. [13]	
	Peak a_x Forehead Impact	Peak Res. a Forehead Impact	Peak α_y Occipital Impact	Peak Res. a Occipital Impact	Peak Res. Upper Neck F	Peak Res. Upper Neck M
P1_F_3.0	-34.74	-	-	-	-	-
P1_F_5.0	-	-68.64	-	-	-	-
P1_R_5.0	-	-	+36.75	-83.64	-	-
P1_S_5.0	-	-	-	-	-157.74	+72.89

6.3.3 Comparison of Hybrid III Neck, PMHS Data, and Phase 1 Neck in Impact

To observe the affect of neck compliancy in impact, additional impacts of the Hybrid III headform when fixed to the Hybrid III neck were completed. The percent differences in peak biomechanical values when compared to PMHS data were then calculated.

Figure 6.7 compares the averaged x-component of the Hybrid III headform COG linear acceleration at 3.0 m/s forehead impact when fixed to the Phase 1 neck and when fixed to the Hybrid III neck to data presented by Advani et al. [12]. The percent difference in peak values between the Hybrid III neck and PMHS data is -26.85%. The negative value indicates the averaged peak x-component of linear acceleration in the Hybrid III tests was larger in magnitude than the data presented by Advani et al.

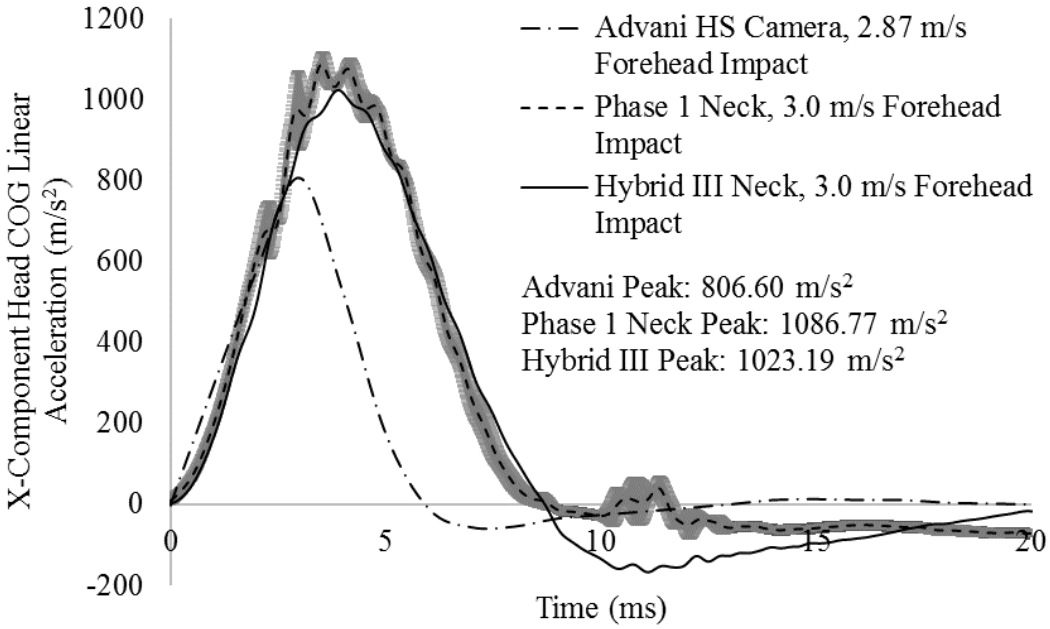

Figure 6.7: Comparison of three averaged x-component linear accelerations at Hybrid III headform COG when fixed to the Phase 1 mechanical surrogate neck prototype and the Hybrid III neck at 3.0 m/s forehead impact to adapted data presented by Advani et al. [12]
Note: Greyed areas show ±1 SD of three averaged Phase 1 neck tests.

Figure 6.8 compares averaged 5.0 m/s impacts to the rear cap of the Hybrid III headform when fixed to the Phase 1 neck and when fixed to the Hybrid III neck to occipital impact data presented by Rizzetti et al. [8]. Figure 6.8a) compares the resultant linear acceleration and Figure 6.8b) compares angular accelerations about the y-axis of head COG. The total time duration of the

Phase 1 neck and Hybrid III neck linear acceleration data is set to 20 ms and the angular accelerations are set to 16 ms to highlight the initial response after the Hybrid III headform impacted the MEP pad. The percent difference in peak resultant linear acceleration between the Hybrid III neck and data presented by Rizzetti et al. is -85.92%, and in rotational acceleration about the y-axis is 31.44%. The negative value indicates the averaged peak resultant linear acceleration in the Hybrid III neck test is larger than the peak magnitude presented by Rizzetti et al.

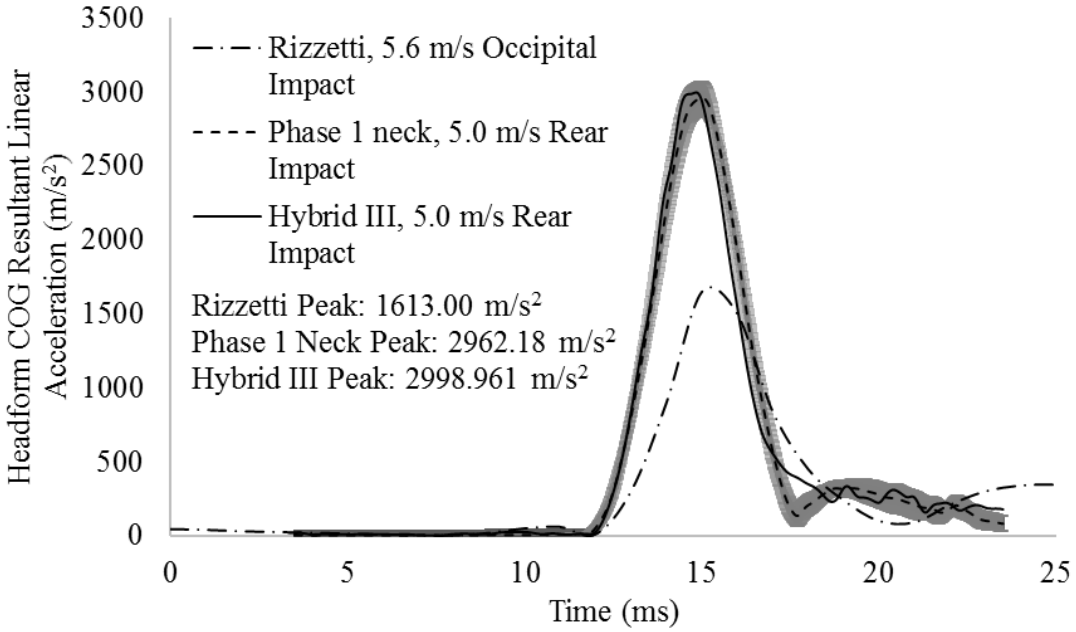

(a)

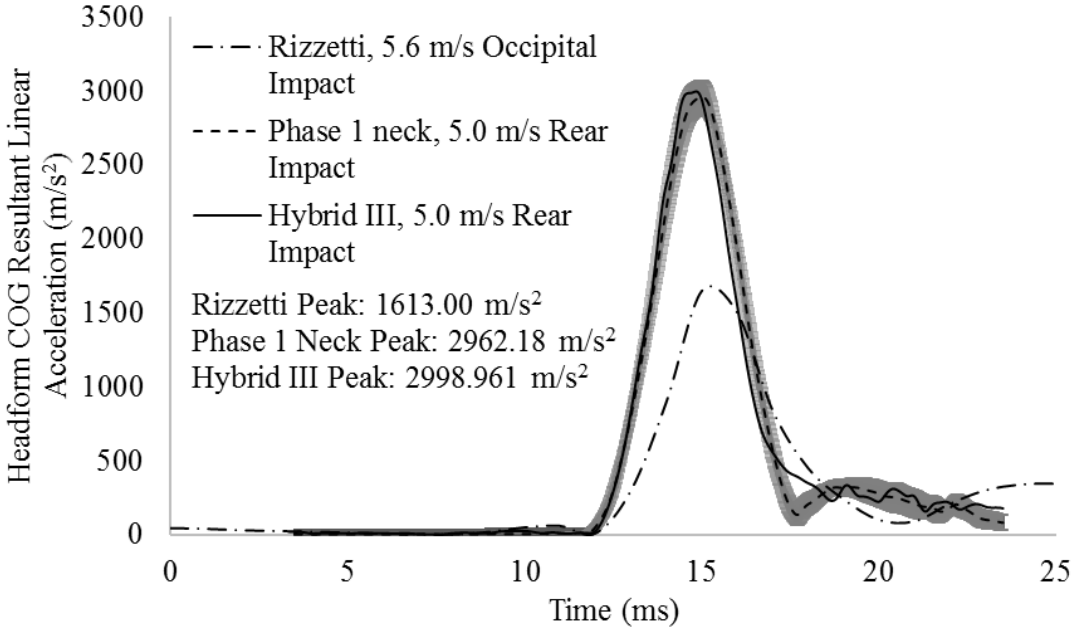

(b)

Figure 6.8: Comparison of three averaged Hybrid III headform COG kinematics at 5.0 m/s impacts to rear cap when fixed to Phase 1 mechanical surrogate neck prototype and when fixed to the Hybrid III neck to adapted 5.6 m/s occipital impacts presented by Rizetti et al. [8], (a) resultant linear acceleration, (b) angular acceleration about y-axis Note: Greyed areas show ±1 SD of three averaged Phase 1 neck tests

Figure 6.9 compares the averaged resultant force and moment responses of 5.0 m/s lateral impacts to the Hybrid III headform when fixed to the Phase 1 neck and when fixed to the Hybrid III neck to data presented by Yoganadan et al. [13]. The total time duration of the Phase 1 neck and Hybrid III neck kinetic data is set to 20 ms to highlight the initial response after the Hybrid III headform impacted the MEP pad. Although the Hybrid III neck model could survive 7.0 m/s impact tests, the Hybrid III neck tests were also limited to 5.0 m/s for consistency between all collected impact tests of the Phase 1 neck and Hybrid III neck model. The percent difference in peak resultant upper neck forces between the Hybrid III neck and data presented by Yoganandan et al. is -1306.11%, and peak resultant upper neck moments is 66.95%. Again, the negative value indicates the averaged peak resultant upper neck force in the Hybrid III neck test is larger than the peak magnitude presented by Yoganandan et al.

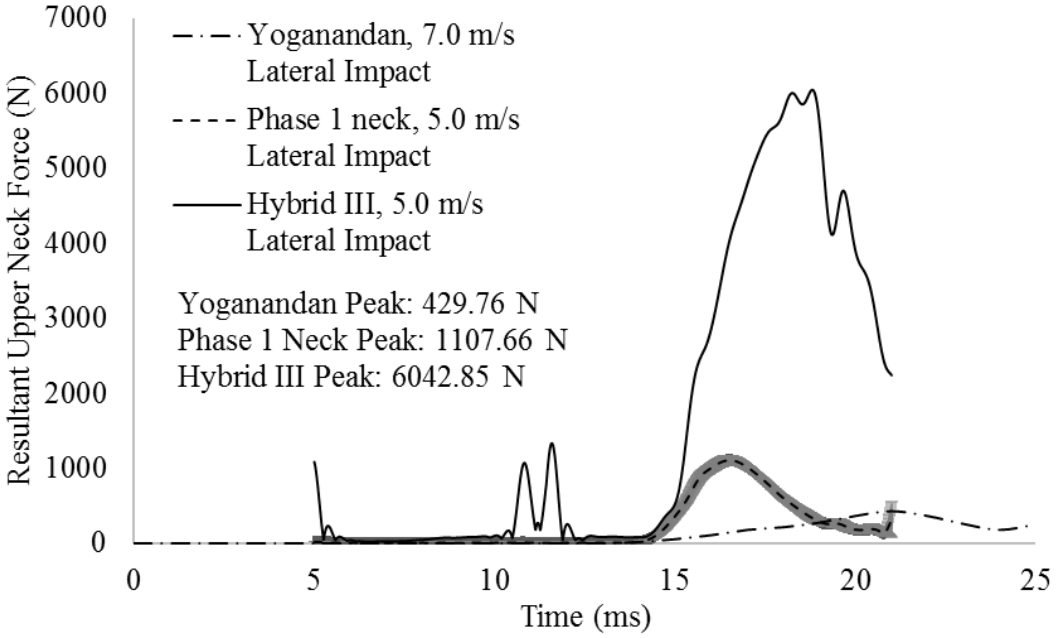

(a)

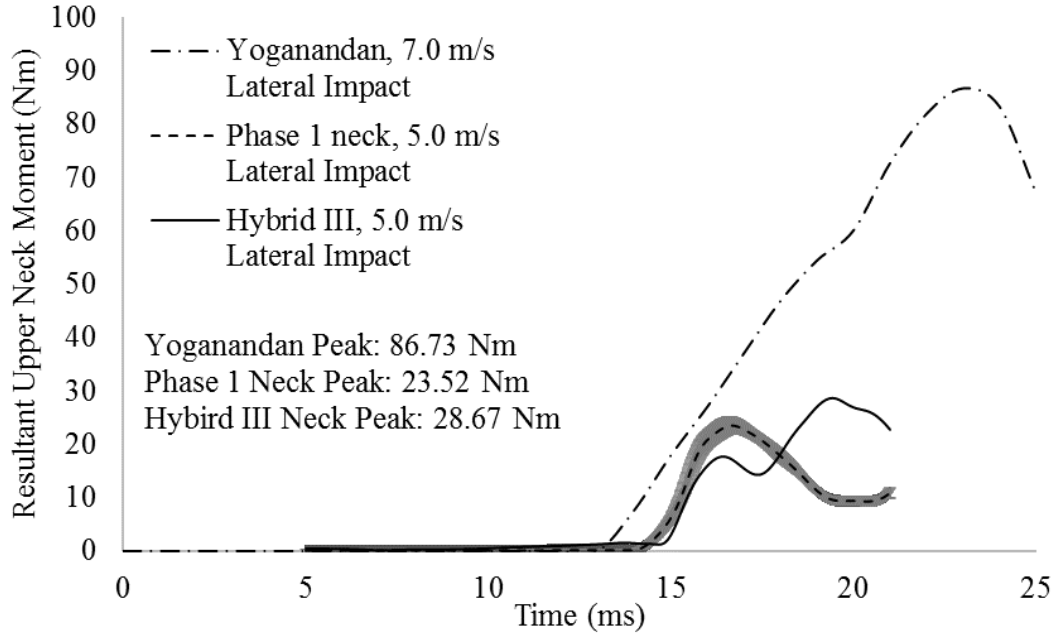

(b)

Figure 6.9: Comparison of three averaged resultant upper neck kinetics of 5.0 m/s lateral impact to Hybrid III headform when fixed to Phase 1 mechanical surrogate neck prototype and when fixed to the Hybrid III neck to adapted 7.0 m/s PMHS lateral impact data presented by Yoganandan et al. [13], (a) resultant upper neck forces, (b) resultant upper neck moments
Note: Greyed areas show ±1 SD of three averaged Phase 1 neck tests

Table 6.5 summarizes the percent differences between peak headform COG kinematics and upper neck kinetics of the Phase 1 neck, the Hybrid III neck and all reported data values presented by Advani et al. [12], Rizzetti et al. [8], and Yoganandan et al. [13]. Specifically, the x-component of the linear acceleration, a_x, the peak angular acceleration about the y-axis, α_y, the peak resultant linear acceleration about the heaform COG, a, the peak resultant upper neck force, and the peak upper neck moments are compared.

As can be seen from the results, when compared to the published PMHS data, the percent difference of the peak Hybrid III headform COG linear and angular acceleration, as well as the peak resultant upper neck moments exceed 30% of the PMHS data. Specifically, the Hybrid III peak resultant upper neck forces are 1300% greater than the reported PMHS data. However, the experimental setup of the guided linear impacts differ from the published PMHS data. Future iterations of the experimental protocol should compare identical Phase 1 neck, Hybrid III neck, and PMHS data to determine the affect of neck compliance on head kinematic and upper neck kinetic data.

Table 6.5: Percent differences in peak head COG kinematic and upper neck kinetic magnitudes between Phase 1 mechanical surrogate neck prototype and the Hybrid III neck to published PMHS data

Test Group ID	% Diff. of Phase 1 Neck and Hybrid III Neck to Advani et al. [12]	% Diff. of Phase 1 Neck and Hybrid III Neck to Rizetti et al. [8]			% Diff. of Phase 1 Neck and Hybrid III Neck to Yoganandan et al. [13]	
	Peak a_x Forehead Impact	Peak Res. a Forehead Impact	Peak α_y Occipital Impact	Peak Res. a Occipital Impact	Peak Res. Upper Neck F	Peak Res. Upper Neck M
P1_F_3.0	-34.74	-	-	-	-	-
H3_F_3.0	-26.85	-	-	-	-	-
P1_F_5.0	-	-68.64	-	-	-	-
H3_F_5.0	-	-46.25	-	-	-	-
P1_R_5.0	-	-	+36.75	-83.64	-	-
H3_R_5.0	-	-	+31.44	-85.92	-	-
P1_S_5.0	-		-	-	-157.74	+72.89
H3_S_5.0	-	-	-	-	-1306.11	+66.95

6.3.4 Variability Analysis

Figure 6.10 presents a sample average (solid line) and one standard deviation (greyed areas) of 3.0 m/s forehead impacts to the Hybrid III headform fixed to the Phase 1 neck. This test group is labeled P1_F_3.0 in Table 6.6. Table 6.6 summarizes all peak resultant Hybrid III headform COG kinematic and upper neck kinetic CV values. Over the 24 test groups, the maximum CV in peak resultant Hybrid III headform COG linear acceleration is 17.82%, peak resultant Hybrid III headform COG angular acceleration is 37.68%, peak resultant upper neck force is 31.55%, and in peak resultant upper neck moment is 21.15%.

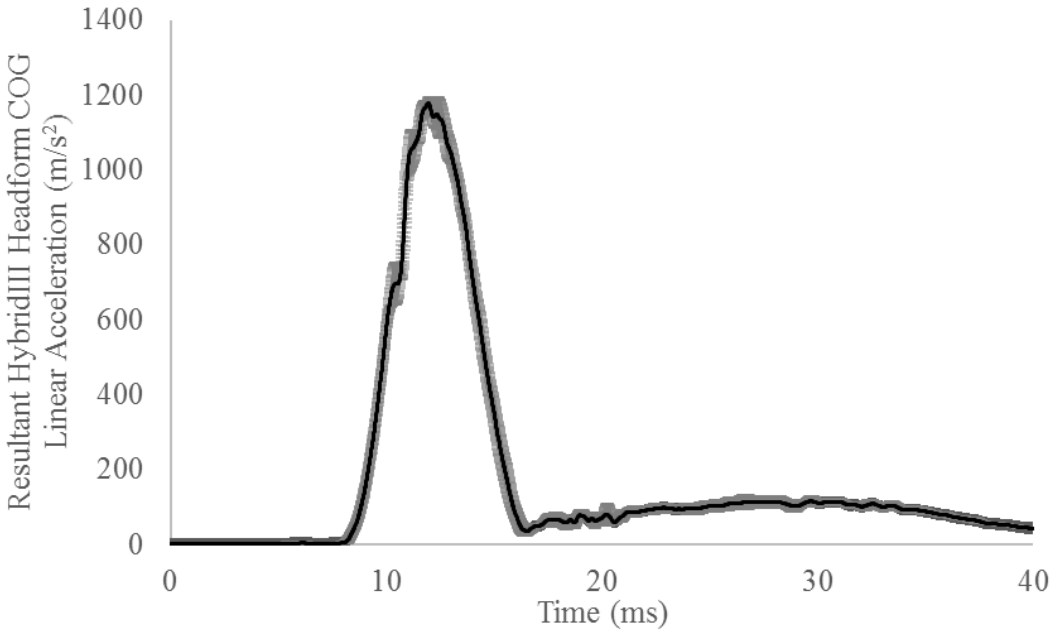
Resultant HybridIII Headform COG
Linear Acceleration (m/s²)
1400
1200
1000
800
600
400
200
0
0
10
20
30
40
Time (ms)

(a)

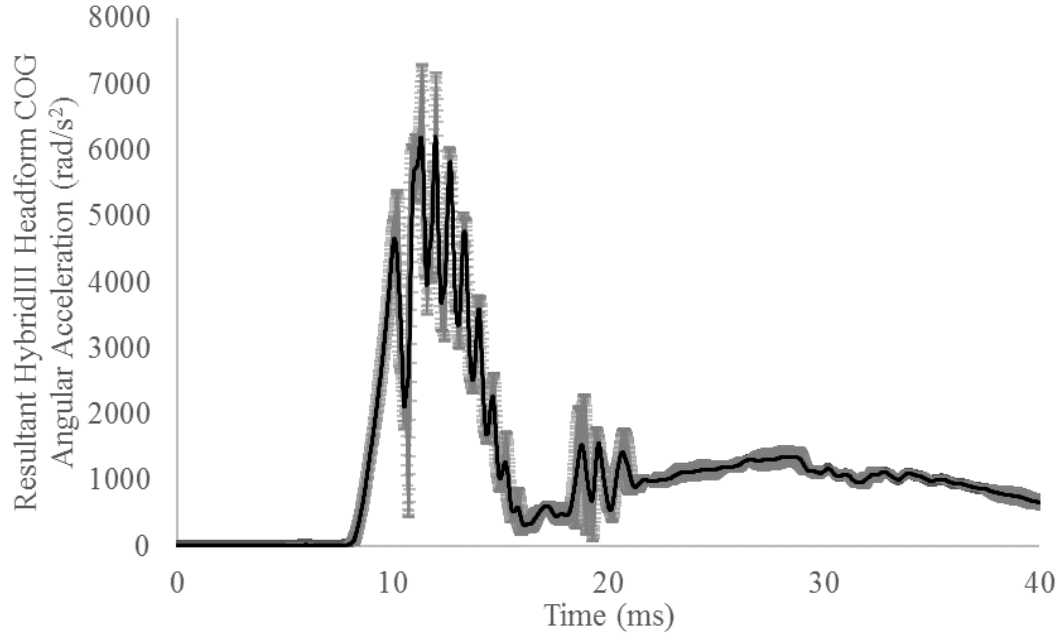
Resultant HybridIII Headform COG
Angular Acceleration (rad/s²)
8000
7000
6000
5000
4000
3000
2000
1000
0
0
10
20
30
40
Time (ms)

(b)

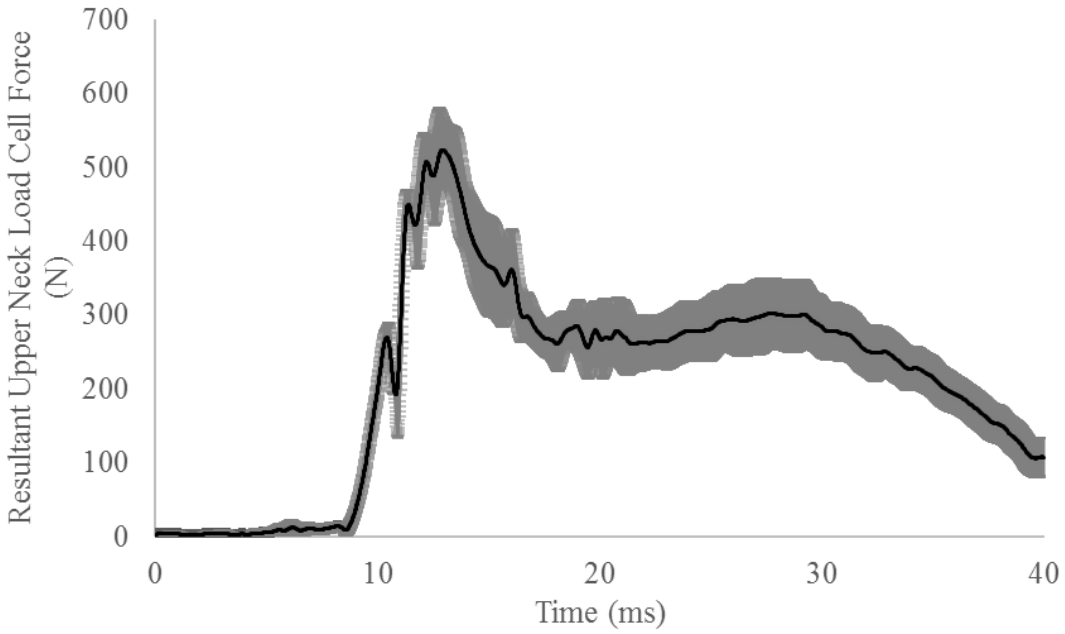

(c)

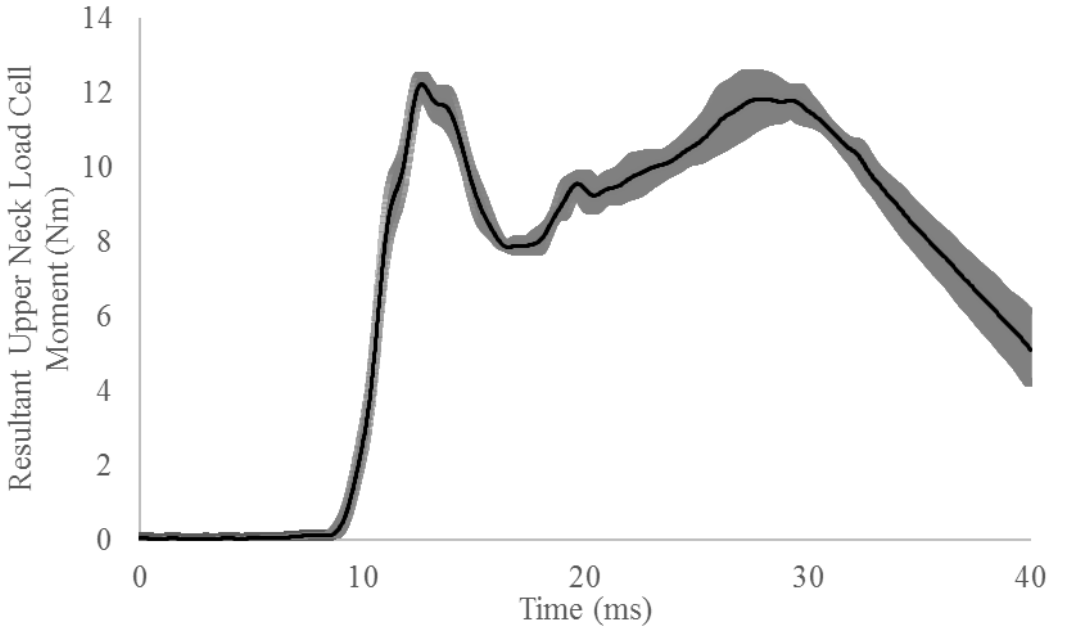

(d)

Figure 6.10: Sample 3.0 m/s forehead impact resultant COG kinematics and upper neck kinetics of the Hybrid III headform fixed to the Phase 1 mechanical surrogate neck prototype, (a) headform COG resultant linear acceleration, (b) headform COG resultant angular acceleration, (c) resultant upper neck forces, (d) resultant upper neck moments. Note: Greyed areas show ±1SD of three averaged Phase 1 neck tests (solid)

Table 6.6: Coefficient of variation analysis of Phase 1 mechanical surrogate neck prototype impact tests

Test Group ID	Peak Resultant COG Linear Acceleration CV (%)	Peak Resultant COG Angular Acceleration CV (%)	Peak Resultant Upper Neck Force CV (%)	Peak Resultant Upper Neck Moment CV (%)
P1_F_1.5	**17.82**	14.54	18.64	**21.15**
P1_F_2.0	7.57	5.29	2.07	6.54
P1_F_2.5	8.35	24.98	7.43	4.13
P1_F_3.0	1.12	13.53	9.35	2.42
P1_F_3.5	1.40	3.80	4.82	5.95
P1_F_4.0	12.31	6.46	8.59	1.99
P1_F_4.5	2.59	8.59	2.56	3.49
P1_F_5.0	5.02	2.75	14.74	4.72
P1_S_1.5	8.86	12.26	4.75	3.77
P1_S_2.0	1.37	7.00	3.02	4.16
P1_S_2.5	7.77	9.64	9.73	13.71
P1_S_3.0	8.18	6.53	5.49	6.24
P1_S_3.5	5.23	8.05	7.31	13.34
P1_S_4.0	7.93	7.57	14.52	10.18
P1_S_4.5	7.02	15.76	8.35	7.51
P1_S_5.0	4.85	6.45	5.01	6.87
P1_R_1.5	5.75	8.41	2.38	4.80
P1_R_2.0	3.32	13.90	5.24	3.30
P1_R_2.5	1.93	7.93	5.39	3.38
P1_R_3.0	0.51	7.13	**31.55**	4.28
P1_R_3.5	4.74	**37.68**	1.03	1.63
P1_R_4.0	4.41	19.76	2.23	2.60
P1_R_4.5	0.94	24.30	24.04	8.88
P1_R_5.0	3.72	18.79	17.87	1.74

6.3.5 Simple Linear Regression Models

Figure 6.11 presents sample simple linear regression models of the peak resultant Hybrid III headform COG kinematics and upper neck kinetics in impact when fixed to the Phase 1 neck with the R^2 values displayed. Table 6.7 summarizes the R^2 values of all impact locations to the Hybrid III headform when fixed to the Phase 1 neck. The results convey the peak biomechanical measures scale approximately linearly with impact speed, as evidenced by R^2 values of 0.90 or greater. However, for forehead and lateral impact locations to the Hybrid III headform, the impact speed explains only 0.25 of the variation in peak resultant Hybrid III heaform COG angular acceleration using a simple linear regression model.

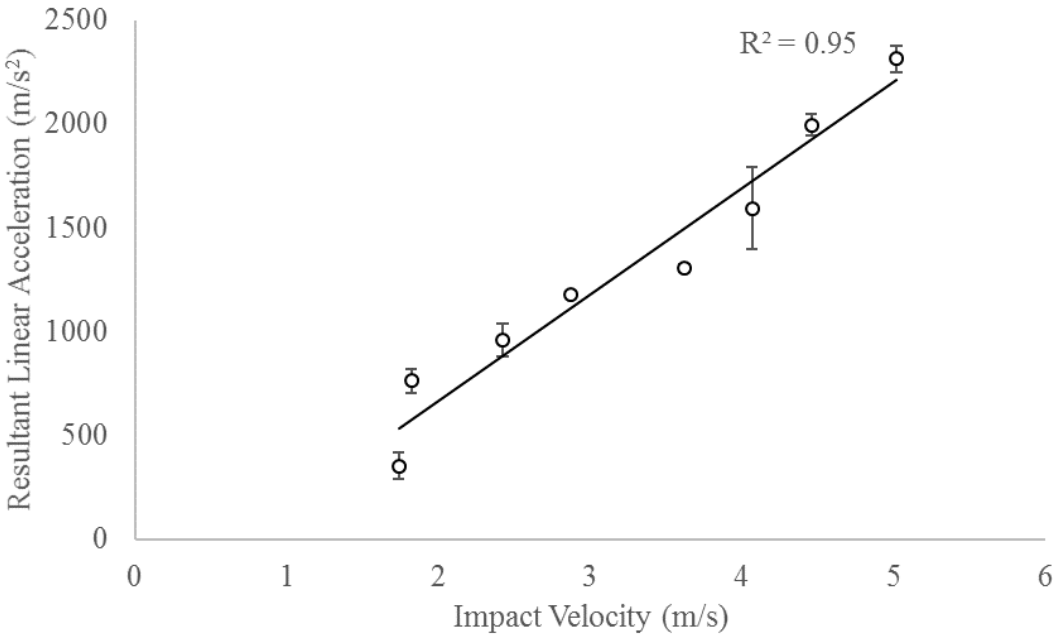
R² = 0.95
Resultant Linear Acceleration (m/s²)
2500
2000
1500
1000
500
0
0
1
2
3
4
5
6
Impact Velocity (m/s)

(a)

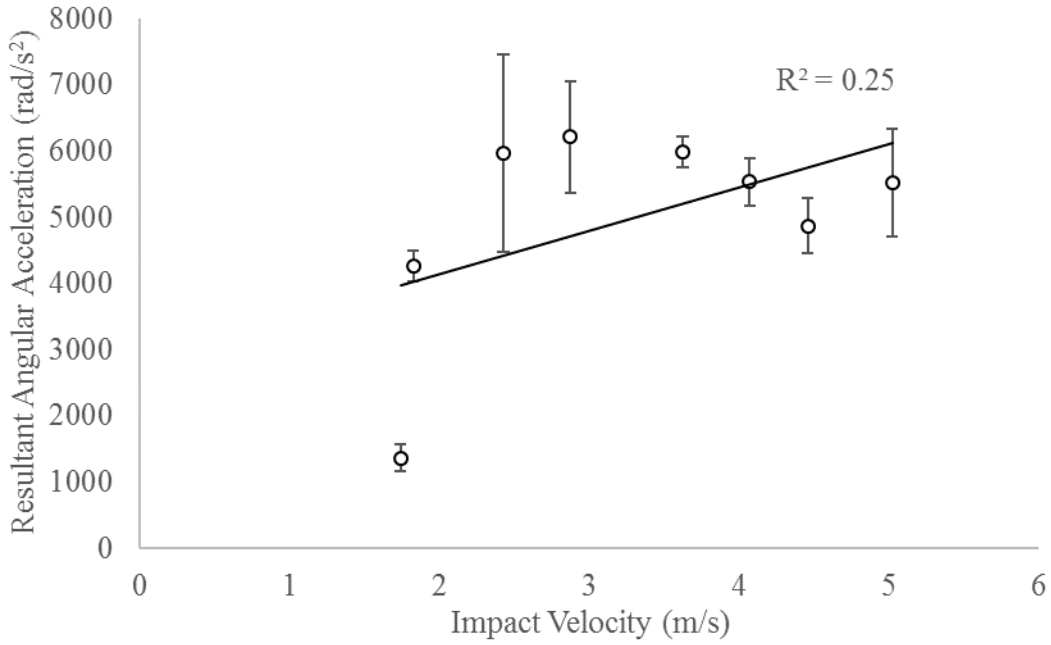
R² = 0.25
Resultant Angular Acceleration (rad/s²)
8000
7000
6000
5000
4000
3000
2000
1000
0
0
1
2
3
4
5
6
Impact Velocity (m/s)

(b)

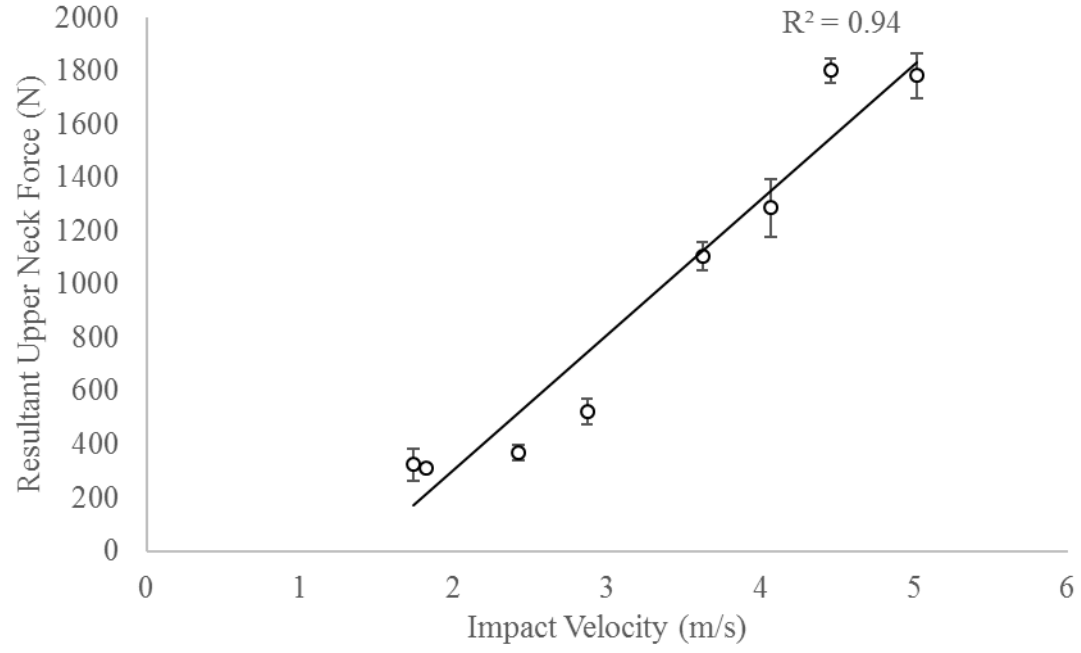

(c)

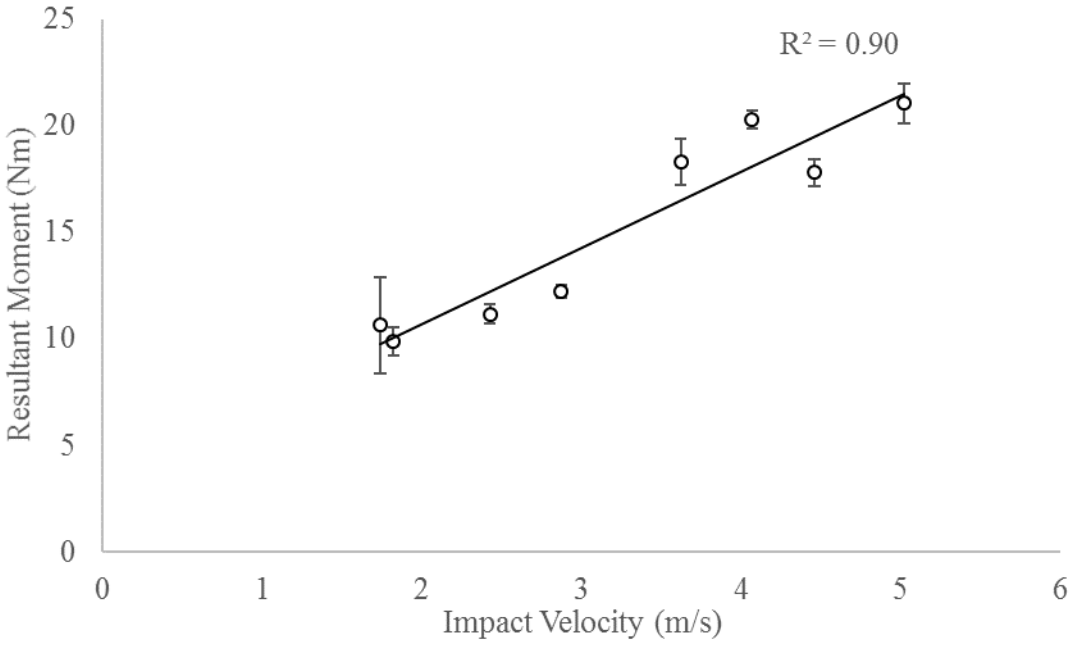

(d)

Figure 6.11: Sample simple linear regression models for forehead impact loading of the Phase 1 mechanical surrogate neck prototype with R^2 value displayed, (a) peak resultant Hybrid III headform COG linear acceleration, (b) peak resultant Hybrid III headform COG angular acceleration, (c) peak resultant upper neck force, (d) peak resultant upper neck moments

Table 6.7: R^2 values for peak resultant head COG kinematics and upper neck kinetics versus increasing impact velocity

Impact Location	Peak Resultant COG Linear Acceleration	Peak Resultant COG Angular Acceleration	Peak Resultant Upper Neck Force	Peak Resultant Upper Neck Moment
Forehead	0.95	**0.25**	0.94	0.90
Side	0.97	**0.23**	0.86	0.98
Rear	0.93	0.97	0.90	0.90

6.4 Discussion

The impact comparison methods presented in this chapter offer an initial observation of the peak resultant headform COG kinematics and upper neck kinetics of the Phase 1 neck to PMHS data. By comparing the collected values to published PMHS data, differences between the two neck segments have been quantified. This information could be used to further develop the Phase 1 neck prototype to closer match realistic human impact response.

The data presented by Advani et al. [12], Rizzetti et al. [8], and Yoganandan et al. [13] offered a range of impact locations to the PMHS head at multiple speeds. The published data sets incorporated time histories of human biomechanical response in direct head impact. At this Phase 1 stage, it was desired to investigate whether the Hybrid III headform COG kinematic and upper neck kinetic data when fixed to the Phase 1 neck was within the range of reported PMHS literature, therefore, peak response analysis was quantified as opposed to observations within whole corridors. In future iterations of the Phase 1 neck, once the peak impact response of the surrogate neck model is optimized to fall with a realistic range of the human, next steps to analyze whether the total time histories of biomechanical corridors are realistic can be investigated.

When fixed to the Phase 1 neck, the Hybrid III headform was impacted three times at multiple impact speeds to the forehead, side, and rear cap. The number of impact speed intervals chosen allowed an initial simple linear regression analysis to be completed on the averaged resulting peak biomechanical values. Additionally, the number of repeated tests allowed for sufficient mean and standard deviation of peak values to be calculated for the initial CV analysis.

The maximum CV value of all peak Hybrid III headform COG kinematics when fixed to the Phase 1 neck was approximately 38% and peak upper neck kinematics was approximately 32%, as shown in Table 6.6. Although the presented maximum CV values in biomechanical data exceed 30%, surpassing the desired 20% target to achieve repeatability, CV values obtained in dynamic

PMHS literature can range from 20% to 140% [29]. Additionally, based on performance requirements outlined by the CFR, the acceptable coefficient of variance within the Hybrid III neck model is 23% in flexion and 50% in extension [19]. The implication of this finding is that the CV of the Phase 1 neck could mimic that of PMHS models, and is within an acceptable range of current neck models. This fact, combined with the evidence that the Phase 1 neck is a durable component, could be interpreted to convey that the Phase 1 neck is a first step towards a durable model that could mimic PMHS response in direct head impact. More realistic neck response could lead to more realistic biomechanical data which, overall, could increase the biofidelity of helmet assessment methods.

Additionally, the R^2 values of 0.90 or greater in Table 6.7 seem promising; however, the R^2 values recorded for peak resultant Hybrid III headform COG angular acceleration range at approximately 0.25. In-house or partnered lab testing of PMHS at a broader range of impact speeds and impact locations than presented in the chosen literature would offer information about how well a simple linear regression model correlates peak biomechanical measures to impact speed for PMHS models. This information could also be used to determine whether the R^2 value obtained for Hybrid III headform COG angular acceleration is realistic when compared to PMHS data.

6.4.1 PMHS Comparisons

The peak Hybrid III headfrom COG linear and angular accelerations when fixed to the Phase 1 neck were within approximately 35% of peak values reported by Advani et al. [12] and approximately 60% of values reported by Rizzetti et al. [8]. Additionally, the peak resultant upper neck force and upper neck moment were within approximately 45% and 73% of peak values reported by Yoganandan et al. [13]. One contributor of this could due to the fact the Phase 1 neck has no neutral zone. As mentioned in Chapter 4, the stiffness of the neutral zone within the human cervical spine is very low and considerable vertebral rotations occur at small-scale moments. In Chapter 4, it was found that the Phase 1 neck is more stiff than the human cadaver neck. As shown in the presented results, the increased stiffness of the Phase 1 neck also affects the headform COG kinematic and upper neck kinetic data upon impact.

The impact experimental method was limited to published PMHS data because live human direct head impact data is more or less nonexistent. It is currently an open question whether the neck of a PMHS is a realistic model for the living human. Live volunteer NBDL sled test results

do exist; however, the resultant biomechanical results are not comparable to direct impact results. The head rotations in these tests are induced by the response of the human torso when the sled is accelerated, and therefore the physical response is different from direct head impacts. Additionally, the volunteer stature and muscle activation are unknown.

Even if refined to match behavior of a cadaveric neck, it is important to acknowledge this Phase 1 neck model might not match the mechanics of a living human. A possible solution could be to attempt to match head kinematics measured from living athletes in a laboratory setting where sport impacts can be recreated.

6.4.2 Limitations

It is important to note the limitations when comparing to published PMHS impact data. First and foremost, the sample size of the PMHS data is exceedingly small, with only 3 impacts, each from separate papers with separate experimental methods. Additionally, the gravitational component in the Phase 1 neck guided free-fall impact experimental methods differs from literature. The data published by Advani et al. were results from pendulum impact to the PMHS head [12]. Rizzetti et al. published data from pneumatic piston impacts [8]. Yoganandan et al. tested PMHS using an electrohydraulic device which pulled a cable to rotate the head [13]. Ongoing efforts will be necessary to assess these head loading paradigms when compared to linearly guided drop tests used in this thesis.

One solution to ensure an exact comparison between PMHS data and the Phase 1 neck would be to undertake in-house or partnered lab PMHS impact testing of a greater number of the test cases than presented in this chapter. Alternatively, creating an experimental protocol to measure head kinematics of living athletes in a controlled laboratory setting, as described in Section 6.4.1, would offer comparisons of biomechanical data of the living human in real athletic impacts to the Phase 1 neck.

A limitation of this impact work is the use of the Hybrid III headform. This surrogate head model was developed by the automotive industry, for use in frontal vehicle collision assessment [15]. A common validation procedure of the Hybrid III headform is to suspend the neckless headfrom and drop it such that the forehead is impacted on a horizontal steel plate, and the peak linear acceleration data is collected [19]. The Hybrid III headform was not validated for rear or lateral impacts. However, previously published works use the Hybrid III head in multiple impact

locations, therefore the use of this headform was justified for this Phase 1 analysis of the surrogate neck model [8], [56].

Additionally, the connection to the upper neck load cell of the Hybrid III headform, which approximates the OC in the human, allows for flexion and extension motions only. The design of the OC in this headform is therefore not realistic, as it does not allow for lateral or axial rotations. This could limit the headform kinematics and upper neck kinematics. Headform COG kinematic and upper neck kinetic responses in other surrogate models validated at other impact locations and contain more realistic OC joints should be investigated to confirm the results when compared to human responses.

At impact speeds approaching 5.0 m/s, small tears in the silicone rubber around areas where the steel cables extruded in the Phase 1 neck. If the experimental protocol of helmet certification methods exceed 5.0 m/s, the durability of the Phase 1 neck will begin to falter. In future iterations of the neck model, silicone rubbers that are stronger in shear, but remain compliant enough to be comparable to human tissue, should be explored.

Figure 6.12 depicts the peak impact response of a 5.0 m/s impact to the rear cap of the Hybrid III headform when fixed to the Phase 1 neck. Due to the compliance of the neck, the silicone rubber did not stick to the gimbal. At the higher speed impacts, the Hybrid III headform rotations where then entirely based upon the tension in the steel cables, and not the effect of the simulated musculature. Additionally, impact tests that exceeded 3.0 m/s caused slippage of the clamping collars that dictated the tension in the steel cables.

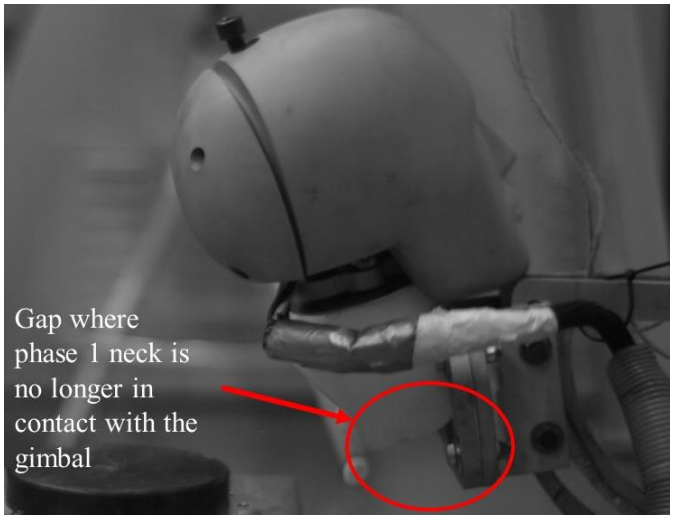

Figure 6.12: Annotated high-speed image of peak impact response of 5.0 m/s rear impact to the Hybrid III headform fixed to the Phase 1 mechanical surrogate neck

The chosen clamping collars are manufactured to clamp to a shaft for power transmission. As described in Section 4.4.3 of Chapter 4, since these collars were used in tension on cables rather than power transmission on shafts, the collars slipped under the impact testing conditions. The slipped collars could change the results in biomechanical measures within repeated tests. However, the magnitudes of these biomechanical measures are large enough that changes in cable tension did not appear to have a considerable effect on the variation results, as shown in Table 6.6, than in the quasi-static bending results (Chapter 4). In future iterations of the Phase 1 neck, adhering the silicone rubber to the gimbal would reduce the additional tension in the steel cables post-impact, possibly reducing the amount the collars slip down the cables.

7 DISCUSSION

The objective of this thesis is to develop and characterize a Phase 1 mechanical surrogate neck prototype that offers a realistic biomechanical response, relative to the human, for use in helmet certification experimental methods. A realistic surrogate neck component is imperative for helmet assessment protocol, because more realistic helmet test methods will lead to measurements of helmet performance that reflect a true representation of mechanics in the human. This could be important if helmet certifications were to include pass/fail thresholds based on realistic head COG rotational kinematics, or the use of brain models that rely on realistic input kinematics to assess risk of injury. Stated another way, if the Phase 1 neck was further optimized to offer realistic biomechanical direct head impact responses relative to the human, helmet assessment tools that give a truer picture of how protective a helmet is could be achieved, as opposed to simply quantifying its ability to attenuate impact in a crude impact experiment.

7.1 Overall Trends

The motivation behind this thesis objective is to design a mechanically robust, repeatable, and reusable surrogate neck model that is less stiff than the currently available Hybrid III neck model. Additionally, one objective was to achieve headform COG kinematics and upper neck kinetics that were within 20% of peak PMHS data. The characterization methods of the Phase 1 neck included comparing the sagittal plane flexural stiffness of the Phase 1 neck to PMHS data, comparing the impact response of the Phase 1 neck to an available surrogate ATD neck model, and comparing the impact response of the Phase 1 neck to PMHS data.

The trends in the presented data show the Phase 1 neck model is more mechanically compliant than the Hybrid III neck component. This is evident from the differences in headform COG kinematics exceeding 40% and upper neck kinetics exceeding 80%, respectively. In many helmet certification methods, the experimental protocol was developed under the assumption that surrogate neck compliance has no effect on peak biomechanical measures. However, based on the results presented in Chapter 5, the compliance of the neck does in fact make a difference on these peak measures. This suggests that the judgement of using the Hybrid III neck model in helmet certification experimental methods may not be sound.

The data presented in Chapter 4 and Chapter 6 show the peak flexural angular displacements, head COG kinematic, and upper neck kinetic data of the Phase 1 neck exceed 20% of current PMHS literature. However, this Phase 1 attempt to characterize a novel mechanical surrogate neck prototype offered valuable and meaningful insight to optimize this neck model to closer match the human response moving forward.

In both the quasi-static bending and impact CV analyses, the variation in the Phase 1 neck data was found to exceed the 20% target to achieve repeatability. However, CV values of PMHS neck models in quasi-static bending literature can be up to 40% [9]–[11], and in dynamic literature can range from 20% to 140% [29], thereby drawing the conclusion that the Phase 1 neck model could mimic PMHS models.

The Phase 1 neck sustained over 10 quasi-static bending experiments and over 80 impacts without failure. The presented impact data suggests peak biomechanical magnitudes scale approximately linearly with impact speed (R^2 value of 0.90 or greater). This finding suggests the Phase 1 neck is a reliable component that can withstand multiple impacts without damage.

The overall trends found in this thesis are that the Phase 1 neck is a durable component with inter-test variance that is comparable to PMHS data. These results can be interpreted such that the Phase 1 neck is a first step towards a reusable neck component that could mimic PMHS response in both quasi-static bending and direct head impact. A neck model that offers realistic response compared to human data could lead to more realistic biomechanical response data obtained in helmet assessment methods which, overall, could increase the biofidelity of these experimental methods.

7.2 Comparison of Thesis Work to Work of Others

While a specific surrogate neck model for helmet testing has not yet been introduced, working towards a realistic neck model in impact is crucial component for realistic testing of human head protection technology and helmet certification protocol. The presented work in this thesis focuses on a Phase 1 characterization of the novel mechanical surrogate neck design, and compare the results to the PMHS response.

The presented characterization protocol, namely quasi-static bending and direct headform impact testing, are not used to calibrate currently available automotive surrogate neck models. Currently available ATD surrogate necks include the Hybrid III and the THOR for use frontal vehicle impacts, the BioRID for use in rear vehicle simulations, as well as the EuroSID and the WorldSID for use in side-impact vehicle collisions. However, the focus of these efforts remain in the automotive industry and not direct head impact testing, therefore, the design and validation of these neck components were all compared to sled test data [19], [39], [60], [61].

Although these ATD neck models are not validated for direct head impact testing, these models contain interesting qualities. For example, the THOR neck model contains components to replicate the OC in the sagittal plane [62]. The EuroSID neck contains a screwed half-sphere at the superior and inferior ends of the neck, which allows lateral rotation [61]. These qualities could be investigated for future iterations of the Phase 1 neck model to increase the biofidelity of this component.

7.3 Phase 1 Mechanical Surrogate Neck Prototype Design Change Suggestions

7.3.1 Quasi-static bending Response Characterization

Generally, the percent difference in peak angular displacement in the sagittal plane between the Phase 1 neck and PMHS literature exceeded 80%. One contributor to this could be the lack of neutral zone in the Phase 1 neck. When comparing the Phase 1 neck ROM results to regions beyond the neutral zone in the PMHS, the maximum percent difference in peak values decrease by 20%, 40%, and 10% when compared to data presented by Camacho et al. [9], Nightingale et al. [10], and Wheeldon et al. [11], respectively. Already, these results show that introducing a neutral zone into the Phase 1 neck design may reduce the difference in ROM.

A possible way to achieve this neutral zone in the Phase 1 neck would be to include ball joints between vertebral levels. The transverse posterior elements of the vertebral body design, as well

as the design of the intervertebral discs, would ensure the rotations of the ball joints do not exceed realistic limits.

Alterations to the Phase 1 neck intervertebral disc design could be completed to increase the biofidelity of the neck model. The intervertebral discs of the Phase 1 neck were 3D printed, homogeneous components. Methods suggested by Vuono-Hawkins et al. suggest thermoplastic multicomponent designs are adequate to mimic the human intervertebral disc [63]. In future designs of the Phase 1 neck, incorporating multi-durometer thermoplastic intervertebral discs that are adhered to the adjacent vertebral bodies may influence the flexibility response to closer match the human.

To keep the design of the Phase 1 neck simple, the geometry of all vertebral bodies and intervertebral disc designs were kept the same. However, the coupled joint movements at the AO and AA joints in the human are quite complex and offer the most motion in head rotational movements [6]. Accurate representations of these joints in the Phase 1 neck design could offer greater flexibility at the superior end of the surrogate spinal segment, and would closer match the movements in a human cervical spine. These improvements to the Phase 1 neck design could also improve the impact response when compared to PMHS data.

The design at the inferior end of the neck effected the quasi-static bending results. The base plate is secured in place using three clamping collars – one for each cable. This design allowed for a temporary setup of each Phase 1 neck prototype replicate. Should the Phase 1 neck incur any damage, the neck model could easily be disassembled and reassembled by hand. At the maximum flexion and extension displacements, enough force on the clamping collars was present to cause them to slip down the cables. Due to the small magnitudes of the angular displacement within the Phase 1 neck, any change in the tests effect the overall flexural results. Now that the Phase 1 neck has been shown to be a durable model, the assembly of future iterations of the neck prototype could secured in a more permanent way. Compression stud end fittings where bolts could be fastened at the end of these fittings with a known torque could be added which would result in a known tension within the cable.

7.3.2 Impact Response Characterization

Typically, the percent difference in peak biomechanical measures in impact between the Phase 1 neck and PMHS literature exceeded 20%. Although the Phase 1 neck was found to be

more compliant than the Hybrid III neck model, the Phase 1 neck remains more mechanically stiff for realistic human impact response. However, implementing a realistic neutral zone, realistic intervertebral discs, and realistic AA and AO joints within the Phase 1 neck, as described in Section 7.1.2, would offer a more realistic head-neck response than one without these features.

In impact, the silicone rubber was not adhered to the gimbal. As a result, the steel cables, and therefore the tension within the cables of the Phase 1 neck assembly, influenced Hybrid III headform motion post-impact. After multiple impact tests, this response caused the clamping collars to slip down the steel cables, resulting in fluctuating tension between repeated tests. Although this fluctuation in cable tension did not appear to influence the results, the impact response of the Hybrid III headform is considered unrealistic if it is purely based on the tension in the cables. If, in the next phase of impact test characterization, the silicone rubber was adhered to the gimbal, the impact response would be influenced by all components of the neck model, such as the spinal column, soft tissue, and tension in the steel cables. This is a more realistic comparison to human impact response.

8 CONCLUSION

The objective of this thesis was to develop and characterize a Phase 1 mechanical surrogate neck model for use in helmet certification experimental methods. Today's helmet certification experimental methods include neck models with varying degrees of stiffness, from rigid metal rods, to ATD surrogate neck models, to no neck whatsoever. These neck models are known not to exhibit realistic head-neck motions upon impact, however, many helmet certification methods are developed to protect against focal head injury where head rotation is not examined. With growing concern of diffuse brain injury, commonly known as concussion, as well as the connection between rotational movement of the head with this type of brain injury, a neck model that offers realistic response relative to the human is necessary. This study proposed a novel neck design and identified possible experimental characterization methods to achieve a durable and repeatable neck design, relative to human response.

One aim of this thesis was to quantify the difference in peak flexion and extension angles in pure moment bending of the Phase 1 neck to PMHS cervical spine segments. Many currently available human surrogate neck models were developed by the automotive industry, and were not validated for quasi-static bending. A quasi-static bending analysis offers valuable information about realistic flexibility and ROM in the human spine, and allows for accurate characterization of surrogate neck models. Overall, the ROM results of the Phase 1 neck were approximately 80% lower than that of a PMHS. The maximum CV of the flexion data was approximately 45%, and of the extension data was 70%.

The other goal of this thesis is to quantify the difference in peak resultant biomechanical magnitudes of the Phase 1 neck to an available ATD surrogate neck model and to the PMHS in

impact. Comparing to an available ATD neck model offers valuable information about how a more compliant neck model may change the headform COG kinematics and the upper neck kinetics in impact. Overall, the results show the Phase 1 neck is more mechanically compliant than the Hybrid III neck model. Additionally, the results show the compliancy of the neck model does in fact make a difference in the rotational results of the headform, contradicting the current assumptions made when developing helmet certification experimental methods.

Comparing to PMHS data offers information about how realistic the Phase 1 neck impact response is to the human. Overall, the peak resultant linear acceleration at the Hybrid III headform COG when fixed to the Phase 1 neck was up to 80% greater and the peak resultant angular acceleration at the Hybrid III headform COG when fixed to the Phase 1 neck was up to 35% less than the PMHS literature values selected. Furthermore, the peak resultant upper neck forces were up to 50% greater and the peak resultant upper neck moments were up to 75% less in the Phase 1 neck, relative to necks of PMHS.

The Phase 1 neck prototype proved to be a robust component and survived over 80 impact tests without mechanical failure. The maximum CV value in peak resultant headform COG kinematics and upper neck kinetics was approximately 35%. Simple linear regression models showed most peak biomechanical measures approximately scale with impact speed, as evidenced by R^2 values of 0.90 or greater in the presented data.

8.1 Contributions

As discussed through the entirety of this thesis, current helmet certification methods do not use a standardized surrogate neck model. When certifying helmets, a surrogate neck model validated against human head impact data is crucial for accurate collection of realistic post-impact head-neck mechanics. This thesis work presents a novel mechanical surrogate neck prototype design, as well as characterizes the quasi-static bending and impact response relative to published human PMHS data. Overall, the contributions of this thesis include:

- A viable baseline surrogate neck characterization experimental protocol. Currently available ATD neck models were developed by the automotive industry, and are often validated against human sled test data, not direct head impact response. The proposed

experimental protocol to characterize surrogate neck models offers a possible method to achieve realistic human impact response corridors.

- Neck model compliancy is important when evaluating headform rotational data. The compliancy of the surrogate neck model affects the neck rotational ROM, which in turn dictates post-impact biomechanical data of the headform used. This finding contradicts the current assumption in helmet certification standards that neck compliancy does not affect biomechanical data.
- The variance within the Phase 1 neck model is comparable to PMHS literature. Coupled with the fact the Phase 1 neck is a durable model, these findings could be interpreted to convey the Phase 1 neck is a reasonable first step towards a reusable model to be used in a controlled laboratory setting that could mimic PMHS response.

The results in this thesis document a Phase 1 analysis of overall flexural stiffness and peak resultant biomechanical data of a novel mechanical surrogate neck design with several limitations. With ongoing work to refine the Phase 1 neck design and characterization procedure, a neck model that accurately represents the human response in impact may be achieved.

8.2 Future Work and Recommendations

Overwhelming evidence in head injury biomechanics research shows angular kinematic evaluation is necessary in helmet certification methods. To achieve this, a neck model that exhibits realistic impact response, relative to the human, is imperative. This thesis presents a novel neck design and a possible characterization protocol for surrogate neck models. Repeating this study with a more refined neck design will offer valuable information in achieving a surrogate neck model with realistic impact response, relative to the human. In particular, such refinements include: adapting a neutral zone in the spinal column, multi-durometer intervertebral discs, more realistic atlanto-occipital and atlano-axial joints at the superior end of the spinal column, and re-designing the base of the neck to reduce errors due to fluctuating tension in the stability cables.

Undertaking in-house or partnered lab PMHS testing will augment the characterization protocol to allow for more direct comparisons between future neck designs and the human quasi-static bending and impact responses. The quasi-static bending PMHS test protocol could include halo to T1 cervical spine segments of the human cadaver and the same robotic platform as

presented in Chapter 4. Elastic flexural bending stiffness experiments could be completed in the sagittal plane to observe flexion and extension bending, as well as in the coronal plane to observe lateral bending responses. Stereoscopic video recording and coordinate transform methods to determine the relative magnitudes of rotation at each vertebral level for both the Phase 1 neck and PMHS neck segments will prove to be valuable, as each vertebral level in the human cervical spine does not contain the same ROM about the COR. Additionally, altering the quasi-static bending experimental protocol such that the COR of the robotic platform moves in an arc following the motion of the neck model, rather than remaining stationary, will allow for a better application of pure moments to the neck model.

The impact PMHS test protocol could include guided-linear free-fall drops, horizontal piston impacts, or pendulum sing impacts to PMHS head-neck segments. It will be important to ensure whichever test protocol is chosen for the PMHS response is also be repeated on the next phase neck prototype design. Additionally, testing a greater number of impact locations and impact speeds to the PMHS than presented in Chapter 6 will offer a more complete characterization protocol for future surrogate neck models. Further, helmeted PMHS impacts could be included in the test protocol to observe the differences human head-neck response in helmeted versus un-helmeted experiments.

When fixed to the Phase 1 neck, small rotations of the Hybrid III headform were observed in the collected high-speed video footage prior to impacting the MEP pad. If the chosen test protocol of the next phase were to include guided-linear free-fall drops, a custom gimbal attachment will be required to guide the headform to strike the anvil with no rotations prior to impact

Alternatively, a characterization protocol using live human data could be implemented. Live human quasi-static bending data could be collected using 3D MRI scans of cervical spines during flexion, extension, and lateral bending movements. Live human impact responses could be collected from athletes in a laboratory setting in which sport impacts can be recreated. Comparing the surrogate neck response to living human data will offer the most realistic response corridors.

A method to evaluate whole response curves of a given biomechanical parameter, rather than peak magnitudes alone, would assist with better characterizing future iterations of the Phase 1 neck prototype design. Additionally, testing more than one replicate of the Phase 1 neck model offer a more robust statistical analysis of the results. A suite of comparison metrics, known as CORA, is a correlation and analysis evaluation method [64]. This method evaluates the data using a corridor

rating and a cross-correlation rating [64]. The corridor rating evaluates the fit of a response curve to a user-defined corridor [64], which, for the purpose of a surrogate neck design characterization, would be the human response corridor. The cross-correlation rating evaluates the phase shift, curve shape, and area below the two corridor curves [64]. This CORA evaluation method has already been used by researchers such as Vavalle et al. to evaluate methods of time history signals to compare simulated human body responses to experimental data [65]. Their results show the CORA method offered the most comprehensive evaluation of their time signals [65], which supports this statistical analysis method as a viable option.

Should a refined surrogate neck model that similarly matches human impact response be achieved, it will then be necessary to implement changes in current helmet certification experimental protocol. If a standardized, repeatable human surrogate neck model was required in all helmet certification methods, more accurate representations of human head-neck motion will be attained. Helmet certification methods must then be assessed to ensure realistic and reasonable linear and angular thresholds are set in place. Additionally, a standardized neck model will reduce any ambiguities between helmet certification methods that use different neck models.

REFERENCES

[1] T. Kay et al., "Definition of mild traumatic brain injury," in *J Head Trauma Rehabil*, vol. 8(3), pp. 86-87, 1993.

[2] *The Cost of Injury in Canada*. Toronto, ON: Parachute, 2015, pp. 1.

[3] J. M. Billette and T. Janz. (2017, April). "Injuries in Canada: Insights from the Canadian Community Health Survey." *Statistics Canada Catalogue*. [Online]. 82-624-X. Available: http://www.statcan.gc.ca/pub/82-624-x/2011001/article/11506-eng.htm. [Accessed: 23-Jan-2017].

[4] E. G. Takhounts, M. J. Craig, K. Moorhouse, and J. McFadden, "Development of Brain Injury Criteria (BrIC)," *Stapp Car Crash Journal*, vol. 57, pp. 243-266, Nov. 2013.

[5] F. Martini et al. *Fundamentals of Anatomy & Physiology,* Eleventh edition. New York: Pearson Education, Inc, 2018.

[6] R. Riascos et al., "Imaging of Atlanto-Occipital and Atlantoaxial Traumatic Injuries: What the Radiologist Needs to Know," *RadioGraphics*, vol. 35(7), pp. 2121–2134, Nov. 2015.

[7] R. Eastell, L. Mosekilde, S. F. Hodgson, and Dr. B. L. Riggs, "Proportion of human vertebral body bone that is cancellous," *Journal of Bone and Mineral Research*, vol. 5(12), pp. 1237-1241, 1990.

[8] A. Rizzetti, D. Kallieris, P. Schiemann, and R. Mattern, "Response and Injury Severity of the Head-Neck Unit During a Low Velocity Head Impact," in *Proc. IRCOBI Conference*, 1997, pp. 193-206.

[9] D. L. Camacho, R. W. Nightingale, J. J. Robinette, S. K. Vanguri, D. J. Coates, and B. S. Myers, "Experimental Flexibility Measurements for the Development of a Computational Head-Neck Model Validated for Near-Vertex Head Impact," in 41st Annual Stapp Car Crash Conference, 1997, pp. 473-486.

[10] R. W. Nightingale et al., "Flexion and extension structural properties and strengths for male cervical spine segments," *J of Biomech*, vol. 40(3), pp. 535–542, Jan. 2006.

[11] J. A. Wheeldon, F. A. Pintar, S. Knowles, and N. Yoganandan, "Experimental flexion/extension data corridors for validation of finite element models of the young, normal cervical spine." *J Biomech*, vol. 39(2), pp. 375–380, 2006.

[12] S. H. Advani, W. R. Powell, J. Houston, and S. J. Ojala, "Human Head Impact Response - Experimental Data and Analytical Simulations," West Virginia University, Morgantown, WV, Rep. 26506, pp. 153-163, (n.d.).

[13] N. Yoganandan, J. Humm, F. A. Pintar, C. E. Wolfla, and D. J. Maiman, "Lateral neck injury assessments in side impact using post mortem human subject tests," *Ann. Adv. Automot. Med.*, vol. 55, pp. 169–179, Oct. 2011.

[14] H. J. Mertz and A. L. Irwin, "Anthropomorphic Test Devices and Injury Risk Assessments," in *Accidental Injury: Biomechanics and Prevention*. N. Yoganandan, Ed. New York: Springer Science+Business Media, 2015, pp. 83-86.

[15] C. VanIngen-Dunn and I. Kaleps, "A Pursuit for a More Biofidelic Manikin Neck," in *Frontiers in Head and Neck Trauma*. N. Yoganandan et al., Ed. Amsterdam: IOS Press, 1998, pp. 131-145.

[16] J. Foster, J. Kortge, and M. Wolanin, "Hybrid III - A Biomechanically-Based Crash Test Dummy," SAE Transactions, vol. 86, Section 4: 770720-771010, 1977, pp. 3268-3283.

[17] E. K. Spittle et al.,"Hybrid II and Hybrid III Dummy Neck Properties for Computer Modeling." Airforce Systems Command, Wright-Patterson Air Force Base, OH, AL-TR-1992-0049, Feb. 1992.

[18] H. J. Mertz, R. F. Neathery, and C. C. Culver, "Performance Requirements and Characteristics of Mechanical Necks" in *Proc. Symposium on Human Impact Response*, 1972, pp. 263-288.

[19] GPO, "Anthropomorphic Test Devices," CFR Standard 49 Part 572, CFR, Oct. 2011.

[20] T. Gibson, N. Shewchenko, and C. Withnall, "Biofidelity Improvements to the Hybrid III Neck," in *Proc. 14th ESV*, 1994, pp. 159-168.

[21] C. Esopenko and B. Levine, "Aging, Neurodegenerative Disease, and Traumatic Brain Injury: The Role of Neuroimaging," *J. Neurotrauma*, vol. 32(4), pp. 209–220, Feb. 2015.

[22] F. A. Fernandes and R. J. A. de Sousa, "Head injury predictors in sports trauma – A state-of-the-art review," *Proc. Inst. Mech. Eng.*, vol. 229(8), pp. 592–608, Aug. 2015.

[23] J. A. Langlois, W. Rutland-brown, and M. M. Wald, "The Epidemiology and Impact of Traumatic Brain Injury: A Brief Overview," *J. Head Trauma Rehabil.*, vol. 21(5), pp. 375–378, Sep. 2006.

[24] ASTM International, "Standard Performance Specification for Ice Hockey Helmets," U.S. Standard F1045-16, n.d.

[25] P. Halldin, “CEN/TC 158 Working Group 11 Rotational test methods,” ASTM New Orleans, Nov-2014.

[26] UNECE, “Uniform provisions concerning the approval of protective helmets and their visors for drivers and passengers of motor cycles and mopeds,” C.H. Standard E/ECE/324: E/ECE/TRANS/505, Sept. 24, 2002.

[27] NOCSAE, “Standard Pneumatic Ram Test Method and Equipment Used in Evaluating the Performance Characteristics of Protective Headgear and Face Guards,” U.S. Standard (ND) 081-14m15, Jan. 2016.

[28] B. Rowson, S. Rowson, and S. M. Duma, “Hockey STAR: A Methodology for Assessing the Biomechanical Performance of Hockey Helmets,” *Ann. Biomed. Eng.*, vol. 43(10), pp. 2429–2443, Oct. 2015.

[29] J. H. Ash, D. J. Lessley, J. L. Forman, Q. Zhang, C. G. Shaw, and J. R. Crandall, “Whole-Body Kinematics: Response Corridors for Restrained PMHS in Frontal Impacts,” in *Proc. IRCOBI Conference 2012*, 2012, pp. 142-154.

[30] C. M. Ringle, R. R. Sinkovics, and J. Henseler, “The use of partial least squares path modeling in international marketing,” in *New Challenges to International Marketing*, Bingley: Emerald Group Publishing Limited, 2009, pp. 277–319.

[31] A. N. Vasavada, J. Danaraj, and G. P. Siegmund, “Head and neck anthropometry, vertebral geometry and neck strength in height-matched men and women,” *J. Biomech.*, vol. 41(1), pp. 114–121, 2008.

[32] H. G. Armstrong, “Anthropometry and Mass Distribution for Human Analogues, Volume I: Military Aviators,” U.S. Army, Air Force, and Navy, 1988.

[33] J. L. Sparks et al., “Use of Silicone Materials to Simulate Tissue Biomechanics as Related to Deep Tissue Injury,” *Wound Care Journal*, vol. 28(2), pp. 59-68, Feb. 2015.

[34] P. H. F. Nicholson et al., “Structural and material mechanical properties of human vertebral cancellous bone,” *Med. Eng. Phys.*, vol. 19(8), pp. 729–737, Oct. 1997.

[35] N.a., “Spine Biomechanics,” MER/BIO Soft Tissue Mechanics, pp. 5-15, n.d.

[36] S. Schleifenbaum et al., “Load and failure behavior of human muscle samples in the context of proximal femur replacement,” *BMC Musculoskelet. Disord.*, vol. 17, pp. 1-7, Apr. 2016.

[37] M. M. Panjabi, J. Duranceau, V. Goel, T. Oxland, and K. Takata, “Cervical human vertebrae. Quantitative three-dimensional anatomy of the middle and lower regions,” *Spine*, vol. 16(8), pp. 861–869, Aug. 1991.

[38] I. Gilad and M. Nissan, “A Study of Vertebra and Disc Geometric Relations of the Human Cervical and Lumbar Spine,” *Spine*, vol. 11(2), pp. 154–157, Mar. 1986.

[39] “Biomechanical Response Requirements of the THOR NHTSA Advanced Frontal Dummy,” GESAC Inc., Boonsboro, MD, Report Bo. GESAC-05-03, 2005.

[40] T. Ishii et al., “Kinematics of the upper cervical spine in rotation: in vivo three-dimensional analysis,” *Spine*, vol. 29(7), pp. E139-144, Apr. 2004.

[41] B. S. Myers et al., “Response of the Human Cervical Spine to Torsion,” in *Proc.33rd Annual Stapp Car Crash Conference*, 1989, pp. 215-222.

[42] T. S. Nelson and P. A. Cripton, “A New Biofidelic Sagittal Plane Surrogate Neck for Head-First Impacts,” *Traffic Inj. Prev.*, vol. 11, no. 3, pp. 309–319, Jun. 2010.

[43] SAE, “(R) Instrumentation for Impact Test - Part 1 - Electronic Instrumentation,” SAE Standard J211-1, SAE International, 2007.

[44] M. M. Panjabi et al., “Mechanical Properties of the Human Cervical Spine as Shown by Three-Dimensional Load-Displacement Curves,” *Spine*, vol. 26 (24), pp. 2692-2700, 2001.

[45] R. W. Nightingale, B. A. Winkelstein, K. E. Knaub, W. J. Richardson, J. F. Luck, and B. S. Myers, “Comparative strengths and structural properties of the upper and lower cervical spine in flexion and extension,” *J. Biomech.*, vol. 35 (6), pp. 725–732, Jun. 2002.

[46] E. E. Swartz, R. T. Floyd, and M. Cendoma, “Cervical Spine Functional Anatomy and the Biomechanics of Injury Due to Compressive Loading,” *J. Athl. Train.*, vol. 40(3), pp. 155–161, 2005.

[47] H. J. Wilke, K. Wenger, and L. Claes, “Testing criteria for spinal implants: recommendations for the standardization of in vitro stability testing of spinal implants,” *Eur. Spine J. Off. Publ. Eur. Spine Soc. Eur. Spinal Deform. Soc. Eur. Sect. Cerv. Spine Res. Soc.*, vol. 7(2), pp. 148–154, 1998.

[48] I. Busscher et al., “The effects of creep and recovery on the in vitro biomechanical characteristics of human multi-level thoracolumbar spinal segments,” *Clin. Biomech.*, vol. 26(5), pp. 438–444, Jun. 2011.

[49] B. P. Meij, N. Suwankong, A. J. Van der Veen, and H. A. W. Hazewinkel, "Biomechanical flexion-extension forces in normal canine lumbosacral cadaver specimens before and after dorsal laminectomy-discectomy and pedicle screw-rod fixation," *Vet. Surg. VS*, vol. 36(8), pp. 742–751, Dec. 2007.

[50] A. J. Padgaonkar, K. W. Krieger, and A. I. King, "Measurement of Angular Acceleration of a Rigid Body Using Linear Accelerometers," *J. Appl. Mech.*, vol. 42, no. 3, pp. 552–556, Sep. 1975.

[51] N. M. Alem, G. S. Nusholtz, and J. W. Melvin, "Superior-Inferior Head Impact Tolerance Levels," US Dep. of Health and Human Services, Rockville, MD, Rep. 210-79-0028, 1982.

[52] D. L. A. Camacho, R. W. Nightingale, and B. S. Myers, "The Influence of Surface Padding Properties on Head and Neck Injury Risk," *J. Biomech. Eng.*, vol. 123, no. 5, pp. 432–439, Apr. 2001.

[53] G. S. Nusholtz, D. E. Huelke, P. Lux, N. M. Alem, and F. Montalvo, "Cervical Spine Injury Mechanisms," in *Proc. 27th Stapp Car Crash Conference with IRCOBI and Child Injury and Restraint Conference with IRCOBI*, 1983, pp. 179-97.

[54] G. S. Nusholtz, J. W. Melvin, D. F. Huelke, N. M. Alem, and J. G. Blank, "Response of the Cervical Spine to Superior-Inferior Head Impact," in *Proc. 25th Stapp Car Crash Conference*, 1981, pp. 197-237.

[55] F. A. Pintar, N. Yoganandan, and J. Baisden, "Characterizing occipital condyle loads under high-speed head rotation," *Stapp Car Crash J.*, vol. 49, pp. 33–47, Nov. 2005.

[56] D. E. Toomey, K. H. Yang, and C. A. Van Ee, "The Hybrid III upper and lower neck response in compressive loading scenarios with known human injury outcomes," *Traffic Inj. Prev.*, vol. 15 Suppl 1, pp. 223-230, 2014.

[57] N. Yoganandan, J. Sances A., and F. Pintar, "Biomechanical Evaluation of the Axial Compressive Responses of the Human Cadaveric and Manikin Necks," *J. Biomech. Eng.*, vol. 111(3), pp. 250–255, Aug. 1989.

[58] N. Yoganandan, F. A. Pintar, J. F. Cusick, and M. Kleinberger, "Head-Neck Biomechanics in Simulated Rear Impact," *Annu. Proc. Assoc. Adv. Automot. Med.*, vol. 42, pp. 209–231, 1998.

[59] N. Yoganandan, F. A. Pintar, J. Zhang, B. D. Stemper, and M. Philippens, "Upper neck forces and moments and cranial angular accelerations in lateral impact," *Ann. Biomed. Eng.*, vol. 36(3), pp. 406–414, Mar. 2008.

[60] A. Linder et al., "Design and Validation of the Neck for a Rear Impact Dummy (BioRID I)," *Traffic Inj. Prev.*, vol. 3(2), pp. 167–174, Jun. 2002.

[61] Seminar European Side-Impact Dummy "Eurosid," *The European side-impact dummy "Eurosid": proceedings of the seminar held in Brussels, 11 December 1986*. Luxembourg: Office for Official Publications of the European Communities, 1987.

[62] "THOR-50M User Manual," Humanetics Innovative Solutions, Farmington Hills, MI, Report No. 472-9900 Rev D, 2017.

[63] M. Vuono-Hawkins, N. A. Langrana, J. R. Parsons, C. K. Lee, and M. C. Zimmerman, "Materials and design concepts for an intervertebral disc spacer. II. Multidurometer composite design," *J. Appl. Biomater.*, vol. 6(2), pp. 117–123.

[64] C. Gehre, H. Gades, and P. Wernicke, "Objective Rating of Signals Using Test and Simulation Responses," in Proc. 21st ESV, 2009.

[65] A. Vavalle et al., "An Evaluation of Objective Rating Methods for Full-Body Finite Element Model Comparison of PMHS Tests." Traffic Injury Prevention, vol. 14, pp. 87-94, 2013.